Max-Planck-Institut für Meteorologie
Max Planck Institute for Meteorology

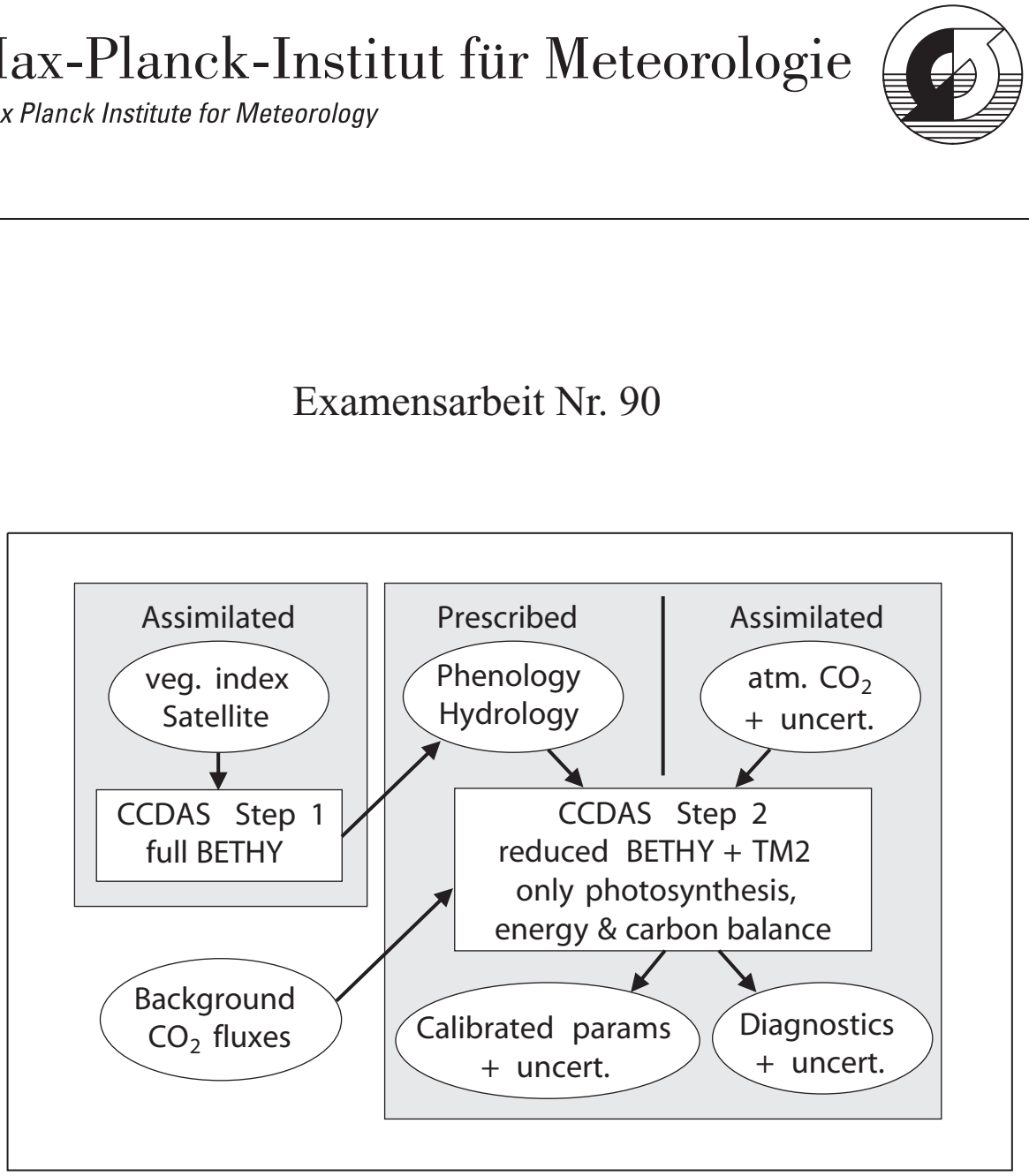

Examensarbeit Nr. 90

Model studies on the response of the terrestrial carbon cycle to climate change and variability

Marko Scholze

Hamburg, Mai 2003

Dissertation zur Erlangung des Doktorgrades

Autor:

Marko Scholze Max-Planck-Institut für Meteorologie

Max-Planck-Institut für Meteorologie
Bundesstrasse 55
D - 20146 Hamburg
Germany

Tel.: +49-(0)40-4 11 73-0
Fax: +49-(0)40-4 11 73-298
e-mail: <name>@dkrz.de
Web: www.mpimet.mpg.de

Model studies on the response of the terrestrial carbon cycle to climate change and variability

Dissertation
zur Erlangung des Doktorgrades
der Naturwissenschaften im Fachbereich
Geowissenschaften
der Universität Hamburg

vorgelegt von

Marko Scholze

aus

Kiel

Hamburg

2003

Als Dissertation angenommen
vom Fachbereich Geowissenschaften der Universität Hamburg
auf Grund der Gutachten von Herrn Prof. Dr. Hartmut Graßl
und Herrn Prof. Dr. Martin Heimann

Hamburg, den 08.05.2003

Prof. Dr. H. Schleicher
(Dekan des Fachbereichs Geowissenschaften)

Abstract

The first part of this thesis describes the further development of a dynamic global vegetation model, LPJ, and its application to selected scientific questions. LPJ has been extended to include isotopic fractionation of ^{13}C at the leaf level during assimilation and includes a full isotopic terrestrial carbon cycle. Hence, it simulates the isotopic signature of the heterotrophic respiration fluxes. The model thus allows a quantitative analysis of the net biosphere exchange of CO_2 and $^{13}CO_2$ with the atmosphere as a function of changes in climate, land cover, atmospheric CO_2, and the isotope ratio of CO_2.

The extended version of LPJ has been used to study the response of the global vegetation distribution to an abrupt climate change event (Younger Dryas) and the thereby incurred changes in the terrestrial carbon pools and fluxes and their isotopic $^{13}C/^{12}C$ ratio. Climate data from a 850-year-long coupled ocean-atmosphere general circulation model (ECHAM3/LSG) is used for these simulations. The comparison of the modelled vegetation distribution and shifts during this idealized Younger Dryas event with reconstructed vegetation maps for North America and Europe based on pollen records shows a reasonable agreement. The impact of the terrestrial carbon release during the Younger Dryas on the atmospheric CO_2 and $\delta^{13}C$ is analyzed using a simplified ocean model and compared to ice core measurements. In the standard case the simulation exhibits a significant change in global total terrestrial carbon stocks of about 180 Pg C leading to an atmospheric CO_2 increase of ≈28 ppmv as a consequence of the climate change event. The robustness of the terrestrial signal during the Younger Dryas is studied by several sensitivity experiments concerning the initial values of the carbon pool sizes as well as the CO_2 fertilization effect and the temperature dependency of the carbon decomposition rates. The resulting increase of atmospheric CO_2 concentrations for the cold event varies between 16 to 33 ppmv among the different experiments. The simulated atmospheric $\delta^{13}C$ values which are about 0.4‰ lower during the cold phase reflect major findings from ice core measurements and are fairly robust against the sensitivity experiments.

The isotope version of LPJ has also been used to study the effects of climate variability, fire, and changes in land use on the exchange fluxes of CO_2 and $^{13}CO_2$ between the terrestrial biosphere and atmosphere for the last 100 years in greater detail. A transient, spatially explicit dataset of C_4 crops and tropical C_4 pastures has been compiled which, in combination with a land use scheme, allows the analysis of the impact of land use and C_4 cultivation on the terrestrial stable isotope composition. LPJ simulates a global mean isotopic fractionation of 17.7‰ at the leaf level with interannual variations of ca. 0.3‰ in the case without land use for the years 1950 to 1998. In this case, interannual variability in the net $^{13}CO_2$ flux between atmosphere and terrestrial biosphere is of the order of 15 Pg C ‰ yr^{-1}. It is reduced to 4 Pg C ‰ yr^{-1} if the leaf-level fractionation factor is held constant at the long term mean. Depending on the chosen

land use scheme modelled values of leaf discrimination vary between 17.9‰ and 17.0‰ with results from the experiment specifying C_4 crops and C_4 pastures being the lowest. Modelled values of isotopic disequilibrium similarly depend on the amount of prescribed C_4 vegetation (crops and pastures) and vary between 37.9 Pg C ‰ yr^{-1} and 23.9 Pg C ‰ yr^{-1} averaged over the years 1985 to 1995. In addition, the effect of fire on the isotopic disequilibrium has been estimated to lead to a reduction of ≈10 Pg C ‰ yr^{-1}.

The second part of the thesis describes the construction and application of a terrestrial Carbon Cycle Data Assimilation System (CCDAS). In the assimilation step parameters of a terrestrial biosphere model, BETHY, are constrained subject to observations. The technique is demonstrated by using atmospheric CO_2 concentration observations from 1979 to 1999 and satellite remote sensing data (identifying vegetation activity) for the years 1989 and 1990 to optimize the tunable parameters in the model (some spatially explicit, some global) and also give an estimate of their uncertainties. Quantities (global and spatially explicit carbon fluxes) derived from the prognostic step of CCDAS are then analyzed with respect to climate anomalies. Processes responsible for the mean terrestrial fluxes and their variability are identified. A highly significant correlation between El Niño/Southern Oscillation and terrestrial CO_2 fluxes, with CO_2 lagging by a few months was found. Net CO_2 outgasing during El Niño events is caused mainly by a reduction of photosynthesis in large parts of the tropics, notably the Amazon basin and Central Africa. The most important deviation of this pattern is found after the eruption of Mount Pinatubo in 1991.

Contents

Chapter 1

Introduction

1.1 Motivation

Carbon dioxide (CO_2) is a naturally abundant trace gas in the atmosphere. Through its radiative properties it is (besides atmospheric water vapour) the most important greenhouse gas. Because of the natural greenhouse effect the mean global surface temperature amounts to around +15 °C compared to -18 °C without any climate relevant trace gases in the atmosphere and therefore is a necessity for our life on earth. CO_2 contributes ≈7.2 °C to the total warming potential of 33 °C of the natural greenhouse effect [Seiler and Hahn, 1998]. The connection between the concentration of CO_2 in the atmosphere and earth's climate has been established as early as 1896 by Svante Arrhenius [Arrhenius, 1896]. More than 100 years later this link between atmospheric CO_2 concentration and the surface temperature of the earth is one of the major issues for our society. It is more than likely that the global warming during the last century is, among other things, the consequence of the increased atmospheric CO_2 content due to anthropogenic emissions of CO_2 [Mitchell and Karoly, 2001].

As part of the natural carbon cycle CO_2 undergoes various exchange processes within the main components of this cycle: gross primary productivity (uptake of CO_2 through photosynthesis) and respiration by the land biosphere and physical air-sea exchange. Measurements on air bubbles enclosed in antarctic ice cores showed that the atmospheric CO_2 concentration remained relatively constant at a level of about 280 ppmv [Indermühle et al., 1999] during the last 10.000 years suggesting that the carbon cycle has been in quasi-equilibrium during that time. During periods of transitions between glacial and warm phases the atmospheric CO_2 content varied substantially by 80 to 100 ppmv [Fischer et al., 1999; Petit et al., 1999], however, these variations occurred on time scales of centuries to millenia. High resolution records revealed, that at least during the last transition the increase of atmospheric CO_2 was strongly modulated accompanying abrupt climate changes [Monnin et al., 2001]: higher rates of atmospheric CO_2 increase during cold phases (e.g., Younger Dryas) and even a decrease during warm phases (e.g., Bølling-Allerød)(Figure 1.1). The origin and mechanismen for these modulations are still not

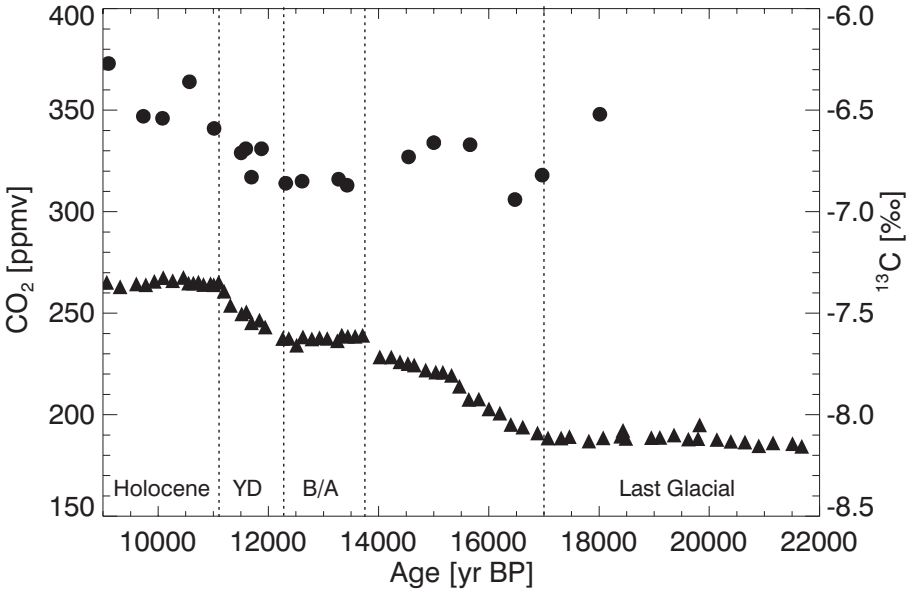

Figure 1.1: CO_2 ice core data from Dome C, Antarctica [Monnin et al., 2001] (triangles) and $\delta^{13}C$ ice core data from Taylor Dome, Antarctica [Smith et al., 1999] (circles).

fully understood.

Since industrialization (the last ≈150 years) atmospheric CO_2 concentration increased by more than 80 ppmv to a total value of around 370 ppmv today, a magnitude which has not been exceeded during the last 420.000 years at a rate which is unique for at least the last 20.000 years [Prentice et al., 2001]. This present increase is caused by anthropogenic emissions of CO_2 mainly due to the burning of fossil fuel and land use change. However, the atmospheric growth rate has been only about half of the fossil fuel emissions during the last century and exhibits a much higher year to year variability (between 1 Pg C yr^{-1} to 4 Pg C yr^{-1}, Figure 1.2) than the emissions. Thus, some of the emitted CO_2 is taken up by the oceans and land biota. The yearly fluctuations seem to be primarily caused by the terrestrial biosphere which itself response to anomalous climate events (e.g., El Niño) [Prentice et al., 2001]. A sketch of the present carbon cycle with the sizes of the main pools and most active exchange fluxes between these pools (land-atmosphere, ocean-atmosphere and anthropogenic emissions) is displayed in Figure 1.3. The numbers only give estimates as the uncertainties are large. Current estimates of the magnitude of the sink capacity for the period 1990 to 1999 are of the order of 1.7 ± 0.5 Pg C yr^{-1} and 1.4 ± 0.7 Pg C yr^{-1} for the oceans and terrestrial ecosystems, respectively [Prentice et al., 2001].

In principle, two methods can be applied to calculate the magnitudes of the carbon fluxes [Heimann, 1997]: First, the measurement of atmospheric trace gases which in combination with simple model estimates can be used to close the global carbon budget (top-down approach). Second, mechanistic modelling of the underlying processes governing the exchange fluxes either between ocean-atmosphere or terrestrial biosphere-atmosphere (bottom-up approach). Much

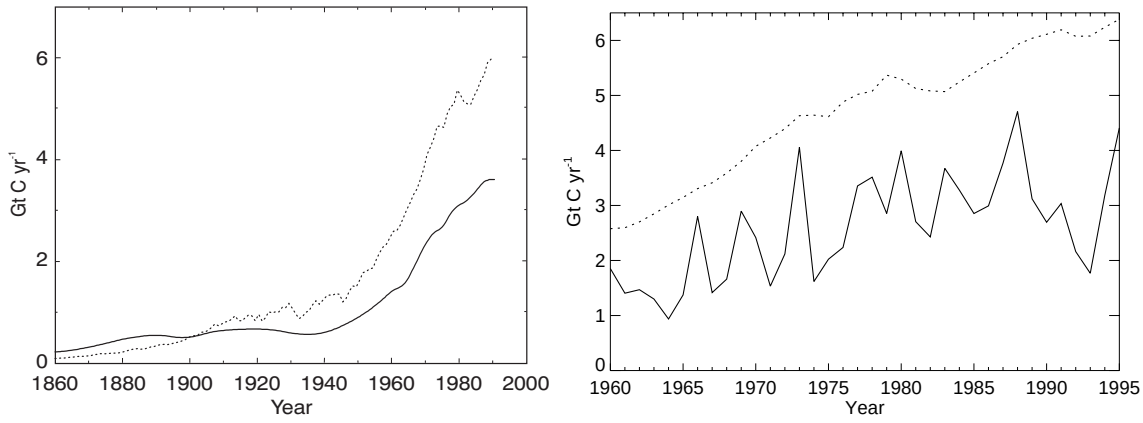

Figure 1.2: Comparison between the annual atmospheric growth rate in CO_2 (solid) and the anthropogenic emissions (dotted) for 1860 to 1990 (left panel, smoothed record adapted from Joos [1996]) and for 1960 to 1995 (right panel).

progress has been made in both attempts. Improvements in the quality and quantity of measurements allow the use of more atmospheric trace gases to constrain the global carbon budget from so-called inversion studies. In particular, measurements of $\delta^{13}C$, the ratio of the abundances of the two stable carbon isotopes, ^{13}C and ^{12}C, in atmospheric CO_2 in conjunction with atmospheric CO_2 measurements can be used to separate the uptake of CO_2 between ocean and land, first described by Keeling et al. [1989]. This partitioning, the so-called "double deconvolution" method, relies on the discrimination against ^{13}C during photosynthesis which leads to plant carbon being depleted in ^{13}C ($\approx$18‰) relative to the atmospheric CO_2 from which it is formed. Only little discrimination is associated with the exchange of carbon between ocean and atmosphere. Consequently, if carbon uptake is dominated by land biota, changes in atmospheric CO_2 concentrations will be accompanied by large changes in atmospheric $\delta^{13}C$, whereas carbon uptake by the oceans will have little effect on $\delta^{13}C$. Complications arise through the fact that burning of fossil fuel which is heavily depleted in ^{13}C constantly lowers atmospheric $\delta^{13}C$. Thus, carbon isotope ratios of respired CO_2 differs slightly from those of photosynthesis leading to an isotopic disequilibrium. Furthermore, the discrimination during photosynthesis itself is highly variable in space and time and depends on the photosynthetic pathway (C_4 photosynthesis discriminates much less than C_3 photosynthesis). These effects have to be estimated by means of models [e.g., Ciais et al., 1999].

On the other hand, the understanding and eventually also the inclusion of more processes into complex models leads to more accurate direct calculations of the exchange fluxes. Here, progress on the terrestrial components relies on including mechanistic descriptions of vegetation dynamical elements as the assumption of the terrestrial biosphere being in equilibrium with climate is certainly not valid under a rapidly changing climate. In order to capture the responses of land ecosystems to climate change, processes such as resource competition, growth, mortality, establishment, soil and litter decomposition have to be included into models of the

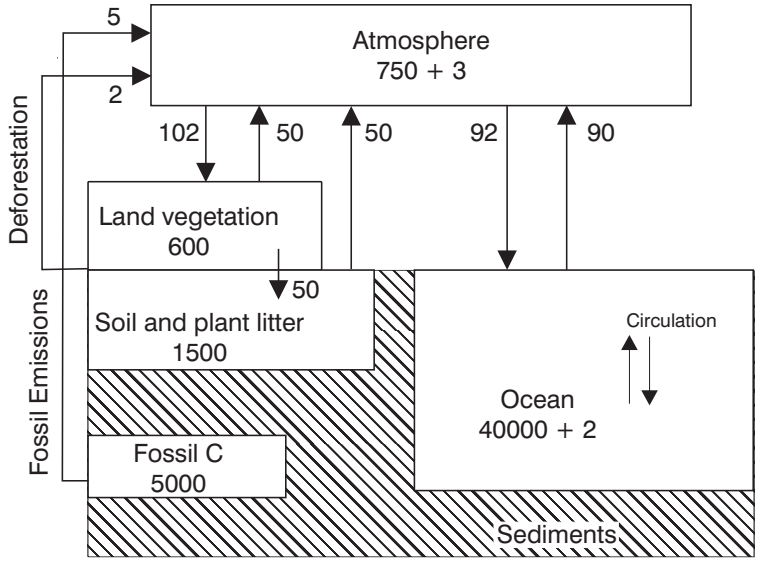

Figure 1.3: A simplified sketch of the present global carbon cycle, pool sizes are given in Pg C and fluxes in Pg C yr^{-1}.

terrestrial biosphere. Several of these so-called "dynamic global vegetation models" exist by now [e.g., Foley et al., 1996; Cox et al., 1998; Sitch et al., 2003]. Process-based modelling of the terrestrial biosphere including atmosphere-land carbon 13 exchange processes for past abrupt climate change events but also for the most recent past will be helpful to understand the past and present terrestrial carbon cycle.

A rather new method is the combination of the two above mentioned approaches (diagnosing the current state of the carbon cycle from atmospheric measurements and predicting the carbon cycle based on models of the physical processes) in which systematic data assimilation methods are used to solve for physical model parameters [Vukićević et al., 2001; Kaminski et al., 2002]. This mathematical method of introducing observations optimally into a modelling framework is already operationally applied in related fields such as, e.g., numerical weather prediction. The two main advantages of such a carbon cycle data assimilation scheme in carbon cycle research are:

- estimation of the magnitudes and uncertainties of surface CO_2 fluxes on high resolution space/time scales consistent with observations, and
- calibration of key model parameters (including also uncertainties) governing carbon fluxes directly to improve the predictive capability of the model.

Furthermore this data assimilation scheme allows the use of multiple observational data, e.g., ecological data, local flux measurements, and satellite radiances, in constraining the terrestrial biosphere model. So far, Kaminski et al. [2002] showed the feasibility of such a formalistic and traditional data assimilation scheme in carbon cycle research for the calibration of two parameters using a simple diagnostic model of the terrestrial biosphere. Extending this study to

a prognostic model of the biosphere would yield a tool for predicting the future evolution of the terrestrial carbon cycle from its current state including uncertainty estimations of the predicted quantities.

1.2 Scientific Objectives

The aim of this Ph.D. thesis is to obtain a better process-based knowledge of the terrestrial carbon cycle. This can be achieved by using the bottom-up modelling approach but also the data assimilation approach. Forward modelling is carried out here in a twofold way. First, to get a better understanding of the behaviour of the land biota during abrupt climate change events and its implications for the atmospheric CO_2 concentration. Second, to obtain a better quantification of the spatial and temporal variations of the stable carbon isotopic composition of the terrestrial biosphere. Using a modified version of the Lund-Potsdam-Jena (LPJ) dynamic global vegetation model [Sitch et al., 2003; Scholze et al., 2003] several model experiments have been performed to investigate the following specific questions:

1. Does LPJ capture the main shifts in vegetation distribution for an abrupt climate change event such as the Younger Dryas cold period (≈12000 years BP)? Does this cold event which is believed to have happened mainly in the northern hemisphere have an impact on vegetation cover in the tropics or the southern hemisphere according to the LPJ simulation?

2. How does the terrestrial carbon cycle change under an abrupt climate change event and what are the characteristic time scales? How does release of terrestrial carbon during a Younger Dryas like event agree with atmospheric CO_2 measurements from ice cores? How robust is the terrestrial signal towards changes in boundary conditions or model parameterizations? Can simulations of the terrestrial carbon 13 cycling during an abrupt climate change event help to clarify the origins of the modulations in atmospheric CO_2 during the last glacial transition (Figure 1.1).

3. Does the fractionation of carbon 13 during photosynthesis vary with climate fluctuations on a global scale and where are the regions exhibiting high variability in fractionation? To what extent is the variability of the fractionation factor caused by changes in the vegetation composition (shifts in C_3/C_4 plants)? What would be the impact of an inter-annually varying fractionation factor on carbon fluxes derived by double deconvolution?

4. Which are the main processes effecting the terrestrial isotopic disequilibrium during the last century and to what extent does the isotopic disequilibrium vary?

In addition to these forward modelling studies a carbon cycle data assimilation system based on a process-based, prognostic terrestrial biosphere model is developed in order to calibrate the model's parameters against observations, to estimate their uncertainties, and to explore which parameters, and thus, also processes are mainly constrained by the observations. Questions

such as how do fluxes which are optimally adjusted to match atmospheric CO_2 concentrations respond to climate variability can be investigated.

1.3 Contents of the Ph.D. Thesis

In order to address the questions and topics listed above, this thesis is organized as follows:

Chapter 2 deals with the first topic, the comparison of the modelled vegetation distribution and shifts during an idealized Younger Dryas event with reconstructed vegetation maps for North America and Europe based on pollen records. Furthermore, parts of the second question are also addressed in Chapter 2. The impact of the terrestrial carbon release during the Younger Dryas on the atmospheric CO_2 is analyzed using a simplified ocean model and compared to ice core measurements. A discussion of the relevant time scales of terrestrial carbon cycling demonstrates the need of dynamic global vegetation models to capture the impact of rapid climate changes on land ecosystems as well as on the global carbon cycle.

In Chapter 3 the question of the robustness of the terrestrial signal during the Younger Dryas is answered by presenting the results of several sensitivity studies concerning the initial values of the carbon pool sizes as well as the CO_2 fertilization effect and the temperature dependency of the carbon decomposition rates. All experiments also calculated the atmosphere-biosphere $^{13}CO_2$ fluxes which were then used to diagnose the atmospheric $\delta^{13}C$ ratio. A comparison with $\delta^{13}C$ ice core data underpins the usefulness the additional tracer for identifying the processes responsible for the modulations of the atmospheric CO_2 concentration during the last transition.

The estimates of the sink capacities of oceans and land biota for the recent past rely also on the results from double deconvolution studies. Up to now these studies assumed a constant isotopic fractionation factor. Chapter 4 answers the third question regarding the influence of climate variability on terrestrial ^{13}C discrimination during photosynthesis. In addition, the impact of changes in the vegetation cover on the inter-annual variability of the fractionation factor as opposed to climate only induced variations is evaluated. A simple estimation of the impact of a varying fractionation underlines the importance of considering a climate dependant fractionation factor in double deconvolution studies.

Chapter 5 resumes the questions of the climate dependant discrimination during photosynthesis and analyzes the spatial pattern of the variance in the fractionation factor and identifies regions with high variability due to climate in contrast to regions mainly affected by fluctuations between C_3 and C_4 photosynthesis. The influence of climate, fire and land use, especially C_4 agriculture (corn, sugar cane, sorghum and millet) and tropical C_4 grazing areas on the isotopic disequilibrium are discussed as the results of double deconvolution studies are particularly sensitive to the isotopic disequilibrium [Heimann and Meier-Reimer, 1996].

Chapter 6 describes the construction and application of a terrestrial carbon cycle data assimilation system (CCDAS). In the assimilation step parameters of a terrestrial biosphere model, BETHY, are constrained subject to observations. The technique is demonstrated by using atmospheric CO_2 concentration observations and satellite remote sensing data to obtain not only

optimized parameter values but also an estimate of their uncertainties. Quantities (global and spatially explicit carbon fluxes) derived from the prognostic step are than analyzed with respect to climate anomalies. Furthermore, Appendix A gives a more technical and computational description of the assimilation system focusing on the use of automatic differentiation.

1.4 Publications

Chapter 2 to Chapter 5 and Appendix A are based on manuscripts which are either published, in press, or in preparation for publication, Chapter 6 is based on a presentation given at the American Geophysical Union Fall Meeting, San Francisco, 2002 and partly on a draft of a manuscript for publication:

Chapter 2: Scholze, M., W. Knorr and M. Heimann, 2003. Modelling terrestrial vegetation dynamics and carbon cycling for an abrupt climate change event. The Holocene, 13(3), 327–333.

Chapter 3: Scholze, M., F. Joos, W. Knorr and M. Heimann, 2003. Response of the terrestrial carbon and carbon 13 cycle to an abrupt climate change event. In preparation for Atmospheric Chemistry and Physics.

Chapter 4: Scholze, M., J.O. Kaplan, W. Knorr and M. Heimann, 2003. Climate and interannual variability of the atmosphere-biosphere $^{13}CO_2$ flux. Geophysical Research Letters, 30(2), 1097, doi:1092/2002GL015631.

Chapter 5: Scholze, M., P. Ciais and M. Heimann, 2003. Modelling terrestrial carbon 13 cycling: climate, land-use and fire. In preparation for Global Biogeochemical Cycles.

Chapter 6: Scholze, M., P. Rayner, W. Knorr, T. Kaminski, R. Giering, 2002. A prototype Carbon Cycle Data Assimilation System (CCDAS): Inferring interannual variations of vegetation-atmosphere CO_2 fluxes. Abstract CG62A-05, Eos Trans. AGU Fall Meeting Supplement 83(47).

Rayner, P., M. Scholze, W. Knorr, T. Kaminski and R. Giering, 2003. The history of terrestrial carbon fluxes from 1980–2000: Results from a Data Assimilation System. In preparation for Global Biogeochemical Cycles.

Appendix A: Kaminski, T., R. Giering, M. Scholze, P. Rayner and W. Knorr, 2003. An example of an automatic differentiation-based modelling system. To appear in Computational Science – ICCSA 2003, Proceedings of the International Conference on Computational Science, Montreal, Canada, May 18-21, 2003, edited by Gavrilova, L., V. Kumar, P. L'Ecuyer and C. J. K. Tan. Lecture Notes in Computer Science, Springer, Berlin.

References

Arrhenius, S., 1896. On the influence of carbonic acid in the air upon the temperature on the ground. Philosophical Magazine 41, 237–276.

Ciais, P., Friedlingstein, P., Schimel, D. S., Tans, P. P., 1999. A global calculation of the δ^{13}C of soil respired carbon: Implications for the biospheric uptake of anthropogenic CO_2. Glob. Biogeochem. Cycles 13 (2), 519–530.

Cox, P. M., Huntingford, C., Harding, R. J., 1998. A canopy conductance and photosynthesis model for use in a GCM land surface scheme. Journal of Hydrology 212–213, 79–94.

Fischer, H., Wahlen, M., Smith, J., Mastroianni, D., Deck, B., 1999. Ice core records of atmospheric CO_2 around the last three glacial terminations. Science 283 (5408), 1712–1714.

Foley, J. A., Prentice, I. C., Ramankutty, N., Levis, S., Pollard, D., Sitch, S., Haxeltine, A., 1996. An integrated biosphere model of land surface processes, terrestrial carbon balance, and vegetation dynamics. Glob. Biogeochem. Cycles 10 (4), 603–628.

Heimann, M., 1997. A review of the contemporary global carbon cycle and as seen a century ago by Arrhenius and Högbom. Ambio 26 (1), 17–24.

Heimann, M., Meier-Reimer, E., 1996. On the relations between the oceanic uptake of CO_2 and its carbon isotopes. Glob. Biogeochem. Cycles 10 (1), 89–110.

Indermühle, A., Stocker, T. F., Joos, F., Fischer, H., Smith, H. J., Wahlen, M., Deck, B., Mastroianni, D., Tschumi, J., Blunier, T., Meyer, R., Stauffer, B., 1999. Holocene carbon-cycle dynamics based on CO_2 trapped in ice at Taylor Dome, Antarctica. Nature 398 (6723), 121–126.

Joos, F., 1996. The atmospheric carbon dioxide perturbation. Europhysics News 27, 213–218.

Kaminski, T., Knorr, W., Rayner, P. J., Heimann, M., 2002. Assimilating atmospheric data into a terrestrial biosphere model: A case study of the seasonal cycle. Glob. Biogeochem. Cycles 16 (4), doi:10.1029/2001GB001463.

Keeling, C. D., Bacastow, R. B., Carter, A. F., Piper, S. C., Whorf, T. P., Heimann, M., Mook, W. G., Roeloffzen, H., 1989. A three-dimensional model of the atmospheric CO_2 transport based on observed winds: 1. Analysis of observational data. In: Peterson, D. H. (Ed.), Aspects of Climate Variability in the Pacific and the Western Americas. Vol. 55. AGU, Washington, D.C., pp. 165–236.

Mitchell, J. F. B., Karoly, D. J., 2001. Detection of climate change and attribution of causes. In: Houghton, J. T., Ding, Y., Griggs, D. J., Noguer, M., van der Linden, P. J., Dai, X., Maskell, K., Johnson, C. A. (Eds.), Climate Change 2001: The Scientific basis. Cambridge University Press, Cambridge, U.K., pp. 695–738.

Monnin, E., Indermühle, A., Dällenbach, A., Fluckiger, J., Stauffer, B., Stocker, T., Raynaud, D., Barnola, J., 2001. Atmospheric CO_2 concentrations over the last glacial termination. Science 291 (5501), 112–114.

Petit, J. R., Jouzel, J., Raynaud, D., Barkov, N. I., Barnola, J. M., Basile, I., Bender, M., Chappellaz, J., Davis, M., Delaygue, G., Delmotte, M., Kotlyakov, V. M., Legrand, M., Lipenkov, V. Y., Lorius, C., Pepin, L., Ritz, C., Saltzman, E., Stievenard, M., 1999. Climate and atmospheric history of the past 420,000 years from the Vostok ice core, Antarctica. Nature 399 (6735), 429–436.

Prentice, I. C., Farquhar, G. D., Fasham, M. J. R., Goulden, M. L., Heimann, M., Jaramillo, V. J., Kheshgi, H. S., Le Quéré, C., Scholes, R. J., Wallace, D. W. R., 2001. The carbon cycle and atmospheric carbon dioxide. In: Houghton, J. T., Ding, Y., Griggs, D. J., Noguer, M., van der Linden, P. J., Dai, X., Maskell, K., Johnson, C. A. (Eds.), Climate Change 2001: The Scientific basis. Cambridge University Press, Cambridge, U.K., pp. 183–237.

Scholze, M., Kaplan, J. O., Knorr, W., Heimann, M., 2003. Climate and interannual variability of the atmosphere-biosphere $^{13}CO_2$ flux. Geophys. Res. Lett 30 (2), 1097, doi:10.1029/2002GL015631.

Seiler, W., Hahn, J., 1998. Der natürliche und anthropogene Treibhauseffekt- Veränderung der chemischen Zusammensetzung der Atmospäre durch menschliche Aktivitäten. In: Lozán, J. L., Graßl, H., Hupfer, P. (Eds.), Warnsignal Klima. Wissenschaftliche Auswertungen, Hamburg.

Sitch, S., Prentice, I. C., Smith, B., Arneth, A., Bondeau, A., Cramer, W., Kaplan, J. O., Levis, S., Lucht, W., Sykes, M. T., Thonicke, K., Venevsky, S., 2003. Evaluation of ecosystem dynamics, plant geography and terrestrial carbon cycling in the LPJ dynamic global vegetation model. Global Change Biology 9, 161–185.

Smith, H. J., Fischer, H., Wahlen, M., Mastroianni, D., Deck, B., 1999. Dual modes of the carbon cycle since the last glacial maximum. Nature 400 (6741), 248–250.

Vukićević, T., Braswell, B. H., Schimel, D., 2001. A diagnostic study of temperature controls on global terrestrial carbon exchange. Tellus 53B (2), 150–170.

Chapter 2

Modelling terrestrial vegetation dynamics and carbon cycling for an abrupt climate change event

---

Abstract. Abrupt climate changes have occurred several times in the past, leading to large-scale modifications of vegetation patterns with important consequences for the global carbon cycle. Dynamic global vegetation models (DGVM) constitute an advanced tool for reconstructing past or predicting future shifts in vegetation distributions in response to climate change on a global scale. The Lund-Potsdam-Jena (LPJ) model is a DGVM that also includes a complete description of terrestrial-vegetation carbon cycling. Here, it is used for a long time integration simulating terrestrial ecosystem responses to an abrupt climate change event. Climatic data from an 850-year-long coupled ocean-atmosphere model (ECHAM3/LSG) experiment representing a highly idealized Younger Dryas (ca. 12 ka BP) like event are used to study the reactions of the vegetation distribution and changes in terrestrial carbon storage. The main feature of the Younger Dryas simulation experiment is the suppression of the Atlantic thermohaline circulation leading to a significant cooling of the northern hemisphere accompanied by a large-scale precipitation decrease. The simulation exhibits a significant shift of the vegetation distribution in the northern hemisphere during the cold period in conjunction with a change in global total terrestrial carbon stocks of 180 x 10^{12} kg C as a consequence of the climate change event. The response time of the terrestrial biosphere lags the climate changes by about 250 years for vegetation and 400 years for soil carbon pools.

2.1 Introduction

The large-scale transitions between glacials and interglacials are often interrupted by abrupt climatic events with large temperature changes happening within only a few decades to centuries, the so-called Dansgaard-Oeschger and Heinrich events [Dansgaard, 1985; Heinrich, 1988]. The

most prominent example of an abrupt climate change event is the Younger Dryas (YD) cold event with a sudden return, within approximately 100 to 200 years [Johnsen et al., 1992; Alley et al., 1993], to almost glacial conditions at the end of the last transition to the Holocene warm period. This event has been dated between 12.7 ka BP and 11.5 ka BP in the GRIP ice core from Central Greenland [Johnsen et al., 1992]. According to a widely believed hypothesis derived from Greenland ice core data analysis, the YD was caused by a reduction in the North Atlantic Deep Water formation induced by a freshwater flux anomaly into the northern North Atlantic from glacial meltwater. The result is a weakened thermohaline circulation associated with a much-reduced northward heat transport [Broecker et al., 1985]. This hypothesis is supported by marine evidence [Lehman and Keigwin, 1992] and several model studies [Wright and Stocker, 1993; Manabe and Stouffer, 1995; Schiller et al., 1997].

Early European pollen studies revealed dramatic changes in vegetation covering Northwest Europe during the YD [Watts, 1980]. More evidence of the response of vegetation composition to an abrupt climatic shift can be found in northern Eurasia [Velichko et al., 1997] and even more pronounced in eastern North America, while it is still questionable if the YD had an influence on the vegetation outside these regions [Peteet, 1995]. Nevertheless, pollen records indicating global impacts during the YD have been found in Colombia, South America [Kuhry et al., 1993].

The synchronization of ice cores from the northern (Greenland) and southern (Antarctica) hemispheres with a relative accuracy of approximately 50 years revealed that during the end of the glacial-Holocene transition the temperatures, derived from the $\delta^{18}O$ proxy in ice, in Greenland and Antarctica were in antiphase [Blunier et al., 1997]: cold temperatures in Antarctica (Antarctic Cold Reversal) simultaneously with the warm Bølling-Allerød period in Greenland followed by already Holocene temperatures in Antarctica at the end of the YD. Atmospheric CO_2 concentrations can most reliably be reconstructed from Antarctic ice cores, because the concentration of impurities known to produce in situ CO_2 is one order of magnitude lower than in Greenland ice cores [Anklin et al., 1997]. The high resolution CO_2 record from Dome C, Antarctica, shows that within the increase from 190 to 265 ppmv during the transition from the last glacial to the Holocene four intervals can be clearly distinguished [Monnin et al., 2001]. In one of those intervals, which corresponds to the YD time period in the GRIP ice core, the CO_2 concentration rises from 237 to 265 ppmv at a rate of about 20 ppmv/ka, with an accelerated increase at the end of the time interval.

The origin of this increase in the atmospheric CO_2 concentration during the Younger Dryas cold climate event is still controversial. Marchal et al. [1999] have shown with model experiments considering only changes in the ocean-atmosphere CO_2 fluxes while keeping terrestrial CO_2 fluxes constant that an atmospheric increase in CO_2 is consistent with a collapse of the Atlantic thermohaline circulation. However, this study strongly relies on the area of cooling being spatially limited, such that the effect of increased solubility of CO_2 in the North Atlantic is over-compensated by other effects, such as outgassing of CO_2 in the Southern Ocean due to warmer sea surface temperatures. A different explanation of the enhanced increase in atmospheric CO_2 during the YD is suggested by changes in the terrestrial carbon cycle. Here, we

Table 2.1: PFTs defined in LPJ with their names and abbreviations as used in Figure 2.2.

PFT No.	PFT Name	Abbrevation
1	Tropical broad-leaved evergreen tree	TrBE
2	Tropical broad-leaved raingreen tree	TrBR
3	Temperate needle-leaved evergreen tree	TeNE
4	Temperate broad-leaved evergreen tree	TeBE
5	Temperate broad-leaved summergreen tree	TeBS
6	Boreal needle-leaved evergreen tree	BNE
7	Boreal summergreen tree	BS
8	C_3 grass	C3G
9	C_4 grass	C4G

assess the plausibility of this hypothesis by modelling both the vegetation dynamics and the terrestrial carbon cycle for a Younger Dryas like abrupt climate change event, thereby keeping ocean-atmosphere fluxes constant.

2.2 Methodology

2.2.1 The Lund-Potsdam-Jena dynamic global vegetation model

The LPJ-DGVM [Sitch et al., 2003] combines process-based descriptions of terrestrial ecosystem structure (vegetation composition, biomass, and height) and function (energy absorption, carbon cycling). Vegetation composition is described by nine different plant functional types (PFT, see Table 2.1 for a complete list), which are distinguished according to their physiological (C_3, C_4 photosynthesis), morphological (tree, grass), and phenological (deciduous, evergreen) attributes. The model is run on a grid cell basis with specified atmospheric CO_2 concentration, soil texture, monthly fields of temperature, precipitation, and radiation. Each grid cell is divided into fractions covered by PFTs and bare ground. Both the presence and the covered fraction of PFTs within a grid cell depend on their specific environmental limits and on resource competition among the PFTs.

Photosynthesis is calculated daily for each PFT based on its current fractional coverage, phenology, and water availability in the rooting zone whose vertical extension is PFT specific. Soil water is represented by a two-layer model following Haxeltine and Prentice [1996]. The water balance calculation also is made with a daily time step. Percolation from the upper to the lower layer, and absolute water holding capacity are soil texture dependant.

Vegetation dynamics is updated annually and is based on the productivity of the different PFTs as well as on disturbance, mortality, and establishment. Plant establishment depends on the fraction of bare ground available for seedlings to successfully establish, whereas natural mortality is a function of PFT vigour and reduces the total number of PFT individuals within

a grid cell. Natural disturbance is modelled as fire, which leads to an additional PFT mortality.

Furthermore, the slower ecosystem-level processes also include tissue, litter, and soil carbon turnover, with soil and litter biogeochemistry updated monthly. Each PFT has an associated below-ground and above-ground litter pool, a fraction of which is respired as CO_2 directly into the atmosphere, and the remainder is divided between the fast and slow soil carbon pools. The litter and the fast and slow soil pools are assigned turnover times at 10 °C of 2, 33 and 1000 years, respectively, with decomposition rates modified by soil temperature and soil moisture [Lloyd and Taylor, 1994], decreasing both at low and very high levels.

2.2.2 Melt-water experiment

The climatic experiments were performed by Mikolajewicz et al. [1997] using the ECHAM3/LSG coupled ocean-atmosphere general circulation model (OAGCM). The atmospheric component consists of the spectral atmosphere model ECHAM3 [Roeckner et al., 1992] with a T21 horizontal resolution (approximately 5.6° x 5.6°) and 19 vertical levels, while the oceanic component is the large-scale-geostrophic (LSG) circulation model [Maier-Reimer et al., 1993] with a 5.6° horizontal resolution and 11 vertical layers. Both components of the OAGCM are periodically synchronously coupled with a simultaneous atmosphere-ocean integration period of 15 months alternating with ocean-only periods of 48 months [Voss and Sausen, 1996]. This coupling technique saves considerable amount of computing time, thus allowing long-time integrations with complex 3D circulation models, while retaining the decadal atmospheric responses.

In the so-called meltwater-experiment, a triangular-shaped freshwater flux (i.e. linear increase (decrease) to (from) the peak value with time) into the Labrador Sea was prescribed, while all other boundary conditions were kept at modern values. The meltwater input lasted for 500 years with a maximum peak value of 0.625 Sv (1 Sv = 10^6 m^3s^{-1}) in the year 250. The total length of the perturbation and of an unperturbated control experiment is 850 years. This meltwater-experiment mimics a highly idealized analogue of the Younger Dryas event; magnitude and length of the prescribed meltwater input are consistent with estimates by Fairbanks [1989].

Figure 2.1 shows the anomalies of the meltwater experiment averaged over the model years 200 to 500 of two of the main input fields for the LPJ model, surface temperature and precipitation. As a result of the freshwater input, the thermohaline circulation of the Atlantic is drastically weakened and thereby the poleward heat transport in the Atlantic is also strongly reduced. This leads to a strong surface cooling over almost the entire northern hemisphere, except for a hot-spot over the Indian subcontinent which is caused by a reduction of the monsoon strength as there is also a significant decrease in precipitation (Figure 2.1b). Temperature changes in the southern hemisphere are much less pronounced and vary regionally between a heating over the South Atlantic and Africa and a cooling over Antarctica. Precipitation is generally less (about 10 to 20 mm/month) for the northern hemisphere in the meltwater experiment than in the control run. Another interesting feature is the reduction of precipitation over the monsoon regions in West Africa, mainly the Sahel zone, and India but also a rather strong

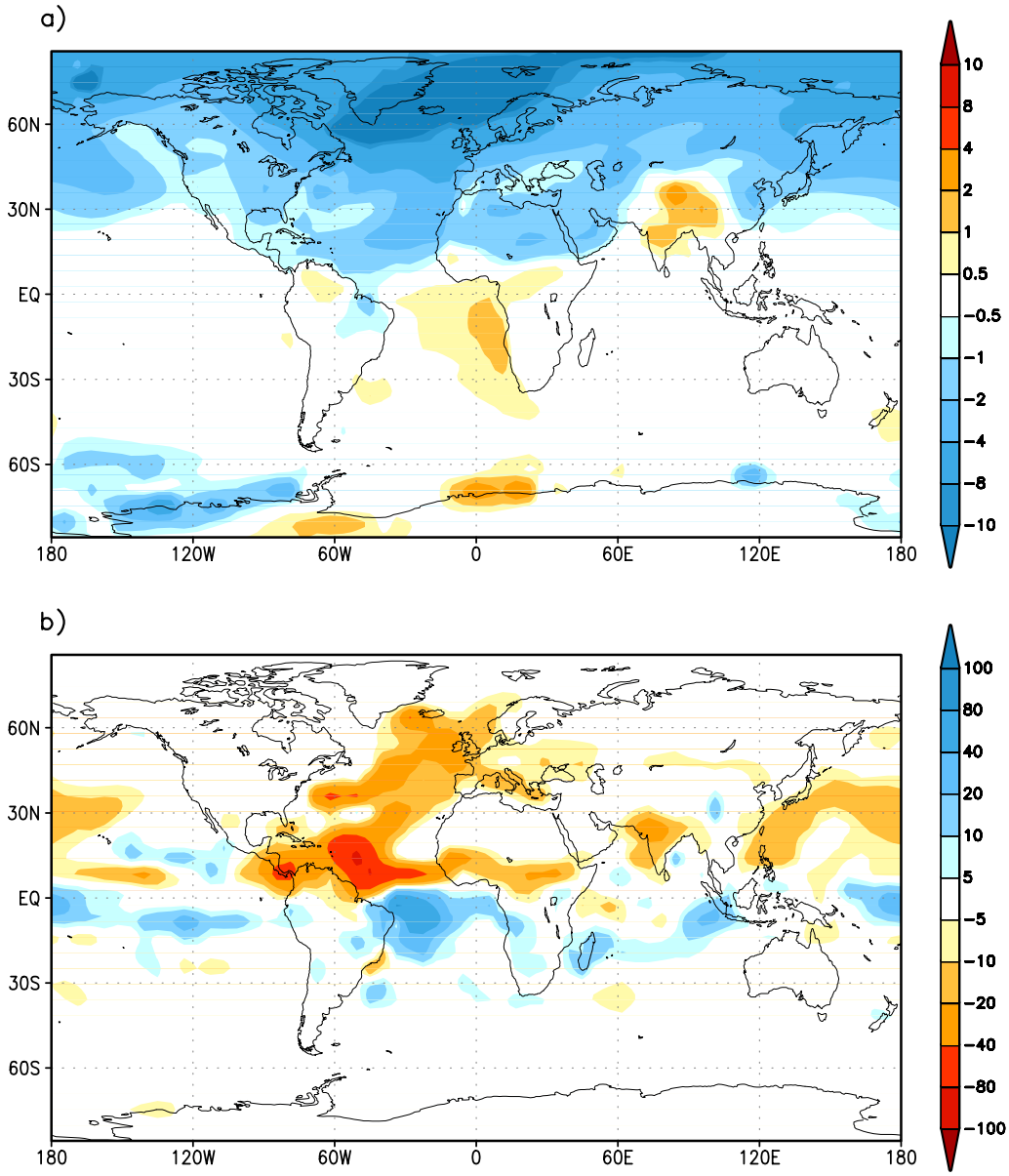

Figure 2.1: Differences between the meltwater and the control experiments averaged over the simulation years 250 to 500: a Annual mean surface temperature [°C], b annual precipitation [mm/month].

reduction of up to 40 mm/month in Central America and northern South America. A more detailed discussion of the meltwater experiment can be found in Schiller et al. [1997].

2.2.3 Modelling protocol

Two experiments were performed with LPJ, first a meltwater and second a control experiment using directly the output from the ECHAM3/LSG meltwater and control integrations. For both experiments the climate input data were interpolated to a 2.5° x 3.75° horizontal resolution according to the soil and topographical boundary conditions of LPJ. The missing climate data for the ocean-only simulation periods were filled up with atmospheric simulation data repetitively from the previous synchronous coupled simulation period, a procedure which may slightly reduce the modelled interdecadal variability and also slightly reduces the total simulation length. As this study focuses on the long-term behaviour of the terrestrial biosphere, this effect is expected to be of minor importance. The vegetation model was spun-up for 1000 years using 30 years control run climate repetitively. Throughout the whole simulation period of 800 years a constant atmospheric CO_2 forcing of 240 ppmv was applied. For the meltwater experiment, an inland ice sheet following the reconstruction by Peltier [1994] was prescribed.

2.3 Results and discussion

2.3.1 Changes in vegetation distribution

The Younger Dryas cold-event was first identified by shifts in the northern European vegetation distribution documented in Scandinavian pollen records [Rodbell, 2000]. These large-scale changes in vegetation coverage at the end of the transition from the last glacial to the present interglacial are caused by the return to almost glacial climatic conditions during the YD event. Because pollen records are often site specific and influenced by local environmental conditions such as topography, we do not directly compare time-series of pollen assemblages with time-series of modelled PFT composition on a 3.75° x 2.5° grid-cell basis.

A few vegetation maps reconstructed from pollen records for the YD time period exist, covering only regional parts of the globe such as Northwest Europe [Peng et al., 1995] or eastern North America [Overpeck et al., 1992]. These reconstructions of past vegetation cover can be accomplished by using various methods (Peng et al. [1998] give a brief overview). For example, the reconstructions made by Overpeck et al. [1992] rely on the modern analogue technique in which the fossil pollen assemblage is compared to modern pollen assemblages. If a good match is found between a fossil and a modern pollen assemblage the area with this specific fossil pollen assemblage is assigned the vegetation producing the modern assemblage. Peng et al. [1995] use the biomization method for their reconstructions. Each pollen taxon is assigned to one or under certain circumstances to several PFTs which are then translated in terms of biomes. In order to reconstruct biomes, the one that most resembles the PFT composition derived from fossil pollen

is chosen to represent the area in question. As LPJ explicitly models PFT distribution, the modelled fractional coverage of the various PFTs averaged over a larger area - to minimize site-specific effects - can be compared among the two different experiments (control and meltwater) and the results can also be compared to those paleo-vegetation maps qualitatively.

Figure 2.2a shows the mean modelled fractional coverage of the present PFTs for northwest Europe (5° E - 20° W, 45° N - 60° N) and Figure 2.2b for southern Europe (10° E - 25° W, 35° N - 45° N) averaged over the simulation years 300 to 500 for both the control (dark grey bars) and the meltwater (light grey bars) experiment. The modelled fractional coverage of the present PFTs for the meltwater experiment are quite different from the ones of the control experiment. The reduction of the temperate tree PFTs (TeNE and TeBS, see Table 2.1 for PFT key) by 30% in fractional coverage is accompanied with an increase in the boreal tree PFTs (BNE and BS) by about 20% and C_3 grass (C3G) by almost 10% in northwest Europe (Figure 2.2a). A more dramatic shift in the vegetation cover in northwest Europe between the YD time period (12 ka) and modern times is described by Peng et al. [1995]. They show that the cold deciduous forest and tundra biomes at 12 ka BP are replaced by a mixed and temperate forest today. As our modelled PFT composition during the meltwater event includes a considerable fraction of temperate PFTs (about 30%, TeNE and TeBS), which according to the reconstructed 12ka BP biomes by Peng et al. [1995] should not have existed at this time period, our simulated vegetation coverage corresponds to a milder climate. This presumably is due to the not fully realistic boundary conditions for the modelled vegetation evolution. The model simulation has a vegetation cover in equilibrium with modern day climate as initial conditions whereas in he real world the vegetation cover was not in equilibrium with the warmer Bølling-Allerød climate but rather still influenced by the previous glacial conditions.

In southern Europe (Figure 2.2b), the temperate broadleaved evergreen tree PFT (TeBE) shows a reduction of 10% in fractional coverage in parallel with an increase of 10% in C_3 grass (C3G) for the meltwater experiment compared to the control run. This PFT (TeBE) is the dominant one for the evergreen/warm mixed forest and xerophytic woods biome. The temperate needle-leaved evergreen and temperate broad-leaved summergreen PFTs (TeNE and TeBS), part of the cool and temperate forest biomes approximately show almost the same amount of coverage for both experiments. Both findings are in qualitative agreement with the reconstructed biome maps of Peng et al. [1995] which show that the temperate deciduous forests and warm grass/shrub steppes at 12 ka PB were replaced by the typical modern Mediterranean biomes, e.g. xerophytic woods/shrub and evergreen/warm mixed forests.

Similar results can be obtained for the east coast of North America, which, according to Overpeck et al. [1992], was covered to a great extent by boreal forest at 12 ka BP, in contrast to a more temperate deciduous and mixed forest today. LPJ shows a large shift from temperate PFTs to boreal PFTs for this region during the cold period. The fractional coverage of temperate PFTs is reduced by 30% from 40% to only 10%, while at the same time boreal PFT coverage increased a similar amount, i.e. from 53% to more than 80%. At 12 ka BP the largest area (south of the Great Lakes and west of the Appalachian mountains) in this reconstructed vegetation map

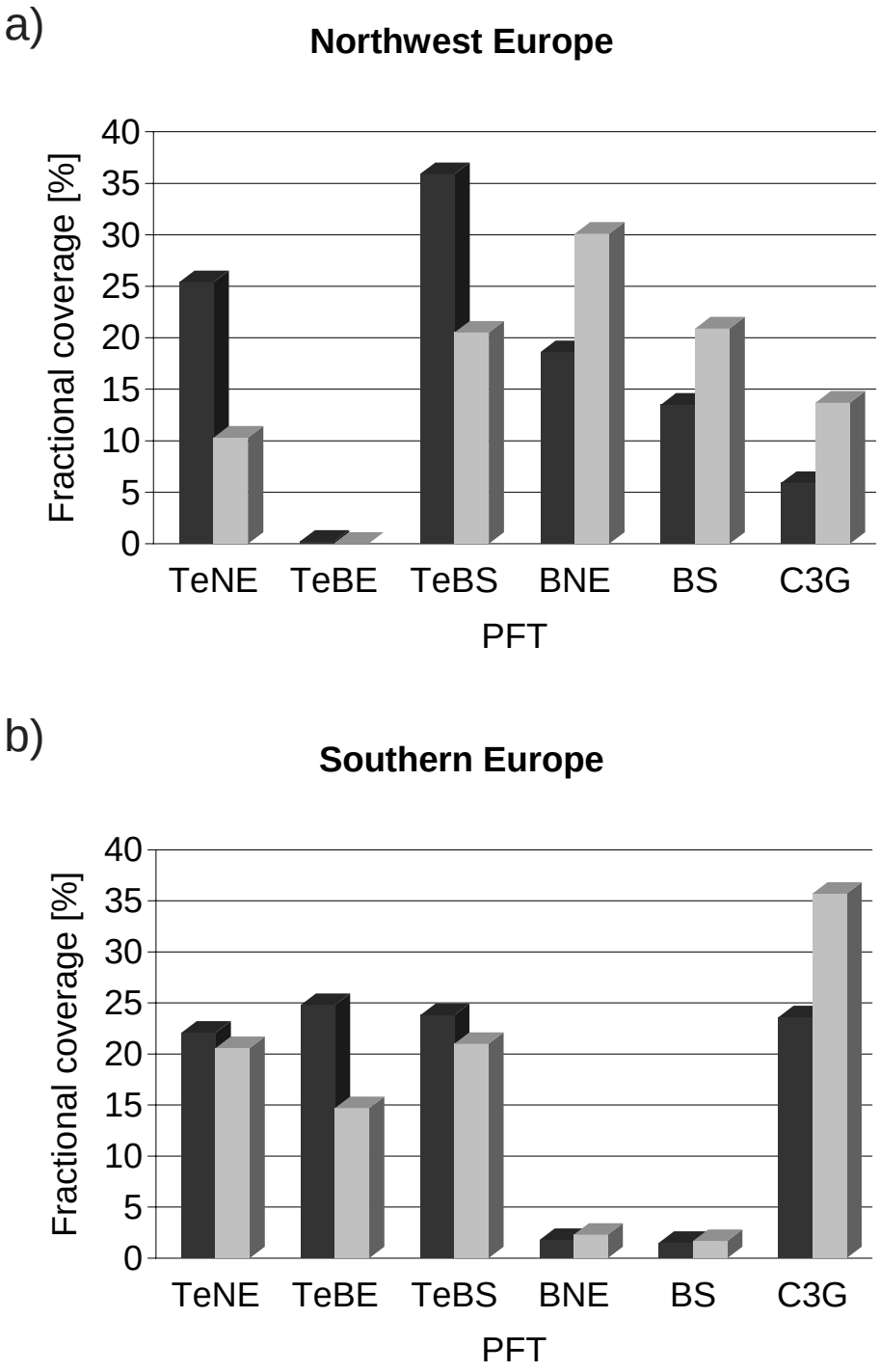

Figure 2.2: Comparison of the mean fractional coverage of the present PFTs averaged over the simulation years 300 to 500 between the control (dark grey) and the meltwater (light grey) experiment for two different regions: a northwest Europe (5° E - 20° W, 45° N - 60° N), b southern Europe (10° E - 25° W, 35° N - 45° N). The PFT key is the same for both figures (see Table 2.1).

is assigned no modern analog vegetation. However, Overpeck et al. [1992] report that this region was essentially dominated by spruce, a boreal tree, which was later (around 9 ka BP) replaced by deciduous and mixed forest represented by temperate PFTs. Here, LPJ simulates a reduction in the boreal PFTs with a concurrent increase in the temperate PFTs of 15% fractional coverage between the meltwater and the control experiment.

2.3.2 Impacts on the carbon cycle

Both, climatic changes but also changes in vegetation composition have an impact on the CO_2 exchange between terrestrial biosphere and atmosphere. As described above the vegetation in the North Atlantic region shifts from mainly temperate to boreal or even herbaceous PFTs, which are naturally lower in productivity compared to the temperate PFTs. However, the major factor reducing the plants' productivity is the colder and drier climate throughout almost the entire northern hemisphere. Figure 2.3 shows the spatial anomalies in the net primary production (NPP) of the meltwater experiment averaged over the model years 200 to 500 with respect to the control experiment. As can be seen in this figure, almost the entire northern hemisphere except central North America and western China had a lower productivity than in the control run. The prominent increase in productivity in western China is due to a simulated warming of up to 4 °C in conjunction with a slight increase in precipitation in this region (see Figure 2.1). The greatest changes in NPP happen around the northern North Atlantic region and the northern edge of the boreal forest zone, which are also the regions with the greatest climatic changes (see Figure 2.1). The reduction in the monsoon strength (less precipitation, higher temperatures) in the AOGCM meltwater experiment is strongly reflected in the terrestrial biospheric productivity in these regions: NPP in subtropical Africa and India is reduced by more than 0.5 kg C m^{-2}, which is almost 50% of the absolute value from the control experiment. The higher precipitation in southern Africa and central South America leads to higher NPP values for the meltwater experiment.

These spatially resolved changes, mainly reductions, in the net productivity of the terrestrial biosphere are also reflected in the total global terrestrial carbon budget. In Figure 2.4, time-series of total terrestrial carbon, vegetation carbon, and soil carbon are shown for both the control- and the meltwater-experiments. A distinct decrease in the amount of total terrestrial carbon of about 180 x 10^{12} kg C from 2,340 x 10^{12} kg C down to 2,160 x 10^{12} kg C occurs in the meltwater experiment, while in the control experiment the total terrestrial carbon stocks stays relatively constant around 2,350 x 10^{12} kg C for the whole simulation period. The reduction of terrestrial carbon stocks in the meltwater experiment starts 100 model years after the beginning of the simulation, which is also 100 years after the onset of freshwater input in the climate simulations. This is in agreement with the climate simulations, as the climate also does not show a strong response to the freshwater input in the first 100 years. Terrestrial carbon reaches its minimum during the simulation years 450 to 500, corresponding to the last 50 years of the freshwater input period in the climate simulations. At the end of the simulation in the model year 800, 300 years

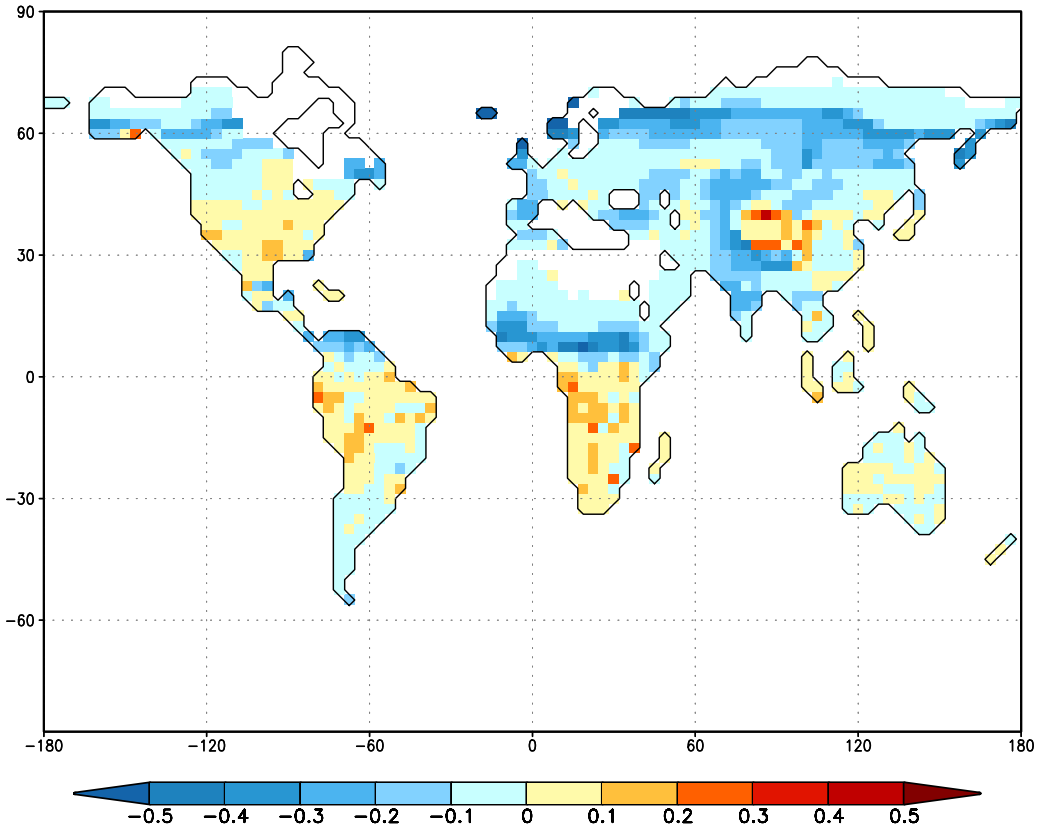

Figure 2.3: Difference in net primary productivity (NPP) [kg C m^{-2} $year^{-1}$] of the terrestrial biosphere between the meltwater and the control experiments averaged over the simulation years 250 to 500. This map only shows the modelled land area (Greenland and Antartica are excluded), no colour represents non-vegetated land points (land ice or desert).

after the end of the additional freshwater flux in the climate experiments, the terrestrial carbon stocks have accumulated only 65% of the lost carbon and have not fully recovered to the original value before the decrease. Therefore, the terrestrial biosphere lags climate by about 200 years or even more for the recovery of the carbon stocks as the climatic changes are most pronounced during the peak value of freshwater input (model year 250) and almost immediately return to control run values after the end of the freshwater input period in the year 500. Obviously, the terrestrial biosphere reacts on two different time scales upon abrupt climate change events: a fast response time of 200 years for the reduction of terrestrial carbon, i.e. a change to colder and drier climate, and a slow response time of 500 years for the build-up of terrestrial carbon due to a change to warmer and wetter climate conditions. Both the vegetation and soil carbon pools decrease almost by the same amount of carbon of about 90 x 10^{12} kg C. However, the vegetation carbon is reacting much faster, recovering almost completely to its original value at the end of the simulation period, whereas the soil carbon, more than twice as large, only starts to decrease when the vegetation carbon has already reached its minimum.

The atmospheric CO_2 concentration was kept constant at 240 ppmv for the present exper-

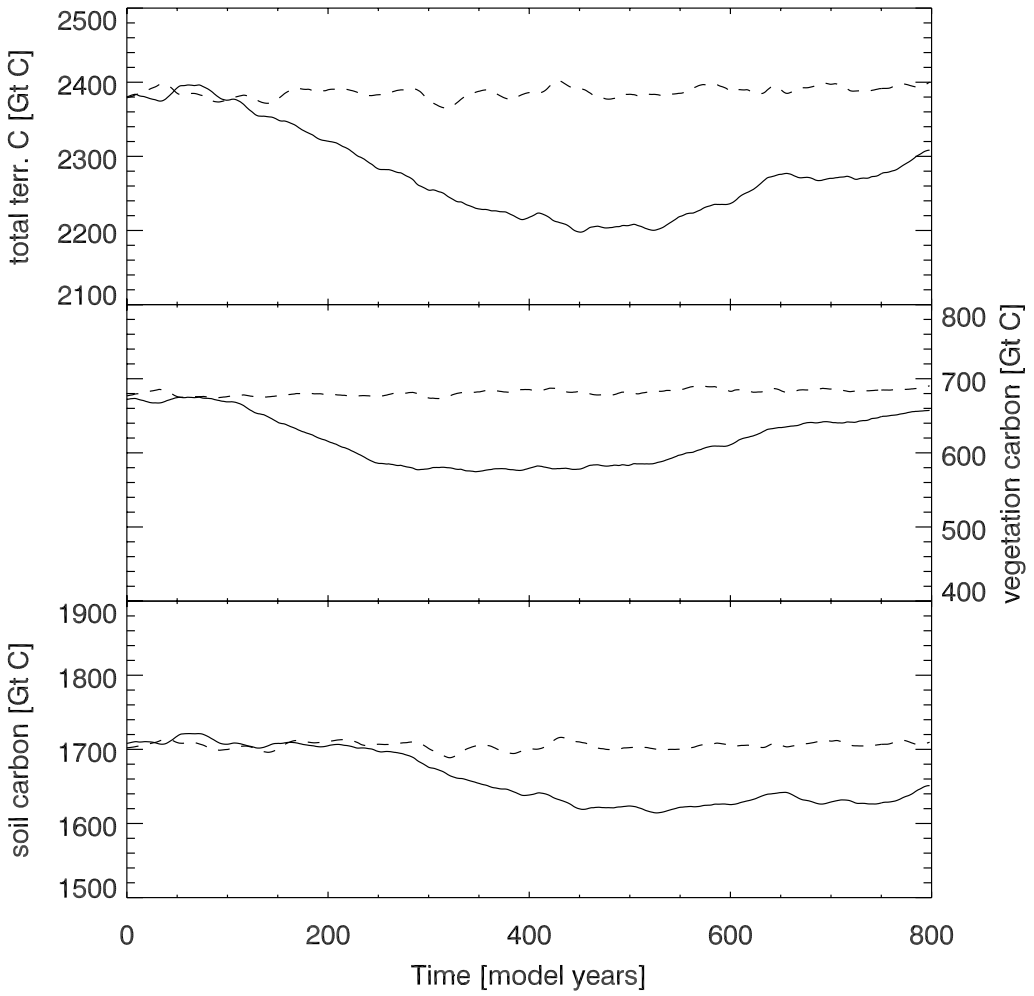

Figure 2.4: Time-series of simulated total terrestrial carbon, vegetation carbon, and soil carbon for the control (dashed line) and the meltwater experiment (solid line).

iments. However, the ice core record shows an increase of 28 ppmv for the YD time period [Monnin et al., 2001]. It is known, that increasing atmospheric CO_2 concentration also increases the rate of photosynthesis, such that the growth of plants is enhanced. In addition to the photosynthetic response, a higher CO_2 concentration also allows partial closure of stomata, less water loss during transpiration and thus an increase of the ratio of carbon gain to water loss. This higher water-use efficiency can lengthen the growing season and increases NPP in plants [Prentice et al., 2001]. Free-air CO_2 enrichment (FACE) experiments in a forest show for a 200 ppmv higher CO_2 concentration than today's an increase of 25% in total NPP [DeLucia et al., 1999]. An overview on the biospheric responses to CO_2 enrichment is given by Körner [2000]. In this study, the "CO_2 fertilization" effect was neglected by keeping atmospheric CO_2 constant. Previous studies using LPJ in a coupled physical-biogeochemical climate model framework showed a

cumulated difference of 416 x 10^{12} kg C in terrestrial carbon uptake between an experiment with constant atmospheric CO_2 at 370 ppm and one with a transient CO_2 increase from 367 ppmv in 2000 to 703 ppmv in 2100 for an IPPC scenario calculation [Joos et al., 2001]. As a simple approach the fertilization effect can be assumed to be independent of climate and ambient CO_2 concentration. Thus, linearly interpolating the amount of cumulated carbon uptake per unit increase in atmospheric CO_2 concentration as reported by Joos et al. [2001] to the 28 ppmv increase in atmospheric CO_2 during the YD period would lead to a decrease of about 35 x 10^{12} kg C of the 180 x 10^{12} kg C terrestrial carbon release in the meltwater experiment.

To estimate the increase of the atmospheric CO_2 content due to the change in terrestrial carbon stocks, we used the net biosphere-atmosphere CO_2 exchange fluxes as an input for a simple ocean carbon model [NICCS, Hooss et al., 2001]. The simulated overall effect is an increase by about 30 ppmv in the atmospheric CO_2 during the YD time period. However, this approximation does not account for changes in the ocean circulation as simulated by the coupled climate model because the ocean carbon model simulations were run with modern boundary conditions. At the end of the simulation atmospheric CO_2 unrealistically decreases because the land biosphere is absorbing some of the previously released carbon again as the climate is going back to "warm" state (see Figure 2.4, years 500 to 800). Besides the missing changes in ocean biogeochemistry, the modelled terrestrial carbon stock changes are probably overestimating the real changes: Although an inland ice sheet was prescribed in the biosphere simulations, and modern-climate initial conditions for the vegetation model are justified by the mild Bølling-Allerød period preceding the YD, the spin-up of the biosphere model was also made with modern climate forcing, but for a longer time than the actual duration of the warm Bølling-Allerød time period. Because of this the initial sizes of the carbon pools, especially of the soil carbon pools, are probably overestimated in the meltwater experiment, resulting in a too large carbon release in the YD perturbation simulation. In addition, the CO_2 fertilization effect would also reduce the amount of carbon release by around 20% as described above.

2.4 Conclusions

The glacial-Holocene increase in atmospheric CO_2 temporarily accelerated during the Younger Dryas cold climate period as revealed by the CO_2 record from the Dome C, Antarctica, ice core. The atmospheric CO_2 content strongly depends on the terrestrial biosphere as one of the key player besides the ocean in the global carbon cycle. Here, we have tested the hypothesis of a terrestrial only response to an abrupt climate change event by modelling both the vegetation dynamics and terrestrial carbon cycling for a highly idealized Younger Dryas. This model study suggests that the terrestrial biosphere may have played an important role during the increase of the atmospheric CO_2 content during the YD time period. Our hypothesis is supported by a qualitatively good agreement of modelled shifts in the vegetation distribution with reconstructed paleo-vegetation maps from pollen records. However, the potential weakness in our interpretation are the sizes of the initial carbon stocks and the initial vegetation distribution

for the meltwater experiment which correspond to modern values, and therefore likely lead us to overestimate the potential release of terrestrial carbon into the biosphere. Consequently, to improve the present model scenario, a longer transient climate experiment representing not only the Younger Dryas but also the preceding time period is necessary. The climate experiment itself should then of course describe a more realistic, i.e. constrained to observational paleo-data such as ice sheets, simulation of the Younger Dryas. The terrestrial vegetation simulations could be further verified by analysing the changes in the tropics, which are already apparent in this simulation, via pollen records or reconstructed paleo-vegetation cover. In a future experiment one should consider the response of the climate to the altered vegetation cover to investigate the vegetation-climate feedback mechanisms through changes in the energy and water balance (e.g. albedo and evaporation). Furthermore, to quantitatively reconstruct the atmospheric CO_2 content for the Younger Dryas time period a coupled biogeochemical ocean-terrestrial biosphere model is necessary to capture the feedbacks in the carbon cycle system.

References

Alley, R. B., Meese, D. A., Shuman, C. A., Gow, A. J., Taylor, K. C., Grootes, P. M., White, J. W. C., Ram, M., Waddington, E. D., Mayewski, P. A., Zielinski, G. A., 1993. Abrupt increase in Greenland snow accumulation at the end of the Younger Dryas event. Nature 362 (6420), 527–529.

Anklin, M., Schwander, J., Stauffer, B., Tschumi, J., Fuchs, A., Barnola, J. M., Raynaud, D., 1997. CO_2 record between 40 and 8 kyr BP from the Greenland Ice Core Project. J. Geophys. Res. 102 (C12), 26539–26545.

Blunier, T., Schwander, J., Stauffer, B., Stocker, T., Dällenbach, A., Indermühle, A., Tschumi, J., Chappellaz, J., Raynaud, D., Barnola, J. M., 1997. Timing of the Antarctic Cold Reversal and the atmospheric CO_2 increase with respect to the Younger Dryas event. Geophys. Res. Lett. 24 (21), 2683–2686.

Broecker, W. S., Peteet, D. M., Rind, D., 1985. Does the ocean-atmosphere system have more than one stable mode of operation. Nature 315 (6014), 21–26.

Dansgaard, W., 1985. Greenland ice core studies. Paleogeogr. Paleoclimatol. Paleoecol. 50 (2-3), 185–187.

DeLucia, E. H., Hamilton, J. G., Naidu, S. L., Thomas, R. B., Andrews, J. A., Finzi, A., Lavine, M., Matamala, R., Mohan, J. E., Hendrey, G. R., Schlesinger, W. H., 1999. Net primary production of a forest ecosystem with experimental CO_2 enrichment. Science 284 (5417), 1177–1179.

Fairbanks, R. G., 1989. A 17,000-year glacio-eustatic sea-level record - influence of glacial melting rates on the Younger Dryas event and deep-ocean circulation. Nature 342 (6250), 637–642.

Haxeltine, A., Prentice, I. C., 1996. Biome 3: An equilibrium terrestrial biosphere model based on ecophysiological constraints, resource availability, and competition among plant functional types. Glob. Biogeochem. Cycle 10 (4), 693–709.

Heinrich, H., 1988. Origin and consequences of cyclic ice rafting in the Northeast Atlantic-Ocean during the past 130,000 years. Quat. Res. 29 (2), 142–152.

Hooss, G., Voss, R., Hasselmann, K., Maier-Reimer, E., Joos, F., 2001. A nonlinear impulse response model of the coupled carbon cycle- climate system (NICCS). Clim. Dyn. 18 (3-4), 189–202.

Johnsen, S. J., Clausen, H. B., Dansgaard, W., Fuhrer, K., Gundestrup, N., Hammer, C. U., Iversen, P., Jouzel, J., Stauffer, B., Steffensen, J. P., 1992. Irregular glacial interstadials recorded in a new Greenland ice core. Nature 359 (6393), 311–313.

Joos, F., Prentice, I. C., Sitch, S., Meyer, R., Hooss, G., Plattner, G. K., Gerber, S., Hasselmann, K., 2001. Global warming feedbacks on terrestrial carbon uptake under the Intergovernmental Panel on Climate Change (IPCCC) emission scenarios. Glob. Biogeochem. Cycle 15 (4), 891–907.

Körner, C., 2000. Biosphere responses to CO_2 enrichment. Ecological Applications 10, 590–619.

Kuhry, P., Hooghiemstra, H., Vangeel, B., Vanderhammen, T., 1993. The El-Abra stadial in the Eastern Cordillera of Colombia (South-America). Quat. Sci. Rev. 12 (5), 333–343.

Lehman, S. J., Keigwin, L. D., 1992. Sudden changes in North-Atlantic circulation during the last deglaciation. Nature 356 (6372), 757–762.

Lloyd, J., Taylor, J. A., 1994. On the temperature-dependence of soil respiration. Funct. Ecol. 8 (3), 315–323.

Maier-Reimer, E., Mikolajewicz, U., Hasselmann, K., 1993. Mean circulation of the LSG OGCM and its sensitivity to the thermohaline surface forcing. Journal of Physical Oceanography 23, 731–757.

Manabe, S., Stouffer, R. J., 1995. Simulation of abrupt climate-change induced by fresh-water input to the North-Atlantic Ocean. Nature 378 (6553), 165–167.

Marchal, O., Stocker, T. F., Joos, F., Indermühle, A., Blunier, T., Tschumi, J., 1999. Modelling the concentration of atmospheric CO_2 during the Younger Dryas climate event. Clim. Dyn. 15 (5), 341–354.

Mikolajewicz, U., Crowley, T. J., Schiller, A., Voss, R., 1997. Modelling teleconnections between the North Atlantic and North Pacific during the Younger Dryas. Nature 387 (6631), 384–387.

Monnin, E., Indermühle, A., Dällenbach, A., Fluckiger, J., Stauffer, B., Stocker, T. F., Raynaud, D., Barnola, J. M., 2001. Atmospheric CO_2 concentrations over the last glacial termination. Science 291 (5501), 112–114.

Overpeck, J. T., Webb, R. S., Webb, T., 1992. Mapping eastern North-American vegetation change of the past 18 ka - no-analogs and the future. Geology 20 (12), 1071–1074.

Peltier, W. R., 1994. Ice-age paleotopography. Science 265 (5169), 195–201.

Peng, C. H., Guiot, J., Van Campo, V. E., 1998. Estimating changes in terrestrial vegetation and carbon storage: Using palaeoecological data and models. Quat. Sci. Rev. 17 (8), 719–735.

Peng, C. H., Guiot, J., Vancampo, E., Cheddadi, R., 1995. Temporal and spatial variations of terrestrial biomes and carbon storage since 13,000 yr BP in Europe - reconstruction from pollen data and statistical-models. Water Air Soil Pollut. 82 (1-2), 375–390.

Peteet, D., 1995. Global Younger-Dryas? Quat. Int. 28, 93–104.

Prentice, I. C., Farquhar, G. D., Fasham, M. J. R., Goulden, M. L., Heimann, M., Jaramillo, V. J., Kheshgi, H. S., Le Quéré, C., Scholes, R. J., Wallace, D. W. R., 2001. The carbon cycle and atmospheric carbon dioxide. In: Houghton, J. T., Ding, Y., Griggs, D. J., Noguer, M., van der Linden, P. J., Dai, X., Maskell, K., Johnson, C. A. (Eds.), Climate Change 2001: The Scientific basis. Cambridge University Press, Cambridge, U.K., pp. 183–237.

Rodbell, D. T., 2000. The Younger Dryas: Cold, cold everywhere? Science 290 (5490), 285–286.

Roeckner, E., Arpe, K., Bengtsson, L., Brinkop, S., Dümenil, L., Esch, M., Kirk, E., Lunkeit, F., Ponater, M., Rockel, B., Sausen, R., Schlese, U., Schubert, S., Windelband, M., 1992. Simulation of the present day climate with the ECHAM model: impact of model physics and resolution. Tech. Rep. 93, Max-Planck-Institut für Meteorologie, Hamburg.

Schiller, A., Mikolajewicz, U., Voss, R., 1997. The stability of the North Atlantic thermohaline circulation in a coupled ocean-atmosphere general circulation model. Clim. Dyn. 13 (5), 325–347.

Sitch, S., Prentice, I. C., Smith, B., Arneth, A., Bondeau, A., Cramer, W., Kaplan, J. O., Levis, S., Lucht, W., Sykes, M. T., Thonicke, K., Venevsky, S., 2003. Evaluation of ecosystem dynamics, plant geography and terrestrial carbon cycling in the LPJ dynamic global vegetation model. Global Change Biology 9, 161–185.

Velichko, A. A., Andreev, A. A., Klimanov, V. A., 1997. Climate and vegetation dynamics in the tundra and forest zone during the late Glacial and Holocene. Quat. Int. 41-2, 71–96.

Voss, R., Sausen, R., 1996. Techniques for asynchronous and periodically synchronous coupling of atmosphere and ocean models. Part II: Impact of variability. Clim. Dyn. 12 (9), 605–614.

Watts, W. A., 1980. Regional variations in the response of vegetation of late-glacial climate events in Europe. In: Lowe, J., Gray, J., Robinson, J. (Eds.), The Late-Glacial of Northwest Europe. Pergamon, New York, pp. 1–22.

Wright, D. G., Stocker, T. F., 1993. Younger Dryas experiments. In: Peltier, W. (Ed.), Ice in the climate system. Springer, Berlin Heidelberg, pp. 395–416.

Chapter 3

Response of the terrestrial carbon and carbon 13 cycle to an abrupt climate change event

---

Abstract. In the past, several rapid climate change events accompanied by large-scale shifts in the vegetation distribution and major changes in the atmospheric CO_2 concentration have occurred. The isotope version of the Lund-Potsdam-Jena (LPJ) dynamic global vegetation model which includes a full description of the isotopic carbon cycle is used for simulating the terrestrial ecosystem response to such an abrupt climate change event. Climate input data is taken from an 850-year-long coupled ocean-atmosphere model (ECHAM3/LSG) experiment representing a highly idealized Younger Dryas (ca. 12 ka BP) like event. Sensitivity experiments are performed to investigate the terrestrial response with respect to different boundary conditions and ecosystem parameterizations. Atmospheric CO_2 and $\delta^{13}C$ are diagnosed using the simulated terrestrial carbon fluxes as input data for the HILDA ocean carbon model. Resulting atmospheric CO_2 concentrations showing an increase of between 16 to 33 ppmv for the cold event are fairly robust against the sensitivity experiments. The simulated atmospheric $\delta^{13}C$ values which are about 0.4‰ lower during the cold phase reflect major findings from ice core measurements. Changes in the terrestrial carbon cycle are a possible explanation for the accelerated increase in atmospheric CO_2 during the Younger Dryas.

3.1 Introduction

Geological records demonstrate that the ending of the last glaciation was accompanied by some abrupt climatic events with major changes in temperature occurring within just a few decades [e.g., Taylor et al., 1993]. The probably best documented event is the Younger Dryas (YD) cold event (12.7 to 11.5 ka BP) that followed the Bølling/Allerød (B/A) warm phase at the end of the last glacial-interglacial transition [Clark et al., 2002]. This sudden return to severe

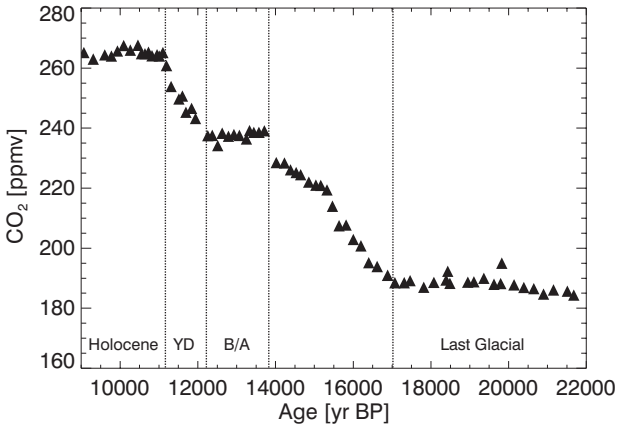

Figure 3.1: CO_2 ice core data from Dome C, Antarctica [Monnin et al., 2001]

glacial climatic conditions is also recorded in ocean sediment cores [Kudrass et al., 1991] and fossil pollen records [Watts, 1980]. The cause for the YD event was possibly a reduction in the meridional overturning circulation and heat transport in the North Atlantic in response to a freshwater flux anomaly from glacial meltwater [Broecker et al., 1985; Sarnthein et al., 1994], producing cooling in the North Atlantic and warming in the southern Hemisphere [Mikolajewicz, 1996; Marchal et al., 1999a; Stocker, 2000]

Analyses of air trapped in ice cores from Greenland and Antarctica show large and abrupt changes in the atmospheric composition in parallel to the climate events [Chappellaz et al., 1993; Blunier et al., 1997; Monnin et al., 2001]. Monnin et al. [2001] show that the atmospheric CO_2 increase from about 190 ppm at the last glacial maximum to an early Holocene value of 265 ppm occurred roughly in four phases (Figure 3.1). CO_2 decreased slightly during the B/A warm phase. Then, CO_2 increased relatively rapidly with an average rate of 23 ppm/ka from 237 ppm to 265 ppm during the YD. The causes of the glacial-interglacial CO_2 increase and of the variations in atmospheric growth rate are still poorly understood. Equally, it is not clear how much of the YD CO_2 increase is related to a long-term trend underlying the whole transition, and how much can be explained by relatively fast oceanic and terrestrial processes. Ocean-sediment processes are associated with typical time scales of millennia and may have contributed to the long-term glacial/interglacial CO_2 increase. Changes in ocean circulation and marine biological production, as well as changes in the terrestrial vegetation distribution and carbon storage in soils and vegetation can occur on decadal time scales.

Earlier studies suggested that both changes in the marine and terrestrial carbon cycle in response to a breakdown in the North Atlantic Deep Water formation contributed to the YD CO_2 increase. Marchal et al. [1999b] forced their 2-dimensional ocean circulation model with freshwater to produce a temporary collapse of the North Atlantic meridional overturning circulation over the length of the YD period. They found that changes in the marine carbon cycle can explain an increase of about 15 ppm during the YD. Scholze et al. [2003b] forced their global dynamic vegetation model with a YD-like climate obtained from an atmosphere/ocean general circulation model and found that terrestrial changes can contribute up to 30 ppmv. A limitation of both studies is that not the overall sequence of events surrounding the YD is simulated. Fully

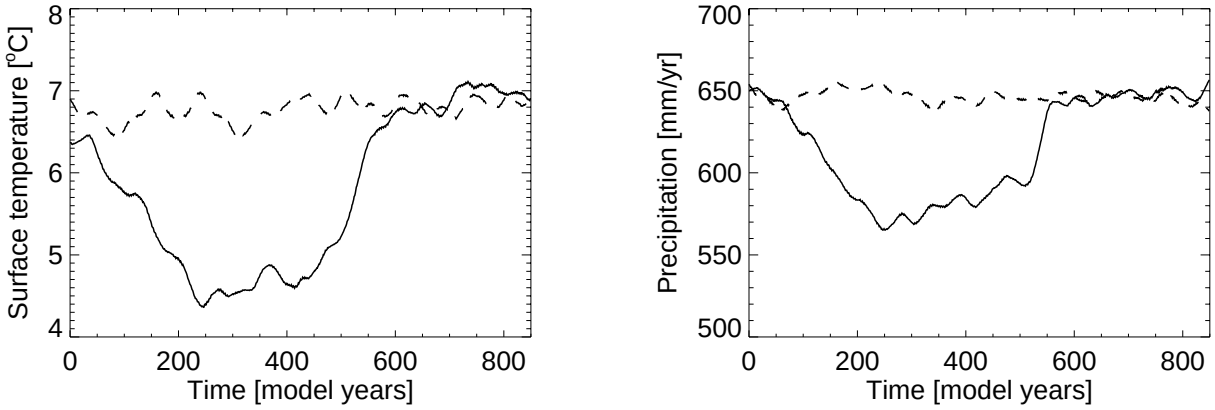

Figure 3.2: Time series of the annual temperature (left panel) and precipitation (right panel) averaged over the land area of the northern hemisphere from the ECHAM3/LSG model simulation.

coupled carbon cycle-climate simulations of the transition and the YD are still missing.

The stable carbon isotope $\delta^{13}CO_2$ could in principle be used to discriminate between oceanic and terrestrial CO_2 sources. However, the source attribution is not straightforward [Heimann and Meier-Reimer, 1996; Indermühle et al., 1999; Joos and Bruno, 1998]) and only a limited number of ice-core measurements exist [Smith et al., 1999].

Here, we extend the study of Scholze et al. [2003b] by (1) simulating changes in the atmospheric stable carbon isotope composition, and (2) presenting sensitivity studies with respect to different parameterizations of the terrestrial carbon cycle. The outline of this paper is as follows: In Section 3.2 we give a brief description of the set-up of the modelling experiments. Results from the different sensitivity experiments and the terrestrial ^{13}C cycling are shown and discussed in Section 3.3. A summary and conclusion is given in the last Section 3.4.

3.2 Model Experiments

The terrestrial biosphere simulations were performed with the Lund-Potsdam-Jena (LPJ) dynamic global vegetation model [Sitch et al., 2003]. LPJ simulates both ecosystem structure (vegetation composition, biomass) and function (energy absorption, carbon cycling). Vegetation composition is described by nine plant functional types (PFT), the presence of a particular PFT in a grid cell being limited by its specific bioclimatic limits. Vegetation dynamics depends on disturbance, mortality, and establishment, but also on the productivity of the different PFTs. As typical for a dynamic vegetation model, vegetation composition does not necessarily have to be in equilibrium with the climate condition at each time step. Terrestrial carbon is represented by living tissue, litter and soil carbon. Decomposition rates are soil moisture and soil temperature dependant [Lloyd and Taylor, 1994]. The LPJ version used in this study also includes a description of terrestrial carbon isotope discrimination [Scholze et al., 2003a].

Table 3.1: LPJ experiments and their specifications.

Experiment.	Specification
CTRL	control climate, no changes
STD	meltwater climate, no changes
CO2	meltwater climate, prescribed transient CO_2
MSD	meltwater climate, modified soil decomposition rate
ASPIN	meltwater climate, spin-up using cold climate

Climate input fields of monthly mean temperature, precipitation and radiation were obtained from a coupled ocean-atmosphere general circulation model experiment [Mikolajewicz et al., 1997]. A highly idealized YD event was simulated with the ECHAM3/LSG by inducing a triangular-shaped freshwater flux (i.e. linear increase (decrease) to (from) the peak value of $0.625*10^6$ m^3 s^{-1} with time) for 500 years while keeping all other boundary conditions at modern values. Main result of this freshwater input is a strong reduction of the thermohaline circulation, which leads to a drastic surface cooling in almost the entire northern hemisphere of about 2 °C to 8 °C, and a reduction of precipitation of the order of 10 to 20 mm/month compared to a control experiment. Figure 3.2 displays the simulated time series of the mean annual temperature and precipitation for the northern hemisphere for both (control and meltwater) ECHAM3/LSG experiments. In the southern hemisphere temperature changes are varying regionally between a warming and a cooling. A more detailed analysis of the climate experiments can be found in Schiller et al. [1997].

A set of experiments were performed following the set-up as described in Scholze et al. [2003b] (Table 3.1). The control (CTRL) and standard meltwater (STD) experiments are the same as presented in this earlier study. For simulation STD, the LPJ model was initialized using climate model output for pre-industrial conditions, and only the climate forcing was changed to YD-like conditions during the experiment. Three additional simulations were performed to investigate the sensitivity of the carbon cycle to (1) increasing atmospheric CO_2 (CO2), (2) varying the temperature dependency of soil carbon decomposition rates (MSD), and (3) the initial state of the land biosphere (ASPIN). These sensitivity experiments were carried out to test the robustness of the inferred terrestrial signal against different boundary conditions or alternative assumptions on terrestrial ecosystem processes.

The extent to which atmospheric CO_2 influences through "CO_2 fertilization" primary productivity and terrestrial storage is under debate. A strong enhancement of productivity was found in field experiments exposing plants to higher than present (370 ppm) atmospheric CO_2 concentrations [e.g., DeLucia et al., 1999; Körner, 2000]. In natural ecosystems this effect might be or become limited by the availability of other nutrients such as nitrate and phosphate. One would expect that co-nutrient limitations were less important during past periods of relatively low atmospheric CO_2 such as the YD. In Experiment CO2, atmospheric CO_2 was prescribed to increase linearly from 237 ppm to 259 ppm during the first 550 simulation years and kept

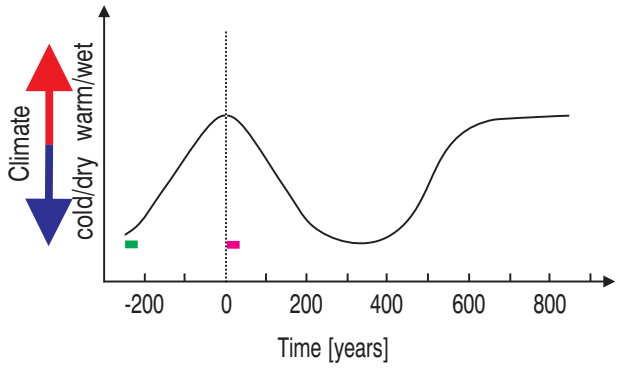

Figure 3.3: A sketch illustrating the different spin-up process for the ASPIN experiment: the first 250 years are mirrored at the year 0, thus increasing the total length of the ASPIN simulation to 1100 years. The green bar indicates the period used for spinning-up the ASPIN and the pink bar for the other experiments.

constant at 259 ppm thereafter.

The temperature dependence of soil and litter respiration has recently been controversially discussed because of conflicting investigations [Trumbore et al., 1996; Giardina and Ryan, 2000]. In the MSD experiment, the temperature dependency of the soil and litter carbon decomposition rate was changed from a doubling of the rate with a temperature increase of 10° C to only a factor of 1.1. Thus, the soil and litter respiration rates are strongly reduced in their temperature dependence [Giardina and Ryan, 2000].

As has been stated by Scholze et al. [2003b] the release of carbon during the cold phase has probably been overestimated in their study as the land biosphere was in equilibrium with a warm climate before the onset of the cooling. For the ASPIN sensitivity experiment, the time history of the terrestrial carbon was taken into account by performing the model spin-up using climate data from the cold phase. This was done mirroring the first 250 years of climate input data,i.e. ECHAM3/LSG model output, at the 0 years point and thus increasing the total simulation length to 1100 years (see Fig. 3.3 for an illustration). The first 30 years which were used for the spin-up resemble a glacial state and the following warm period mimics the B/A. Analyses are presented only for the last 850 years, as for the other experiments.

All experiments cover a simulation period of 850 years, and, except for the CO2 experiment, a constant atmospheric CO_2 forcing of 240 ppmv with a $\delta^{13}C$ value of -6.8‰ was prescribed. For all experiments the resulting atmospheric CO_2 and $\delta^{13}C$ was diagnosed with the Bern ocean carbon model HILDA [Joos et al., 1996] using the simulated biospheric fluxes as input. The physical state of the ocean was kept at modern values.

3.3 Results and Discussions

3.3.1 Vegetation Composition

Pollen records indicate major vegetation shifts during the YD period for North America and Europe but also for regions such as Colombia or South East Asia [Peteet, 1995]. A detailed

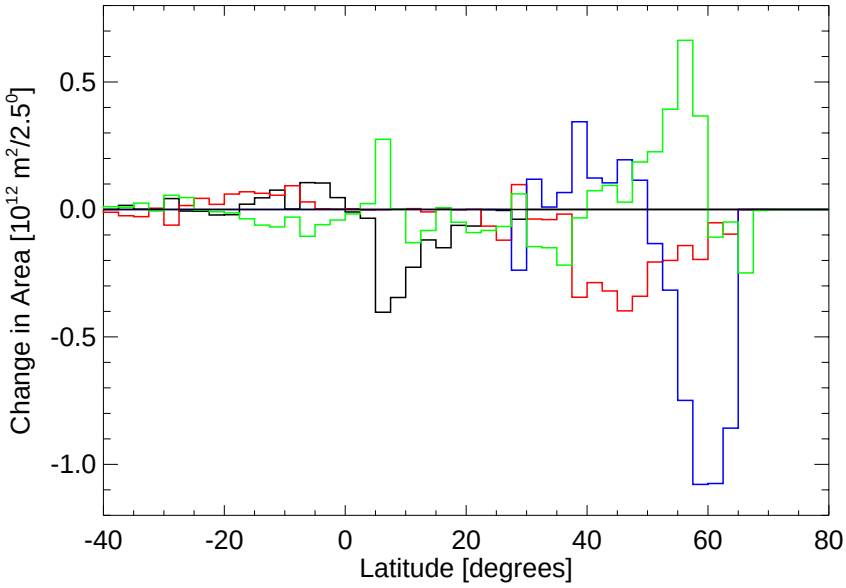

Figure 3.4: Difference in the zonal area between the STD and CTRL experiment of the four main vegetation types (black - tropical, red - temperate, blue - boreal, and green - grass PFTs) averaged over the simulation years 300 to 500.

comparison and validation of the modelled vegetation distribution for the YD time with reconstructed vegetation maps from pollen data has already been done by Scholze et al. [2003b] for the STD experiment. Here, we only recall the major changes in vegetation composition for the STD experiment. All YD experiments show the same vegetation cover as the vegetation representation has not been changed in the sensitivity experiments. Figure 3.4 shows the latitudinal differences in area covered by the main vegetation types between the STD and CTRL experiment. The biggest changes occur at latitudes higher than 50° N, where woody plants (temperate and boreal trees) are partly replaced by herbaceous plants and the remainder by barren land. Between 50° N and 30° N the woody temperate vegetation cover is mainly replaced by boreal trees in the YD experiments. A decline in area of the tropical trees between 5° N and 15° N goes along with an increase in area for C_3 as well as C_4 grasses. These changes in vegetation cover reflect major findings from pollen records [Peteet, 1995].

3.3.2 Carbon Cycle

The return to almost glacial conditions during the YD has a twofold influence on the terrestrial carbon fluxes: directly through the climate response of photosynthesis and respiration, and indirectly through the change in the vegetation distribution. The spatial changes in the CO_2 exchange between the terrestrial biosphere and the atmosphere have already been described by Scholze et al. [2003b] for the STD experiment. Here, we focus our analysis on changes in global fluxes between the sensitivity experiments, including stable carbon isotopes, and their impact on the atmospheric CO_2 content.

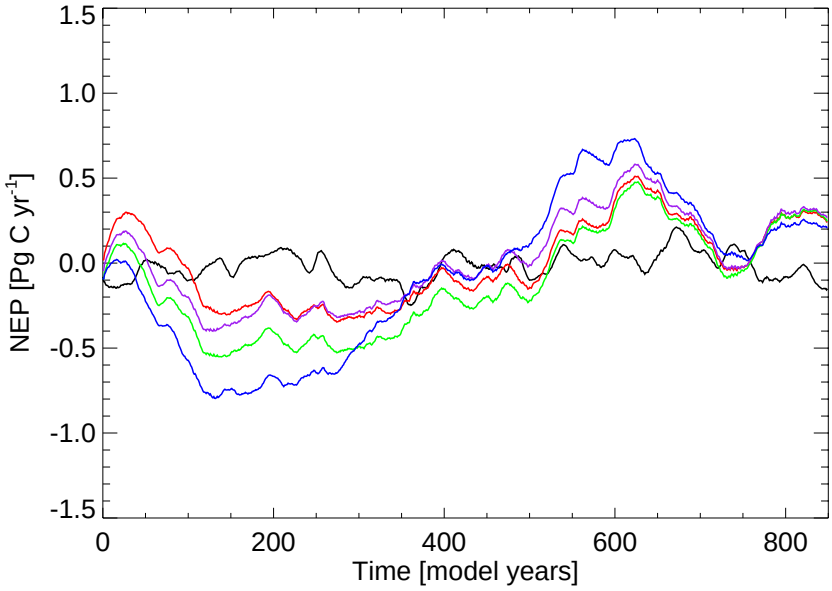

Figure 3.5: Global terrestrial net carbon flux (NEP; negative release, positive uptake of carbon to/from the atmosphere) for the different experiments (black - CTRL, green - STD, blue - MSD, purple - CO2, and red - ASPIN), smoothed with a 50 year running mean filter.

Sensitivity Experiments

The net ecosystem production (NEP) for all five experiments is shown in Figure 3.5. The terrestrial carbon balance for the CTRL experiment is almost neutral through the entire simulation period, whereas all meltwater experiments show a strong release of carbon to the atmosphere during the cold period, and followed by a smaller uptake at the beginning of the following warm period. The MSD experiment shows the biggest carbon release of almost 0.8 petagrams (10^{15}g) of carbon (Pg C) yr^{-1} the first 200 years as the soil carbon decomposition rates does not change much with temperature compared to the other experiments. Therefore, a reduced temperature sensitivity of soil carbon decomposition rates causes a reduced/increased terrestrial carbon storage capability with colder/warmer temperatures as has been shown in a different study using LPJ as well [Joos et al., 2001]. This is also the reason for the stronger uptake of carbon after the cold period because soil carbon fluxes do not increase much with the warming. The total terrestrial carbon storage decreases by about 180 Pg C during the first 300 years (Figure 3.6). Both, the CO2 and the ASPIN experiment exhibit a less pronounced release of carbon during the cold period than the STD experiment. The release from the soil carbon decomposition in the CO2 experiment is partly compensated by the higher productivity due to the CO_2 fertilization. Therefore the change in total terrestrial carbon storage is also only about half the size (80 Pg C) of the STD experiment. LPJ shows a rather strong response of the terrestrial carbon sequestration to changes in atmospheric CO_2 content as already has been found in other studies as well [e.g. Joos et al., 2001; McGuire et al., 2001]. The change in total terrestrial carbon in the ASPIN experiment is only about 100 Pg C although the size of the carbon stock at the end of

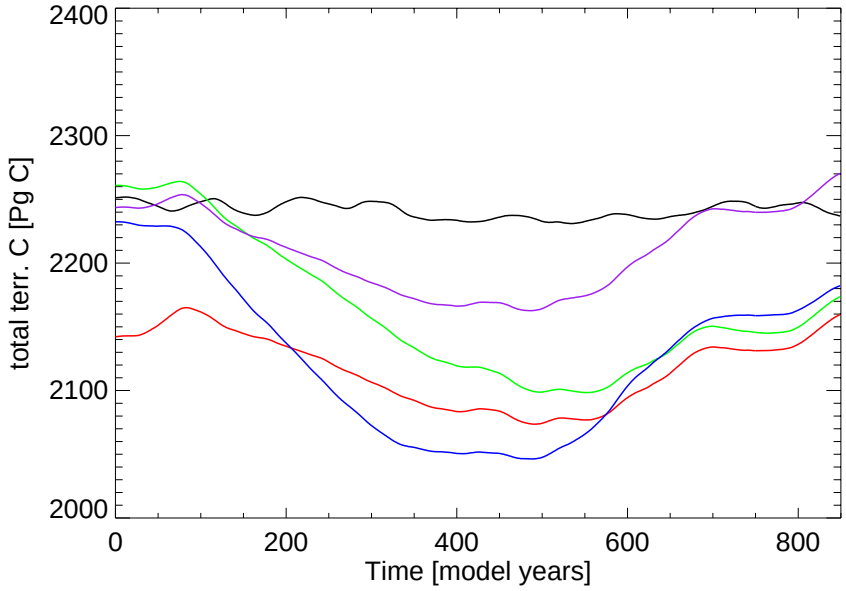

Figure 3.6: Global total terrestrial carbon storage including living biomass, litter and soil carbon for the different experiments (black - CTRL, green - STD, blue - MSD, purple - CO2, and red - ASPIN), smoothed with a 50 year running mean filter.

the cold period (2080 Pg C) is comparable to the STD experiment (2100 Pg C). As can be seen from Figure 3.6, the size of the terrestrial carbon stock was about 5% lower in the ASPIN experiment as in the other experiments at the beginning of the simulation. Therefore the terrestrial biosphere was not completely in equilibrium with the warm climate in the ASPIN experiment due to the different spin-up procedure. There is also still a slight increase of 20 Pg C during the first 100 years which is not apparent in the other experiments. Except for the CO2 experiment no simulation has reached the equilibrium state with the warm climate after the cold period as total terrestrial carbon is still about 80 Pg C lower than what it is in the CTRL experiment.

Figure 3.7 shows the differences in the zonal mean NPP (left panel) and heterotrophic respiration (right panel) fluxes averaged over the years 200 to 400 between the meltwater and CTRL experiments. In the northern hemisphere NPP and also heterotrophic respiration is almost always lower in the meltwater experiments than in the CTRL experiment. Remarkable is the strong decrease in productivity and respiration in the northern tropics (5° N to 10° N). In general the tropics are the region with the highest productivity rates on the globe. A climate change in this region leads to major changes in terrestrial carbon cycling. Between 30° S and 5° N productivity and respiration are higher in the meltwater experiments than in the CTRL simulation because of the warmer and wetter climate. This has also been discussed already for the STD experiment in Scholze et al. [2003b]. Due to CO_2 fertilization productivity and also respiration are always higher in the CO2 experiment compared to the other meltwater simulations. This is especially pronounced in the tropical regions where changes in climate are smaller compared to higher northern latitudes. The modeled CO_2 fertilization mechanism is most effective in tropical

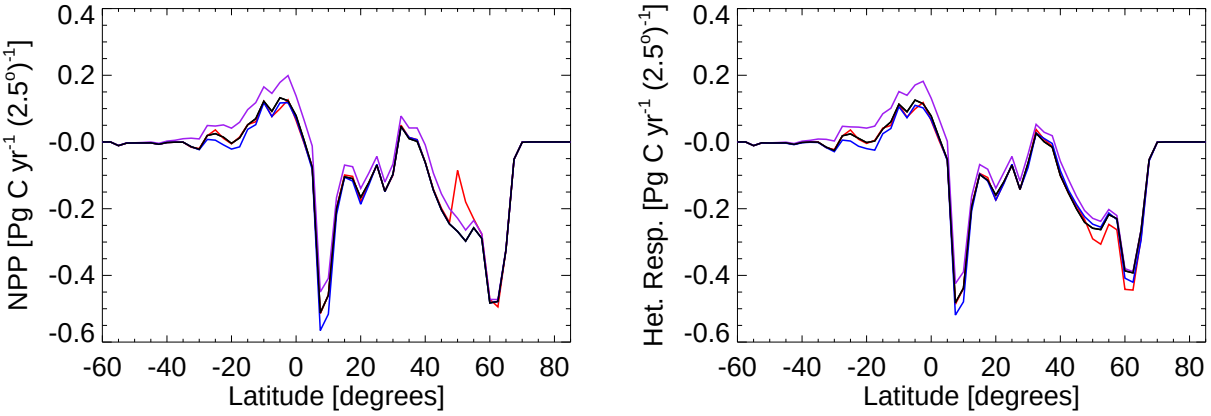

Figure 3.7: Difference in the zonal mean terrestrial carbon fluxes averaged over the simulation years 200 to 400 between the meltwater and CTRL experiments: left panel net primary productivity (NPP, uptake from the atmosphere) and right panel heterotrophic respiration (release to the atmosphere). Colors are: black: STD-CTRL, blue: MSD-CTRL, purple: CO2-CTRL, and red: ASPIN-CTRL.

forests, because of their high NPP, high photorespiration rates (which are reduced in high CO_2), and long timescales for turnover of vegetation carbon.

Terrestrial Isotopic Discrimination

Isotopic discrimination during photosynthesis is defined as

$$\Delta_{leaf} = \frac{\delta^{13}C_{atm} - \delta^{13}C_{leaf}}{1 + \delta^{13}C_{leaf}} \tag{3.1}$$

where $\delta^{13}C_{atm}$[1] is the $^{13}C/^{12}C$ ratio of atmospheric CO_2 and $\delta^{13}C_{leaf}$ is the $^{13}C/^{12}C$ ratio of the photosynthate. The discrimination does not vary much among the sensitivity experiments because, except for the CO2 experiment, nothing has been changed in the photosynthetic carbon uptake routines. The closure or opening of the stomata, which mainly controls the isotopic fractionation during photosynthesis, is dominated by the climatic conditions (more close during the cold, dry phase leading to lower discrimination) even for the CO2 experiment in which the CO_2 fertilization can also influence the stomatal opening.

The left panel in Figure 3.8 shows the flux (NPP) weighted average photosynthetic discrimination for northwest Europe (10° W - 20° E and 50° N - 65° N). The mean isotopic discrimination is reduced by about 1.3 ‰ in this region. However, there is a strong multidecadel (40-60 years) variability in the discrimination of 0.6‰ during the cold phase which is twice the size as in the CTRL experiment. Beerling [1996] reports a reduction of 1.5‰ in isotopic discrimination during the YD deduced from fossil leaves from a specific measurement site in western Norway. Turney

[1] $\delta^{13}C$ is calculated as the deviation with respect to a standard: $\delta^{13}C = [\frac{(^{13}C/^{12}C)}{(^{13}C/^{12}C)_{std}} - 1]1000‰$

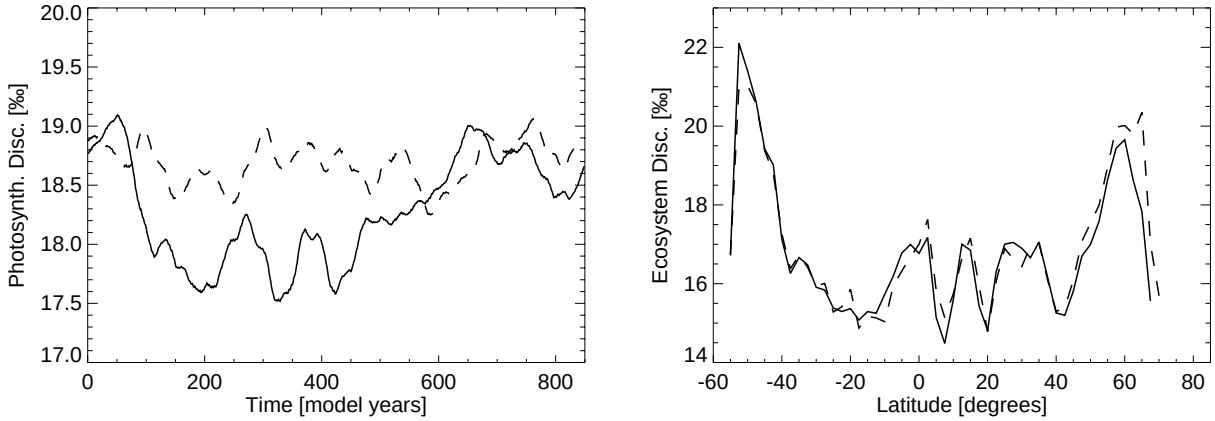

Figure 3.8: Modelled isotopic carbon discrimination for the STD (solid line) and CTRL (dashed line) experiment: the left panel shows the flux weighted average photosynthetic discrimination for Northwest Europe (10° W - 20° E and 50° N - 65° N), smoothed with a 50 year running mean filter and the right panel shows the flux weighted zonal mean ecosystem discrimination averaged over the years 200 to 400.

et al. [1997] have found an increase in the δ^{13}C content of plant material by about the same amount of 1.5‰ for three sites (including the Norway site) in northwest Europe during the YD period. This increase in δ^{13}C is in agreement with a decrease in discrimination.

Zonal mean ecosystem discrimination (see Buchmann et al. [1998] for the concept of ecosystem discrimination), calculated as the flux weighted difference in discrimination against ^{13}C from NPP and heterotrophic respiration, is displayed in the right panel of Figure 3.8 for the CTRL and STD experiment. All meltwater simulations show the same behaviour in the zonal mean ecosystem discrimination: a reduction in almost the entire northern hemisphere with the greatest difference between CTRL and meltwater experiments in the high latitudes north of 55° N. In the southern hemisphere discrimination is especially in the tropics slightly higher for the STD experiment.

Atmospheric CO_2 and δ^{13}C

The simulated terrestrial carbon fluxes from the various experiments have been used as input data for the HILDA ocean carbon model. The boundary conditions for the ocean model have been hold constant at modern values during the ocean simulations. The outcome estimates the changes in atmospheric CO_2 and δ^{13}C values due to the changes in terrestrial carbon fluxes; results are shifted to yield an atmospheric CO_2 content of 240 ppm and a δ^{13}C value of -6.5‰ for the last year of the spin-up period (Figure 3.9 and Figure 3.10).

Atmospheric CO_2 and δ^{13}C are relatively constant in the CTRL experiment with variations of approximately 5 ppmv and 0.2‰, respectively. These variations reflect the variability in the control climate. The strongest amplitude exhibits the MSD experiment with an increase of 33

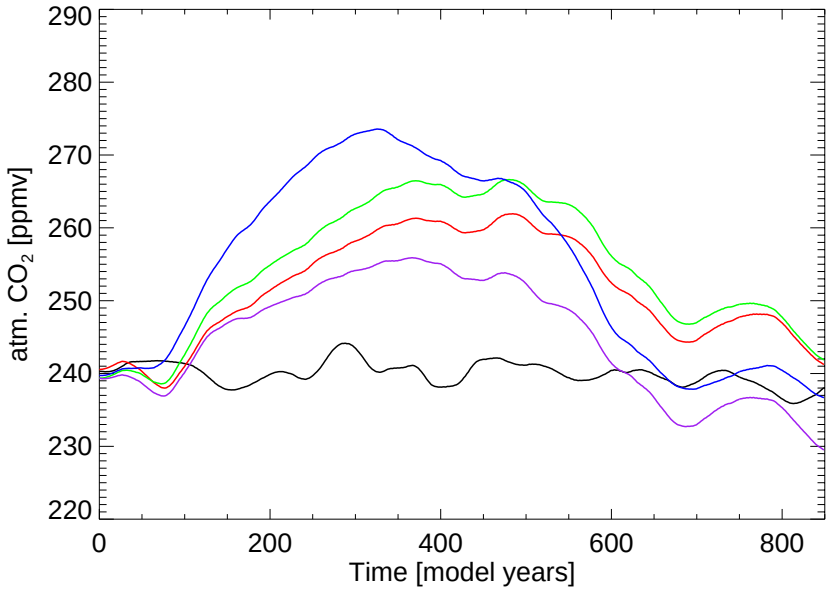

Figure 3.9: Resulting atmospheric CO_2 concentration using the simulated terrestrial carbon fluxes and a simple ocean carbon cycle model (HILDA, Joos et al. [1996]), smoothed with a 50 year running mean filter. Colors are the same as in Figure 3.5: black - CTRL, green - STD, blue - MSD, purple - CO2, and red - ASPIN.

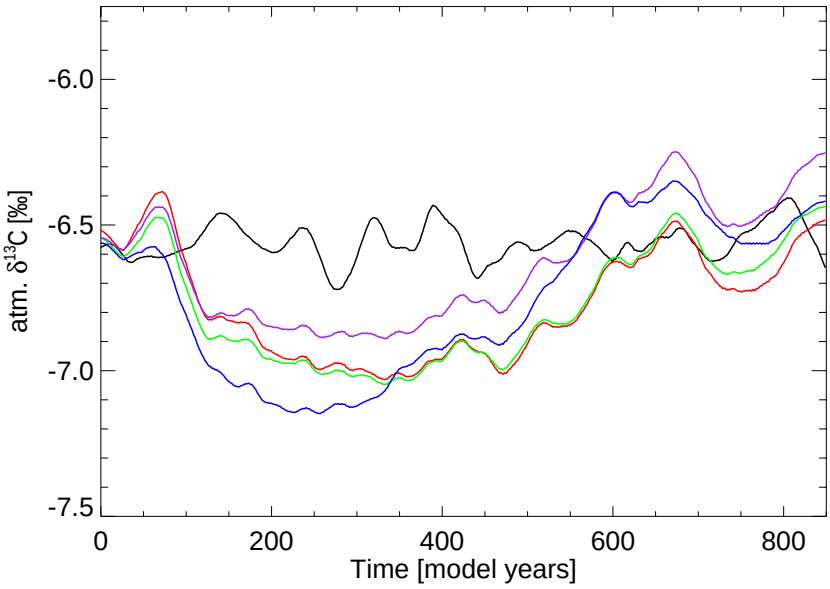

Figure 3.10: Resulting atmospheric $\delta^{13}C$ values using the simulated terrestrial isotopic carbon fluxes and a simple ocean carbon cycle model (HILDA, Joos et al. [1996]), smoothed with a 50 year running mean filter. Colors are the same as in Figure 3.5: black - CTRL, green - STD, blue - MSD, purple - CO2, and red - ASPIN.

ppmv CO_2 and a reduction of 0.6‰ in $\delta^{13}C$. Atmospheric CO_2 is strongly increased because of the reduced carbon storage capability with colder temperatures as described above. This is also the reason for the large drop in $\delta^{13}C$ as more isotopic light (depleted in ^{13}C) carbon is respired than taken up by the biosphere. Terrestrial emissions from the CO2 experiment produce the smallest changes in atmospheric CO_2 (16 ppmv) and $\delta^{13}C$ (0.4‰). The increasing atmospheric CO_2 forcing for LPJ results in a higher productivity and thus, resulting into smaller net emissions to the atmosphere. Compared to the other sensitivity experiments relatively more isotopic light CO_2 is taken up by the biosphere, leaving a larger fraction of ^{13}C enriched CO_2 in the atmosphere and therefore, leading also to the smallest change in atmospheric $\delta^{13}C$. Although terrestrial carbon was not in equilibrium with climate at the beginning of the ASPIN simulation and sizes of soil carbon stocks were smaller than in the STD experiment, atmospheric results for the STD and ASPIN experiment are almost the same with an increase of 26 ppmv and 22 ppmv in atmospheric CO_2, respectively. Also, both experiments show a similar decrease of 0.45‰ in atmospheric $\delta^{13}C$ This suggests that results are not very sensitive to the initial state of the land biosphere.

Our results lie well in the range of the increase in atmospheric CO_2 of about 29 ppmv and also in the range of the decrease in atmospheric $\delta^{13}C$ of approximately 0.3‰ as measured from ice cores [Monnin et al., 2001; Smith et al., 1999] for the YD time period. However, our simulations only focus on changes in the terrestrial carbon cycle and neglect changes in the ocean carbon cycle. Simulated atmospheric CO_2 decreases at the end of the simulation period because the land biosphere is partly taking up again the previously released carbon as climate is changing to warmer conditions. The simulated rates of increase in atmospheric CO_2 for the cold period vary between 19 (CO2 experiment) and 24 ppmv/ka, however, these rates are for a simulated YD period of approximately only 500 years. The observed rate of 23 ppmv/ka spans over a time period of more than 1200 years. A simulation covering the real length of the cold period would result into a considerably lower rate of atmospheric CO_2 increase. During the following warm period the land biota is expanding again and taking up carbon which leads to a decrease in atmospheric CO_2 with approximately the same rate as for the increase during the cold period.

This study supports the hypothesis by Broecker [1987] that the overall increase in atmospheric CO_2 during the glacial to interglacial is due to the ocean carbon cycle (physical air-sea gas exchange, changes in nutrient content and $CaCO_3$ compensation). The terrestrial biosphere acts as an modulator on the overall rate of atmospheric CO_2 rise: during a cold event such as the YD the increase is accelerated by terrestrial carbon emissions and during the following warm phase the increase is damped or in an extreme case reversed to a slight decrease by the uptake of carbon from an expanding land biosphere. For the early Holocene it has already been shown by Broecker et al. [2001], that the removal of atmospheric CO_2 due to the increase in terrestrial biomass after the YD cold period is compensated by a release of carbon from the ocean due to the slow process of $CaCO_3$ compensation, and thus, keeping the atmospheric CO_2 concentration relatively stable.

3.4 Conclusions

Results from ice core measurements show that the rate of increase in atmospheric CO_2 during the glacial-Holocene transition largely varies between a doubling of the overall rate for e.g. the Younger Dyras period and almost a reversal to a decrease for the Bølling-Allerød or the early Holocene [Monnin et al., 2001]. Here, we propose that the modulations of the rate in the atmospheric CO_2 rise are caused by the land biosphere responding to changing climate conditions. We analyzed the terrestrial carbon cycle for a highly idealized YD period followed by a warm period representing the early Holocene. This model study suggests that during the cold YD period the terrestial biosphere acts as a source while for the following warm early Holocene period it acts as s sink for atmospheric CO_2 until the land is in quasi-equilibrium with the climate. Three sensitivity experiments support this hypothesis as they all show the same behaviour as the standard experiment. However, the proposed reduction in the temperature dependence of the soil and litter respiration rates [Giardina and Ryan, 2000] seem to overestimate the source/sink capacity of the land biosphere for our rapid climate change simulation (MSD experiment) as the released terrestrial carbon could explain alone the increase in atmospheric CO_2 during the Younger Dryas. The terrestrial carbon release is strongly reduced (but still sufficient to modulate the measured rate) in the CO2 experiment because of the CO_2 fertilization effect. A rather small impact has the initial value of the terrestrial carbon pools as the carbon release simulated in the ASPIN experiment is close to the STD experiment. The decrease of $\approx$0.4‰ in modelled atmospheric δ^{13}C values is a fairly robust signal found in all sensitivity experiments and is also in agreement with ice core measurements [Smith et al., 1999].

This theory has to be tested in a future study using a coupled ocean-terrestial biosphere carbon cycle model simulating preferable the whole transition period. Of course, detailed measurements of CO_2 and especially atmospheric δ^{13}C would be very valuable to further investigate the concurrent roles of the ocean carbon cycle versus the land carbon cycle during the interglacial.

References

Beerling, D. J., 1996. ^{13}C discrimination by fossil leaves during the late-glacial climate oscillation 12-10 ka BP: measurements and physiological controls. Oecologia 108, 29–37.

Blunier, T., Schwander, J., Stauffer, B., Stocker, T., Dällenbach, A., Indermühle, A., Tschumi, J., Chappellaz, J., Raynaud, D., Barnola, J. M., 1997. Timing of the Antarctic Cold Reversal and the atmospheric CO_2 increase with respect to the Younger Dryas event. Geophys. Res. Lett. 24 (21), 2683–2686.

Broecker, W. S., 1987. The role of $CaCO_3$ compensation in the glacial to interglacial atmospheric CO_2 change. Glob. Biogeochem. Cycles 1, 15–29.

Broecker, W. S., Lynch-Stieglitz, J., Clark, E., Hajdas, I., Bonani, G., 2001. What caused the atmosphere's CO_2 content to rise during the last 8000 years? Geochem. Geophys. Geosyst. 2 (U1–U13).

Broecker, W. S., Peteet, D. M., Rind, D., 1985. Does the ocean-atmosphere system have more than one stable mode of operation. Nature 315 (6014), 21–26.

Buchmann, N., Brooks, R. J., Flanagan, L. B., Ehleringer, J. R., 1998. Carbon isotope discriminiation of terrestiral ecosystems. In: Griffiths, H. (Ed.), Stable Isotopes. BIOS Sci., Oxford, pp. 203–222.

Chappellaz, J., Blunier, T., Raynaud, D., Barnola, J. M., Schwander, J., Stauffer, B., 1993. Synchronous changes in atmospheric CH_4 and Greenland climate between 40-kyr and 8-kyr bp. Nature 366 (6454), 443–445.

Clark, P. U., Pisias, N. G., Stocker, T. F., Weaver, A. J., 2002. The role of the thermohaline circulation in abrupt climate change. Nature 415 (6874), 863–869.

DeLucia, E. H., Hamilton, J. G., Naidu, S. L., Thomas, R. B., Andrews, J. A., Finzi, A., Lavine, M., Matamala, R., Mohan, J. E., Hendrey, G. R., Schlesinger, W. H., 1999. Net primary production of a forest ecosystem with experimental CO_2 enrichment. Science 284 (5417), 1177–1179.

Giardina, C., Ryan, M., 2000. Evidence that decomposition rates of organic carbon in mineral soil do not vary with temperature. Nature 404 (6780), 858–861.

Heimann, M., Meier-Reimer, E., 1996. On the relations between the oceanic uptake of CO_2 and its carbon isotopes. Glob. Biogeochem. Cycles 10 (1), 89–110.

Indermühle, A., Stocker, T. F., Joos, F., Fischer, H., Smith, H. J., Wahlen, M., Deck, B., Mastroianni, D., Tschumi, J., Blunier, T., Meyer, R., Stauffer, B., 1999. Holocene carbon-cycle dynamics based on CO_2 trapped in ice at Taylor Dome, Antarctica. Nature 398 (6723), 121–126.

Joos, F., Bruno, M., 1998. Long-trem variability of the terrestrial and oceanic carbon sinks and the budgets of the carbon isotopes ^{13}C and ^{14}C. Glob. Biogeochem. Cycles 12, 277–295.

Joos, F., Bruno, M., Fink, R., Stocker, T. F., Siegenthaler, U., Le Quere, C., Sarmiento, J. L., 1996. An efficient and accurate representation of complex oceanic and biospheric models of anthropogenic carbon uptake. Tellus 48B, 397–417.

Joos, F., Prentice, I. C., Sitch, S., Meyer, R., Hooss, G., Plattner, G. K., Gerber, S., Hasselmann, K., 2001. Global warming feedbacks on terrestrial carbon uptake under the Intergovernmental Panel on Climate Change (IPCC) emission scenarios. Glob. Biogeochem. Cycle 15 (4), 891–907.

Körner, C., 2000. Biosphere responses to CO_2 enrichment. Ecological Applications 10, 590–619.

Kudrass, H. R., Erlenkeuser, H., Vollbrecht, R., Weiss, W., 1991. Global nature of the Younger Dryas cooling event inferred from oxygen isotope data from Sulu sea cores. Nature 349 (6308), 406–409.

Lloyd, J., Taylor, J. A., 1994. On the temperature-dependence of soil respiration. Funct. Ecol. 8 (3), 315–323.

Marchal, O., Stocker, T. F., Joos, F., 1999a. On large-scale physical and biogeochemical responses to abrupt climate changes in the Atlantic thermohaline circulation. In: Clark, P. U., Webb, R. S., Keigwin, L. D. (Eds.), Mechanisms of Millennial-Scale Global Climate Change. Vol. 112 of Geophysical Monograph. AGU, Washington, D.C., pp. 263–284.

Marchal, O., Stocker, T. F., Joos, F., Indermühle, A., Blunier, T., Tschumi, J., 1999b. Modelling the concentration of atmospheric CO_2 during the Younger Dryas climate event. Clim. Dyn. 15 (5), 341–354.

McGuire, A. D., Sitch, S., Clein, J., Dargaville, R., Esser, G., Foley, J., Heimann, M., Joos, F., Kaplan, J., Kicklighter, D. W., Meier, R. A., Melillo, J. M., III, B. M., Prentice, I. C., Ramankutty, N., Reichenau, T., Schloss, A., Tian, H., Wittenberg, U., 2001. Carbon balance of the terrestrial biosphere in the twentieth century: Analyses of CO_2, climate and land use effects with four process-based ecosystem models. Glob. Biogeochem. Cycles 15, 183–206.

Mikolajewicz, U., 1996. A meltwater-induced collapse of the 'conveyor belt' thermohaline circulation and its influence on the distribution of $\Delta^{14}C$ and $\delta^{18}O$ in the oceans. Tech. Rep. 189, Max-Planck-Insitut für Meterorologie, Hamburg.

Mikolajewicz, U., Crowley, T. J., Schiller, A., Voss, R., 1997. Modelling teleconnections between the North Atlantic and North Pacific during the Younger Dryas. Nature 387 (6631), 384–387.

Monnin, E., Indermühle, A., Dällenbach, A., Fluckiger, J., Stauffer, B., Stocker, T. F., Raynaud, D., Barnola, J. M., 2001. Atmospheric CO_2 concentrations over the last glacial termination. Science 291 (5501), 112–114.

Peteet, D., 1995. Global Younger-Dryas? Quat. Int. 28, 93–104.

Sarnthein, M., Winn, K., Jung, S. J. A., Duplessy, J. C., Labeyrie, L., Erlenkeuser, H., Ganssen, G., 1994. Changes in East Atlantic deep-water circulation over the last 30,000 years - 8 time slice reconstructions. Paleoceanography 9 (2), 209–267.

Schiller, A., Mikolajewicz, U., Voss, R., 1997. The stability of the North Atlantic thermohaline circulation in a coupled ocean-atmosphere general circulation model. Clim. Dyn. 13 (5), 325–347.

Scholze, M., Kaplan, J. O., Knorr, W., Heimann, M., 2003a. Climate and interannual variability of the atmosphere-biosphere $^{13}CO_2$ flux. Geophys. Res. Lett 30 (2), 1097, doi:10.1029/2002GL015631.

Scholze, M., Knorr, W., Heimann, M., 2003b. Modelling terrestrial vegetation dynamics and carbon cycling for an abrupt climate change event. The Holocene 13 (3), 327–333.

Sitch, S., Prentice, I. C., Smith, B., Arneth, A., Bondeau, A., Cramer, W., Kaplan, J. O., Levis, S., Lucht, W., Sykes, M. T., Thonicke, K., Venevsky, S., 2003. Evaluation of ecosystem dynamics, plant geography and terrestrial carbon cycling in the LPJ dynamic global vegetation model. Global Change Biology 9, 161–185.

Smith, H. J., Fischer, H., Wahlen, M., Mastroianni, D., Deck, B., 1999. Dual modes of the carbon cycle since the last glacial maximum. Nature 400 (6741), 248–250.

Stocker, T. F., 2000. Past and future reorganizations in the climate system. Quat. Sci. Rev. 19 (1-5), 301–319.

Taylor, K. C., Lamorey, G. W., Doyle, G. A., Alley, R. B., Grootes, P. M., Mayewski, P. A., White, J. W. C., Barlow, L. K., 1993. The flickering switch of late Pleistocene climate change. Nature 361 (6411), 432–436.

Trumbore, S. E., Chadwick, O. A., Amundson, R., 1996. Rapid exchange between soil carbon and atmospheric carbon dioxide driven by temperature change. Science 272 (5260), 393–396.

Turney, C. S. M., Beerling, D. J., Harkness, D. D., Lowe, J. J., Scott, E. M., 1997. Stable carbon isotope variations in northwest Europe during the las glacial-interglacial transition. Journal of Quaternary Science 12, 339–344.

Watts, W. A., 1980. Regional variations in the response of vegetation of late-glacial climate events in Europe. In: Lowe, J., Gray, J., Robinson, J. (Eds.), The Late-Glacial of Northwest Europe. Pergamon, New York, pp. 1–22.

Chapter 4

Climate and interannual variability of the atmosphere-biosphere $^{13}CO_2$ flux

Abstract. We present a bottom-up approach to simulate the terrestrial isotopic carbon variations using the Lund-Potsdam-Jena dynamic global vegetation model (LPJ-DGVM). LPJ is extended to include isotopic fractionation of ^{13}C at the leaf level during assimilation and includes a full isotopic terrestrial carbon cycle. The model thus allows a quantitative analysis of the net biosphere exchange of CO_2 and $^{13}CO_2$ with the atmosphere as a function of changes in climate, atmospheric CO_2, and the isotope ratio of CO_2. LPJ simulates a global mean isotopic fractionation of 17.7‰ at the leaf level with interannual variations of ca. 0.3‰. Interannual variability in the net $^{13}CO_2$ flux between atmosphere and terrestrial biosphere is of the order of 15 PgC‰ yr^{-1}. It is reduced to 4 PgC ‰ yr^{-1} if the leaf-level fractionation factor is held constant at the long term mean. Taking climate driven variable fractionation effects into account in double deconvolution studies we estimate that this could imply shifts of up to 0.8 PgC yr^{-1} in the inferred partitioning between terrestrial and oceanic carbon sinks.

4.1 Introduction

Over the last 50 years anthropogenic emissions of CO_2 added a total of ca. 210 petagrams (10^{15}g) of carbon (PgC) into the atmosphere [Marland et al., 2001]. During the same period the atmospheric CO_2 content increased by 55 ppmv from 310 ppmv CO_2 in 1950 to 365 ppmv CO_2 in 1998 which is equivalent to ca. 115 PgC only [Prentice et al., 2001]. The remaining carbon has been absorbed by the oceans and the land biosphere. Changes in the concentration and $^{13}C/^{12}C$ ratio of atmospheric CO_2 can be used to constrain the global carbon budget and derive location and magnitude of carbon sources and sinks [e.g. Keeling et al., 1989; Ciais et al., 1995; Heimann and Maier-Reimer, 1996]. A common method to infer the ocean and land contributions to these variations is the double-deconvolution of measured records of atmospheric CO_2 and $\delta^{13}C$[1][Keeling et al., 1989; Francey et al., 1995; Joos and Bruno, 1998]. This "top-down" partitioning calculation is sensitive to various quantities, including the assumed isotopic

signature of terrestrial carbon, which is usually held constant [e.g. Keeling et al., 1989; Joos and Bruno, 1998].

However, the isotopic signature of the terrestrial biosphere is highly variable in space and time. The $\delta^{13}C$ of assimilated CO_2 itself depends strongly on interannual climatic variability and on vegetation composition [Kaplan et al., 2001]. Because of their different anatomy, C_4 plants discriminate against heavy isotopes to a much smaller degree than C_3 plants. Furthermore, the $\delta^{13}C$ of assimilated CO_2 is based on today's atmospheric $\delta^{13}C$, whereas the $\delta^{13}C$ of the respired CO_2 is based on the atmospheric $\delta^{13}C$ of the time when the plant assimilated the CO_2 now being respired, resulting in the so-called isotopic disequilibrium flux. Therefore, changes in the isotopic signature of the land biosphere are controlled not only by atmospheric $\delta^{13}C$, but also by the age distribution of decomposing organic matter, shifts in the terrestrial photosynthesis from C_3 to C_4 plants, and the effects of climatic variability on isotope discrimination in C_3 plants [Battle et al., 2000]. The sum of the above mentioned processes results in an extremely heterogenous $^{13}CO_2$ biosphere-atmosphere exchange flux field.

The double-deconvolution inversion method requires an *a priori* representation of the global $^{13}CO_2$ flux field. Our ability to characterize this $^{13}CO_2$ flux field in space and time based on field-scale measurements has not been possible. To date, most inversions have made simplifying assumptions to describe this flux field, e.g. a constant fractionation factor in space in time. Recently, several process-based model representations of the global $^{13}CO_2$ flux field have appeared [Fung et al., 1997; Wittenberg and Esser, 1997; Kaplan et al., 2001]. However, none of these studies have demonstrated how interannual variability in climate affects plant physiology and vegetation dynamics, and through these processes, the $^{13}CO_2$ flux field and its, potentially large, implications for inverse modeling studies.

Here, the dynamic global vegetation model LPJ is used to simulate CO_2 and $^{13}CO_2$ exchange between the atmosphere and biosphere for the last century in a consistent terrestrial carbon cycling framework. A set of experiments are performed to investigate the impact of the processes on the interannual variations in terrestrial carbon isotope discrimination, and to estimate the importance of considering a temporally-variable flux field for inverse modelling studies.

4.2 Methodology

4.2.1 The LPJ Dynamic Global Vegetation Model

LPJ [Sitch et al., 2003] combines mechanistic treatment of terrestrial ecosystem structure (vegetation composition, biomass) and function (energy absorption, carbon cycling). Vegetation dynamics are updated annually based on the productivity, disturbance, mortality, and establishment of nine different plant functional types (PFTs, seven woody C_3 plants, two herbaceous: C_3 and C_4 grass). Modelled potential vegetation cover (including C_3/C_4 plant distribution)

[1] $\delta^{13}C$ is calculated as the deviation with respect to a standard: $\delta^{13}C = [\frac{(^{13}C/^{12}C)}{(^{13}C/^{12}C)_{std}} - 1]1000‰$

depends on both the bioclimatic limits of the PFTs and the competition among them. Thus, LPJ does not require the assumption of the vegetation distribution in equilibrium with climate.

The enhanced version of LPJ used here fully incorporates ^{13}C as a tracer in the carbon cycle simulated by the model. The carbon isotope module is based on Kaplan et al. [2001] which has been validated with measurements at the leaf, canopy, and background atmosphere scales. LPJ, as the successor of the BIOME model used by Kaplan et al. [2001], is based on an almost identical formulation of ecosystem structure and function except for the vegetation dynamical elements. The module includes the calculation of isotope fractionation during photosynthesis, the addition of an extra above ground litter pool to represent the age spectrum of decomposing organic matter in a more realistic way, and separate accounting of all internal carbon pools for ^{12}C and ^{13}C. Incorporation of the carbon isotope module in LPJ led to the reparameterization of several of the PFT-specific physiological parameters.

The isotope discrimination during assimilation is calculated as described by Lloyd and Farquhar [1994]. LPJ explicitly simulates the actual inter-cellular-to-atmospheric CO_2 concentration (c_i/c_a) ratio through a coupled photosynthesis and water-balance canopy conductance scheme. Photosynthesis and carbon isotope discrimination are calculated on a daily time step representing daily average values; assimilated CO_2 and $^{13}CO_2$ is allocated to the four different tissue pools (leaves, sap- and heart-wood, roots) on an annual basis. Soil and litter total C and ^{13}C pools are updated monthly. Each PFT has an associated below-ground, fast-, and slow-above-ground litter pool. A fraction of the decomposing litter is respired directly into the atmosphere; the remainder is divided between the fast and slow soil carbon pools. The fast and slow litter and the fast and slow soil pools are assigned turnover times at 10°C of 2, 20, 33 and 1000 years, respectively. Decomposition is temperature and moisture dependent. As isotope fractionation processes during respiration are poorly understood, no fractionation is assigned for the decomposition.

4.2.2 Atmospheric CO_2 and $^{13}CO_2$ budget

The atmospheric CO_2 budget is given by

$$\frac{d}{dt}N_a = F_{fossil} + F_{oc,net} + F_{bio,net} = F_{other} + (F_{ba} - F_{ab}) \tag{4.1}$$

where F_{other} is the sum of net ocean and fossil fuel fluxes, F_{ab} is the flux from the atmosphere to the biosphere (here taken as the net primary production, NPP), and F_{ba} is the flux from the biosphere to the atmosphere, i.e. the heterotrophic respiration which here is the sum of the carbon emissions to the atmosphere from the litter and soil pools respectively, and the CO_2 flux due to fire disturbance. Correspondingly the atmospheric $^{13}CO_2$ budget can be formulated as

$$\begin{aligned} \frac{d}{dt}\,{}^{13}N_a &= {}^{13}F_{fossil} + {}^{13}F_{oc,net} + {}^{13}F_{bio,net} \\ &= {}^{13}F_{other} + (F_{ba}R_b - F_{ab}\alpha_{ab}R_a) \end{aligned} \tag{4.2}$$

where R_a and R_b are the isotopic ratios of atmospheric and biospheric carbon, respectively, and α_{ab} is the fractionation factor for the atmosphere-biosphere flux. Here, we assume that gross

assimilation and autotrophic respiration are in isotopic equilibrium on an interannual time scale [Ekblad and Högberg, 2001]. The change in the atmospheric $^{13}CO_2$ can be separated into the temporal change of two components, isotopic ratio (R_a) and CO_2 (N_a):

$$\frac{d}{dt}\ {}^{13}N_a = N_a\frac{d}{dt}R_a + R_a\frac{d}{dt}N_a \tag{4.3}$$

Now focusing only on the time dependency of R_a and considering only biospheric fluxes it follows with $F_{bio,net} = F_{ba} - F_{ab}$ that

$$[N_a\frac{d}{dt}R_a]_{bios} = F_{bio,net}(R_b - R_a) + F_{ab}R_b - F_{ab}\alpha_{ab}R_a \tag{4.4}$$

Reformulating Equation 4.4 in terms of the δ-Notation (for nomenclature see e.g. Mook [1986]) and inserting a temporal mean (1950-98) fractionation term $\overline{\epsilon_{ab}}$ the temporal change in $\delta^{13}C$ from terrestrial biospheric fluxes can be described with three different terms:

$$\begin{aligned}[N_a\frac{d}{dt}\delta^{13}C_a]_{bios} = {} & F_{bio,net}(\delta^{13}C_b - \delta^{13}C_a) \\ & + F_{ab}(\delta^{13}C_b - (\delta^{13}C_a + \overline{\epsilon_{ab}})) + F_{ab}(\overline{\epsilon_{ab}} - \epsilon_{ab})\end{aligned} \tag{4.5}$$

The first term in Equation 4.5 approximates the influence of the variability in the net terrestrial flux on the temporal change in $\delta^{13}C$, the second term represents the terrestrial ^{13}C Suess-Effect [Suess, 1955] and the third term $F_{ab}(\overline{\epsilon_{ab}} - \epsilon_{ab}) = \Delta^{13}F_{ab}$ shows the influence of a time-varying fractionation factor on the global $^{13}CO_2$ budget. Global values are obtained by the flux-weighted sum of the quantities (e.g. F_{ab} for the global fractionation factor) at each grid cell, which are then averaged over the globe.

4.2.3 Set-up of model experiments

Two experiments were performed at 0.5° spatial resolution. For both experiments (ISOVAR and ISOFIX) climate forcing data (monthly mean fields of temperature, precipitation, and cloud cover) was taken from the CRU05 1901-1998 monthly climate time-series [New et al., 2000]. In the ISOVAR experiment discrimination was calculated according to the Lloyd and Farquhar [1994] scheme as described above, while for the ISOFIX experiment we prescribed a constant discrimination of 18.7‰ for C_3 plants and 3.4‰ for C_4 plants (global mean values from the ISOVAR experiment). For both experiments, we used the time-series of atmospheric CO_2 as described in McGuire et al. [2001] and an extended version of the atmospheric $\delta^{13}C$ time-series of Francey et al. [1999]. Soil physical parameters are based on the FAO soil data set [FAO, 1991]. The model was spun-up for 1000 years using the first 30 years of the climate input data repetitively to reach an equilibrium state.

4.3 Results and Discussion

The modelled leaf discrimination (ϵ_{ab}) varies from 3 ‰ to 4‰ for C_4 grasses and 10‰ to 23‰ for C_3 plants. This high variability of up to 13‰ in the leaf discrimination in C_3 PFTs

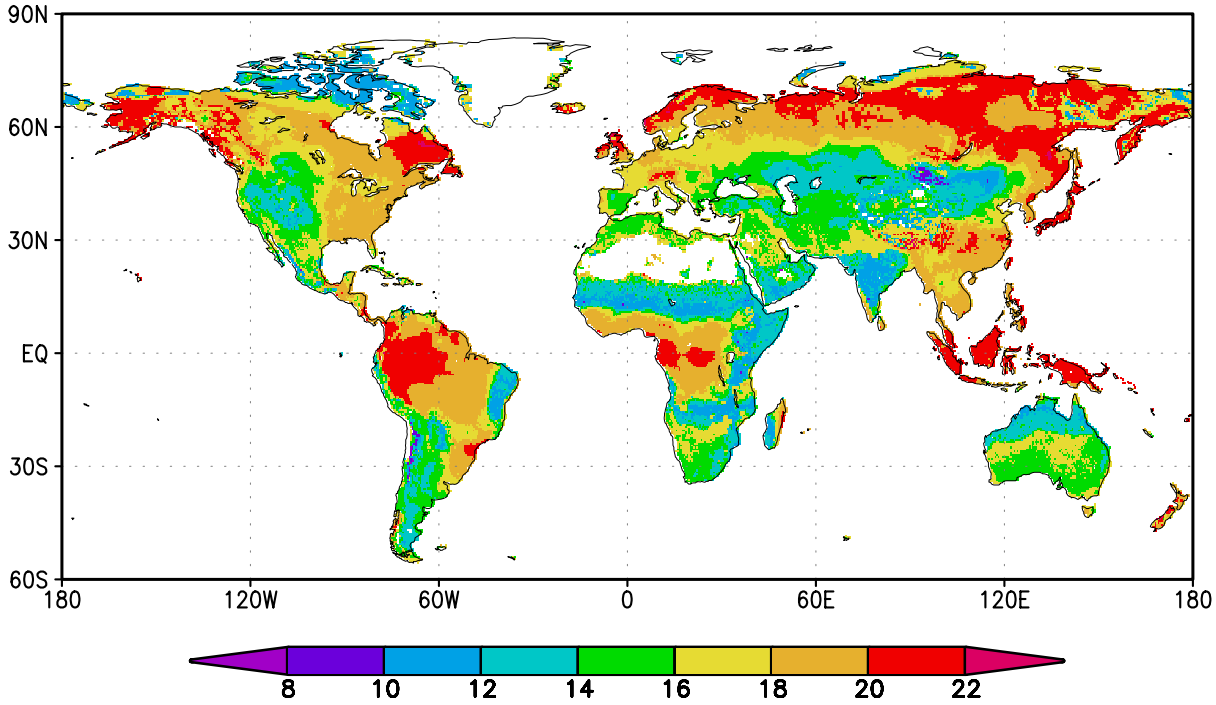

Figure 4.1: Modelled average (1950-1998) annual values for discrimination against ^{13}C during photosynthesis.

reflects the sensitivity of the discrimination to climate conditions in different regions. The water stress induced by decreasing soil moisture and high water vapour pressure deficit controls the stomatal closure and therefore the c_i/c_a ratio, which is the main variable governing the isotope discrimination. Figure 4.1 displays the spatial heterogeneity of the global pattern in the modelled leaf discrimination. The impact of arid climates on discrimination is clearly visible in regions such as central North America and southern South America, Central Asia and in parts also Australia. The influence of C_4 photosynthesis can mainly be seen in the eastern Brazilian grasslands, the African subtropics and the northern region of Australia with discrimination values between 10‰ and 12‰.

The mean globally averaged flux weighted isotopic fractionation $\overline{\epsilon_{ab}}$ over the years 1901-1930 and 1950-1998, the maximum interannual variability of ϵ_{ab}, and of $\Delta^{13}F_{ab}$ are summarized in Table 4.1 for both experiments. The value from the ISOVAR experiment for the years 1950 to 1998 of 17.7‰ is within the range of values from 14.8‰ to 18.6‰ reported in recent studies [Keeling et al., 1989; Tans et al., 1993; Lloyd and Farquhar, 1994; Fung et al., 1997; Kaplan et al., 2001]. Differences arise especially from different amounts of C_4 photosynthesis: while Lloyd and Farquhar [1994] (reported value of 14.8 ‰) prescribe an amount of 25 %, in LPJ less then 10 % of total C is assimilated by C_4 plants, this is partly because of the absence of C_4 land use (pastures and crops). In the ISOFIX experiment, the mean fractionation factor for the period 1950 to 1998 is 17.8‰, almost identical to the ISOVAR experiment.

The interannual variability of ϵ_{ab} in ISOFIX is greatly reduced to 0.1‰ compared to 0.3‰ in

Table 4.1: Mean discrimination for two averaging periods (1901-1930 and 1950-1998) [‰], the max. interannual variability in discrimination [‰], and in $\Delta^{13}F_{ab}$ [PgC ‰ yr^{-1}] for both experiments.

Experiment	specifications		$\overline{\epsilon_{ab}}$	IAVϵ_{ab}	IAV $\Delta^{13}F_{ab}$
ISOVAR	variable fract.	17.40	17.67	0.3	15
ISOFIX	constant fract.	17.72	17.75	0.1	4

ISOVAR as a consequence of the constant fractionation factor (see Figure 4.2). This remaining variability of ≈0.1‰ is entirely caused by changes from C_3 to C_4 plants and their productivity. The long-term trend in discrimination in the ISOVAR experiment could have two possible explanations: first increasing atmospheric CO_2 content changed the c_i/c_a ratio and the discrimination factor, or second a long-term trend in climate had a direct effect on discrimination. In a third experiment with constant climate but variable CO_2, the discrimination factor did not show any trend over the 98 years. Therefore we assume that the trend in the ISOVAR experiment is mainly a climate effect and most likely a response of the plants to increased water stress due to global warming during the 20^{th} century. For the same time period, McGuire et al. [2001] already found a small declining trend in NPP leading to net carbon loss when considering climate only.

Globally averaged time-series of the three terms yielding the temporal variations in atmospheric $\delta^{13}C_a$ from Equation 4.5 and their corresponding CO_2 fluxes (F_{ab} and $F_{bio,net}$, top panel) are plotted in Figure 4.3. The net atmosphere-biosphere flux ($F_{bio,net}$) shows mainly an uptake of C by the land biosphere for the last 50 years, the amount of uptake is comparable to other model studies [McGuire et al., 2001]. Interannual variability in the net flux is related to the variability in the El Niño Southern Oscillation (ENSO) [Keeling et al., 1989]. As $F_{bio,net}$ is the same for both experiments, the values from the first term representing the influence of the net flux (upper middle panel) are almost identical for both experiments. The variability closely follows the variability of the net flux (solid line, top panel).

A secular increasing trend in the terrestrial Suess-Effect from 17.5 PgC ‰ yr^{-1} in 1950 to more than 30 PgC ‰ yr^{-1} in 1998 caused by the invasion of isotopically light anthropogenic CO_2 into the biosphere is simulated (lower middle panel in Figure 4.3). High frequency (interannual) variability is strongly reduced as the ^{13}C entering the terrestrial biosphere is damped in the $\delta^{13}C_b$ emitted from the biosphere because of the relatively long residence time of carbon in the land biosphere. The offset between the two experiments is caused by the difference in the fractionation factor at the beginning of the simulation period as mentioned above. This offset is also seen in the terrestrial ^{13}C soil and litter pools in the latter period of the simulation because of their relatively long time constants for C turnover.

The bottom panel of Figure 4.3 displays $\Delta^{13}F_{ab}$. Calculating $\Delta^{13}F_{ab}$ using the mean global

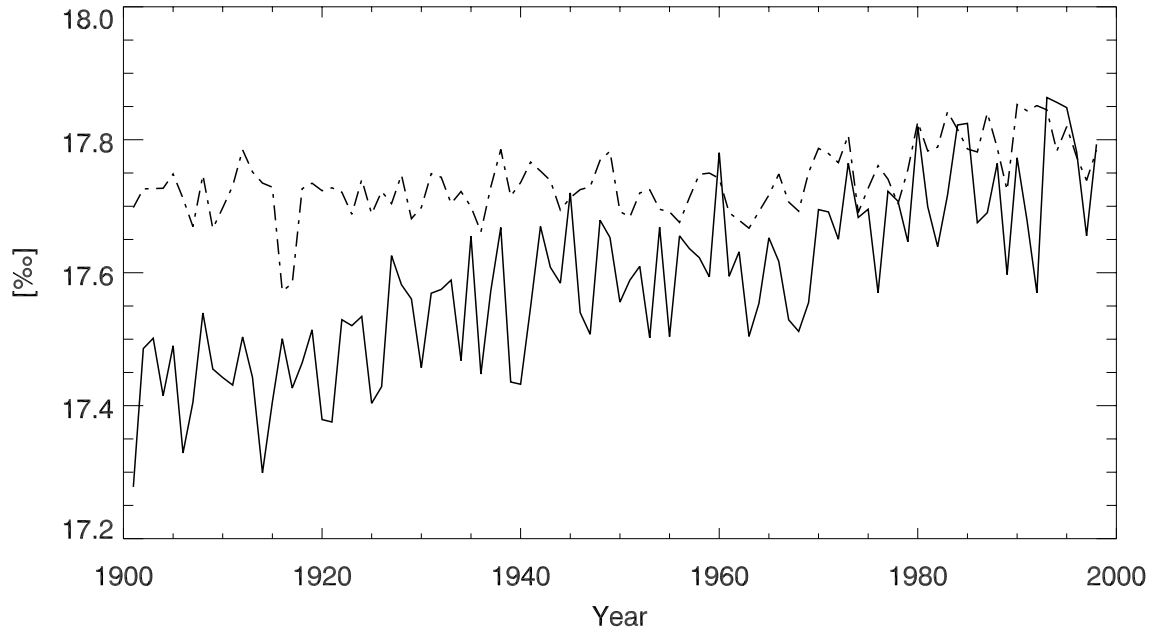

Figure 4.2: Global annual time-series of modelled discrimination against ^{13}C during photosynthesis, solid line ISOVAR and dashed line ISOFIX.

average $\overline{\epsilon_{ab}}$ for the years 1920-1995 gives the magnitude of changes in the ^{13}C fluxes due to climate variability in the fractionation factor ϵ_{ab} opposed to a constant ϵ_{ab}. In Table 4.1 the differences in the interannual variability of $\Delta^{13}F_{ab}$ are summarized. In the ISOFIX experiment the variations are only about 4 PgC ‰ yr^{-1}, whereas the ISOVAR experiment with climatic dependant discrimination exhibits interannual variations up to 15 PgC ‰ yr^{-1}. The difference in the variability in $\Delta^{13}F_{ab}$ between the two experiments is controlled only by the impact of climate variability on isotope discrimination during photosynthesis. In general, interannual variability is especially pronounced during pronounced ENSO events (e.g. 1992/93 and 1997/98). During El Niño years widespread drought conditions lead to a decrease in the isotopic fractionation factor and therefore to a smaller atmosphere to biosphere $^{13}CO_2$ flux.

Using a variable climatic dependent discrimination in double deconvolution studies would certainly lead to a modification of the derived terrestrial sinks. Taking a variable fractionation factor into account we estimate that this could lead to a year-to-year shift of up to 0.8 PgC yr^{-1} in the inferred partitioning between terrestrial and oceanic carbon sinks. In general, a transient decrease in the terrestrial isotopic discrimination factor would imply a corresponding reduction in the inferred terrestrial source by means of a double deconvolution calculation.

4.4 Conclusions

This study demonstrates that large interannual variations in ^{13}C fractionation, induced by anomalous climate events (e.g. ENSO) have a strong impact on the globally integrated ter-

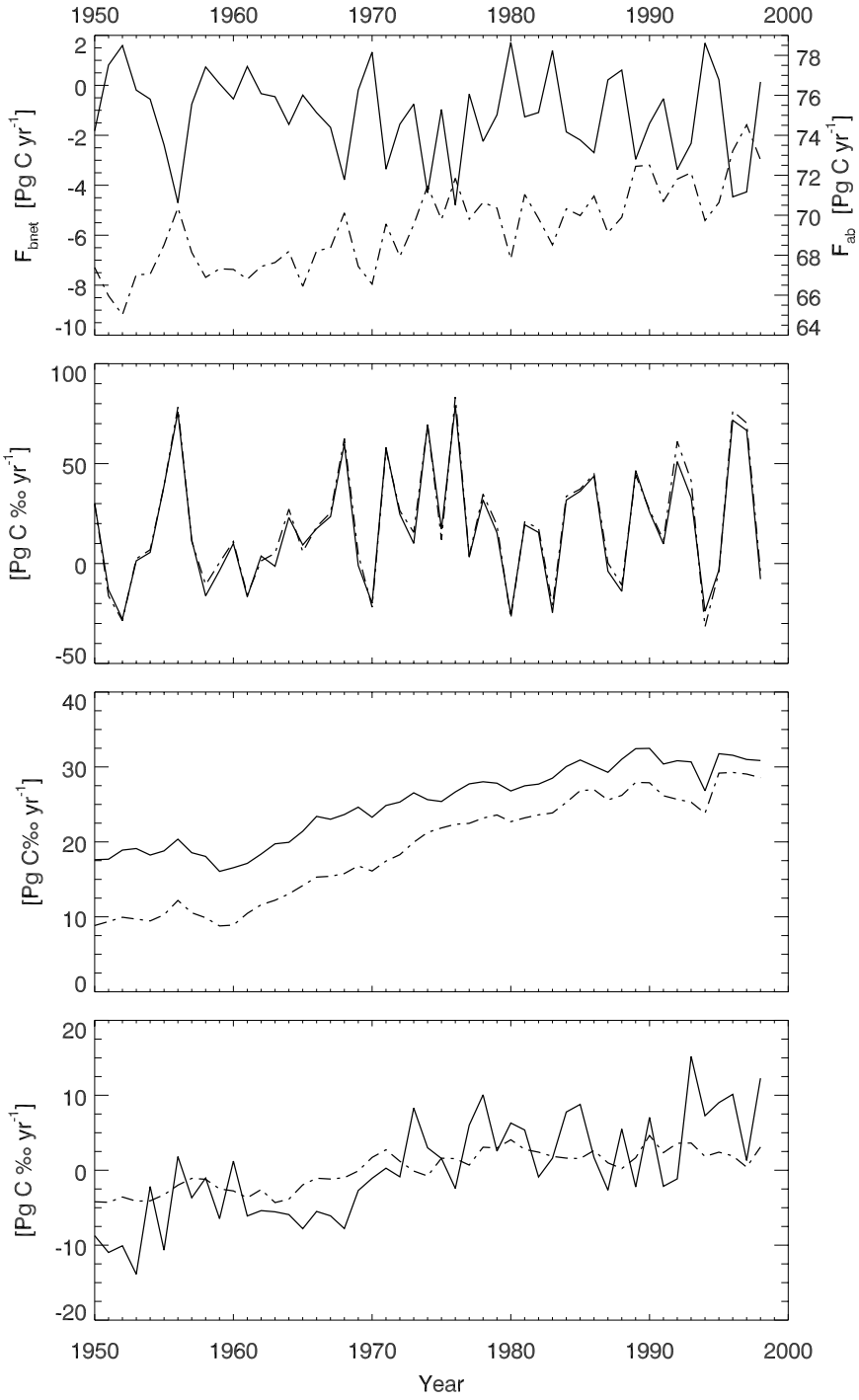

Figure 4.3: Global annual time-series of modelled $F_{bio,net}$ (solid line, negative values indicate net storage in land biosphere) and F_{ab} (dashed line), top panel, and the three terms giving the time dependency of $\delta^{13}C_a$ (see Equation 4.5; in the following: solid ISOVAR and dashed ISOFIX): upper middle panel influence of the net flux (first term), lower middle panel Suess-Effect (second term) and bottom panel $\Delta^{13}F_{ab}$ (third term).

restrial $^{13}CO_2$ fluxes. These fluctuations result primarily from plant physiological responses and to a minor extent from changes in vegetation composition (shifts between C_3 and C_4 plants) induced by climate variations. Ignoring these effects in global double deconvolution studies may result in significant errors in the inferred annual net atmosphere-biosphere flux of up to 0.8 PgC/yr, more than half of the global estimated biospheric sink during the 1990's [Francey et al., 1995]. So far, these simulations do not consider land use change which influences the global discrimination values mainly through tropical C_4 pastures [Townsend et al., 2002] and C_4 crops, e.g. maize cultivation in the northern hemisphere. However, we assume that the effect of land use change on the interannual variability is small compared to the climate effect. Future inverse modeling studies, which may lead to important revision of published carbon budgets for the past two decades, may wish to use the isotope LPJ framework for prescribing variations in terrestrial isotopic discrimination.

References

Battle, M., Bender, M. L., Tans, P. P., White, J. W. C., Ellis, J. T., Conway, T., Francey, R. J., 2000. Global carbon sinks and their variability inferred from atmospheric O_2 and $\delta^{13}C$. Science 287, 2467–2470.

Ciais, P., Tans, P. P., Trolier, M., White, J. W. C., Francey, R. J., 1995. A large northern hemisphere terrestrial CO_2 sink indicated by the $^{13}C/^{12}C$ ratio of atmospheric CO_2. Science 269 (1098-1102).

Ekblad, A., Högberg, P., 2001. Natural abundance of ^{13}C in CO_2 respired from forest soils reveals speed of link between tree photosynthesis and root respiration. Oecologia 127, 305–308.

FAO, 1991. The digitized soil map of the world. No. 67/1. Food and Agriculture Organization of the United Nations.

Francey, R. J., Allison, C. E., Etheridge, D. M., Trudinger, C. M., Enting, I. G., Leuenberger, M., Langenfelds, R. L., Michel, E., Steele, L. P., 1999. A 1000-year high precision record of $\delta^{13}C$ in atmospheric CO_2. Tellus 51B, 170–193.

Francey, R. J., Tans, P. P., Allison, C. E., Enting, I. G., White, J. W. C., Trolier, M., 1995. Changes in oceanic and terrestrial carbon uptake since 1982. Nature 373, 326–330.

Fung, I., Field, C. B., Berry, J. A., Thompson, M. V., Randerson, J. T., Malmström, C. M., Vitousek, P. M., Collatz, G. J., Sellers, P. J., Randall, D. A., Denning, A. S., Badeck, F., John, J., 1997. Carbon 13 exchanges between the atmosphere and biosphere. Glob. Biogeochem. Cycles 11 (507-533).

Heimann, M., Maier-Reimer, E., 1996. On the relations between the oceanic uptake of CO_2 and its carbon isotopes. Glob. Biogeochem. Cycles 10, 89–110.

Joos, F., Bruno, M., 1998. Long-trem variability of the terrestrial and oceanic carbon sinks and the budgets of the carbon isotopes ^{13}C and ^{14}C. Glob. Biogeochem. Cycles 12, 277–295.

Kaplan, J. O., Prentice, I. C., Buchmann, N., 2001. The stable carbon isotope composition of the terrestrial biosphere. In: Geophysical Applications of Vegetation Modeling. J. O. Kaplan, Ph.D. thesis, Lund University, Lund, pp. 89–109.

Keeling, C. D., Bacastow, R. B., Carter, A. F., Piper, S. C., Whorf, T. P., Heimann, M., Mook, W. G., Roeloffzen, H., 1989. A three-dimensional model of the atmospheric CO_2 transport based on observed winds: 1. Analysis of observational data. In: Peterson, D. H. (Ed.), Aspects of Climate Variability in the Pacific and the Western Americas. Vol. 55. AGU, Washington, D.C., pp. 165–236.

Lloyd, J., Farquhar, G., 1994. ^{13}C discrimination during CO_2 assimilation by the terrestrial biosphere. Oecologia 99, 201–215.

Marland, G., Boden, T. A., Andres, R. J., 2001. Global, regional, and national CO_2 emissions. In: Trends: A Compendium of Data on Global Change. Carbon Dioxide Information Analysis Center, Oak Ridge National Laboratory, U.S. Department of Energy, Oak Ridge, Tenn., U.S.A.

McGuire, A. D., Sitch, S., Clein, J., Dargaville, R., Esser, G., Foley, J., Heimann, M., Joos, F., Kaplan, J., Kicklighter, D. W., Meier, R. A., Melillo, J. M., III, B. M., Prentice, I. C., Ramankutty, N., Reichenau, T., Schloss, A., Tian, H., Wittenberg, U., 2001. Carbon balance of the terrestrial biosphere in the twentieth century: Analyses of CO_2, climate and land use effects with four process-based ecosystem models. Glob. Biogeochem. Cycles 15, 183–206.

Mook, W. G., 1986. ^{13}C in atmospheric CO_2. Neth. J. Sea Res. 20, 211–223.

New, M., Hulme, M., Jones, P., 2000. Representing twentieth-century space-time climate variability. Part II: Development of 1901-96 monthly grids of terrestrial surface climate. Journal of Climate 13, 2217–2238.

Prentice, I. C., Farquhar, G. D., Fasham, M. J. R., Goulden, M. L., Heimann, M., Jaramillo, V. J., Kheshgi, H. S., Le Quéré, C., Scholes, R. J., Wallace, D. W. R., 2001. The carbon cycle and atmospheric carbon dioxide. In: Houghton, J. T., Ding, Y., Griggs, D. J., Noguer, M., van der Linden, P. J., Dai, X., Maskell, K., Johnson, C. A. (Eds.), Climate Change 2001: The Scientific basis. Cambridge University Press, Cambridge, U.K., pp. 183–237.

Sitch, S., Prentice, I. C., Smith, B., Arneth, A., Bondeau, A., Cramer, W., Kaplan, J. O., Levis, S., Lucht, W., Sykes, M. T., Thonicke, K., Venevsky, S., 2003. Evaluation of ecosystem dynamics, plant geography and terrestrial carbon cycling in the LPJ dynamic global vegetation model. Global Change Biology 9, 161–185.

Suess, H. E., 1955. Suess effect. Science 122, 415.

Tans, P. P., Berry, J. A., Keeling, R. F., 1993. Oceanic $^{13}C/^{12}C$ observations: a new window on ocean CO_2 uptake. Glob. Biogeochem. Cycles 7, 353–368.

Townsend, A., Asner, G., White, J., Tans, P., 2002. Land use effects on atmospheric ^{13}C imply a sizable terrestrial CO_2 sink in tropical latitudes. Geophys. Res. Lett. 29 (10), 68–1–68–4.

Wittenberg, U., Esser, G., 1997. Evaluation of the isotopic disequilibrium in the terrestrial biosphere by a global carbon isotope model. Tellus 49B, 263–269.

Chapter 5

Modelling terrestrial carbon 13 cycling: climate, land use and fire

Abstract. The isotope LPJ framework, which includes isotopic fractionation of ^{13}C during assimilation and a full isotopic terrestrial carbon cycle, has been used to calculate the atmosphere-biosphere exchange flux of CO_2 and its $\delta^{13}C$ for the years 1901 to 1998. A transient, spatially explicit dataset of C_4 crops and tropical C_4 pastures has been compiled. In combination with a land use scheme this allows the analysis of the impact of land use and C_4 cultivation, besides climate, atmospheric CO_2 and the isotope ratio of atmospheric CO_2, on the terrestrial stable isotope composition. Modelled values of leaf discrimination vary between 17.9‰ and 17.0‰ depending on the chosen land use scheme and also the year of the simulation, with results from the experiment specifying C_4 crops and C_4 pastures being the lowest. Modelled values of isotopic disequilibrium similarly depend on the amount of prescribed C_4 vegetation and vary between 37.9 Pg C ‰ yr^{-1} and 23.9 Pg C ‰ yr^{-1} averaged over the years 1985 to 1995. In addition, the effect of fire on the isotopic disequilibrium has been diagnosed; generally fire leads to a reduction of ≈10 Pg C ‰ yr^{-1}.

5.1 Introduction

Atmospheric CO_2 concentrations are strongly influenced by anthropogenic emissions (combustion of fossil fuel, biomass burning, and cement manufacture). However, only about half of these emissions stay in the atmosphere and cause the increase in atmospheric CO_2, the remainder is taken up by the oceans and terrestrial biosphere. An understanding of the mechanism and also the temporal and spatial patterns of this uptake is of high political and scientific importance in the context of future carbon emissions [Prentice et al., 2001]

Measurements of atmospheric CO_2 and $\delta^{13}C$[1] can be used to estimate carbon sources and sinks by solving for the respective atmospheric budget equations [e.g. Keeling et al., 1989;

[1] $\delta^{13}C$ is calculated as the deviation with respect to a standard: $\delta^{13}C = [\frac{(^{13}C/^{12}C)}{(^{13}C/^{12}C)_{std}} - 1]1000$ ‰

Francey et al., 1995; Ciais et al., 1995; Rayner et al., 1999; Morimoto et al., 2000]. In particular, this 'double deconvolution' method distinguishes between ocean and land fluxes, because of the differences in isotopic fractionation between terrestrial-atmosphere and ocean-atmosphere fluxes. Therefore, the assumed isotopic signature of terrestrial carbon is, among others, one of the sensitive variables in this method.

Due to the heterogeneity and complexity of land ecosystems the terrestrial $^{13}CO_2$ flux field is highly variable in space and time. ^{13}C fractionation during photosynthesis depends on both climatic variability [Scholze et al., 2003; Ito, 2003] and vegetation composition (C_4 plants fractionate ^{13}C to a much smaller extent than C_3 plants) [Kaplan et al., 2002; Scholze et al., 2003]. The $\delta^{13}C$ value of assimilated and respired CO_2 can also be offset by a trend in atmospheric $\delta^{13}C$ since the respired carbon may have been fixed when the $\delta^{13}C$ was different from the current atmosphere, and also that there hence can be a net ^{13}C flux without a net CO_2 flux due to fossil fuel combustion. This isotopic disequilibrium flux is a function of both the rate of change in atmospheric $\delta^{13}C$ and the residence times of carbon in terrestrial ecosystems. Therefore, the $^{13}CO_2$ flux field of the land biosphere is affected by various quantities, e.g. atmospheric $\delta^{13}C$, the age distribution of decomposing organic matter, vegetation composition, and climate [Battle et al., 2000]. The use of atmospheric CO_2 to study the global carbon cycle depends upon both various, accurate measurements of atmospheric $\delta^{13}C$ and the application of models to characterize the terrestrial carbon isotope discrimination in space and time.

Several process-based terrestrial biosphere models have calculated the spatial and seasonal patterns in terrestrial ^{13}C discrimination [Fung et al., 1997; Wittenberg and Esser, 1997; Kaplan et al., 2002]. Recently, two model studies also analysed the impact of climate variability on the ^{13}C fractionation during photosynthesis [Ito, 2003; Scholze et al., 2003]. Land use, especially the conversion of forests into C_4 pastures in the tropics, has also been shown to effect the biosphere-atmosphere $\delta^{13}C$ exchange and therefore, implies a change in the tropical land/ocean carbon sink distribution [Townsend et al., 2002].

Here, the study by Scholze et al. [2003] is extended using the isotope version of LPJ to investigate the impact of climate, ecosystem disturbance (fire), and land use change on the terrestrial carbon isotope discrimination in a consistent terrestrial carbon cycling framework. The outline of this paper is as follows: In Section 5.2 we give a brief description of the model and the experiments. Model validation and results from the experiments are shown and discussed in Section 5.3. A summary and conclusion is given in the last Section 5.4.

5.2 Methodology

5.2.1 The Lund-Potsdam-Jena dynamic global vegetation model

Reported results are based on simulations using the LPJ dynamic global vegetation model [Sitch et al., 2003]. The version of LPJ used here includes terrestrial carbon isotope discrimination. A description of the carbon isotope module within LPJ is given by Scholze et al. [2003]. Only the

main features and the experimental set-up are described.

LPJ combines the simulation of vegetation function (energy absorption, carbon and water cycling calculated daily) and structure (vegetation composition and biomass updated annually). Vegetation composition is described by nine plant functional types (PFT) which are distinguished according to their physiological (C_3, C_4 photosynthesis), morphological (tree, grass), phenological (deciduous, evergreen) and bioclimatic (heat/cold tolerance) attributes.

Vegetation dynamics depends on disturbance, mortality, and establishment, but also on the productivity of the different PFTs. Ecosystem disturbance is modelled as fire events which are calculated based on litter moisture content, a fuel load threshold, and PFT specific fire resistances [Thonicke et al., 2001]. Terrestrial carbon is represented by living tissue (leaves, sapwood, heartwood, and fine-roots), litter (above ground fast and slow, below ground) and soil (intermediate and slow) carbon. The fast and slow litter and the intermediate and slow soil pools are assigned turnover times at 10° C of 2, 20, 33 and 1000 years, respectively. Decomposition rates are soil moisture and soil temperature dependant [Foley, 1995; Lloyd and Taylor, 1994].

Isotopic discrimination during CO_2 photosynthesis is calculated following Lloyd and Farquhar [1994] as a daily average value and depends mainly on the inter-cellular-to-atmospheric CO_2 concentration ratio. Gross photosynthesis and autotrophic respiration are assumed to be in isotopic equilibrium on time scales (longer than seasonal) relevant for this study [Ekblad and Högberg, 2001]. All internal carbon pools are accounted for ^{12}C and ^{13}C separately. As isotope fractionation processes during respiration are poorly understood, no fractionation is assigned for the decomposition. The carbon isotope module used here is based on Kaplan et al. [2002] which has been compared with measurements at various scales (leaf,canopy, and background atmosphere), therefore model results are only briefly compared to measurements. A sketch of the carbon cycling within LPJ is given in Figure 5.1.

In addition to the two experiments described by Scholze et al. [2003] (ISOVAR and ISOFIX) three more experiments are performed (see Table 5.1). All experiments are calculated on a 0.5° spatial resolution using the CRU05 1901-1998 monthly climate (temperature, precipitation and cloud cover) time-series [New et al., 2000]. The time-series of atmospheric CO_2 as described in McGuire et al. [2001] and an extended version of the atmospheric $\delta^{13}C$ time-series of Francey et al. [1999] are used as further input data in all experiments. In the ISOVAR, ISOLU, ISOLUC, and ISOLUCP experiments the ^{13}C fractionation factor is calculated according to the Lloyd and Farquhar [1994] scheme as described above, while for the ISOFIX experiment a constant fractionation factor of -18.7 ‰ for C_3 plants and -4.9 ‰ for C_4 plants (global mean values from the ISOVAR experiment) is prescribed. For all experiments, reported isotopic values are calculated as flux-weighted sums first over time and second over space if applicable.

5.2.2 Land use scheme

The ISOLU simulation follows the land use scheme developed by McGuire et al. [2001]. This land use scheme includes the 1) conversion from natural vegetation to cultivation, 2) production

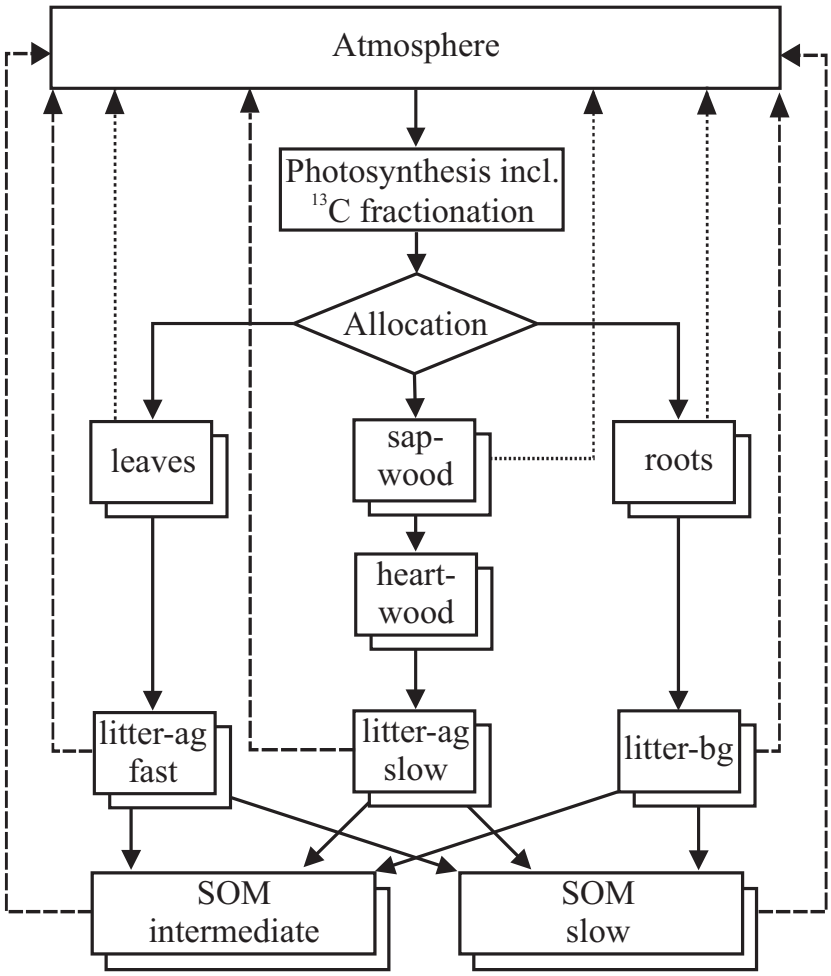

Figure 5.1: Carbon cycling within LPJ: all carbon pools are doubled with respect to ^{13}C, autotrophic respiration (dotted arrows) is assumed to have the same isotopic signature as the photosynthate, while heterotrophic respiration (dashed arrows) is in disequilibrium with carbon uptake.

Table 5.1: Performed LPJ experiments and prescribed input data.

Experiment.	Prescribed
ISOVAR	atm. CO_2 and $\delta^{13}C$, climate
ISOFIX	atm. CO_2 and $\delta^{13}C$, climate, fractionation factor
ISOLU	atm. CO_2 and $\delta^{13}C$, climate, land use, no pastures
ISOLUC	atm. CO_2 and $\delta^{13}C$, climate, land use incl. C_4 crops, no pastures
ISOLUCP	atm. CO_2 and $\delta^{13}C$, climate, land use incl. C_4 crops and C_4 pastures

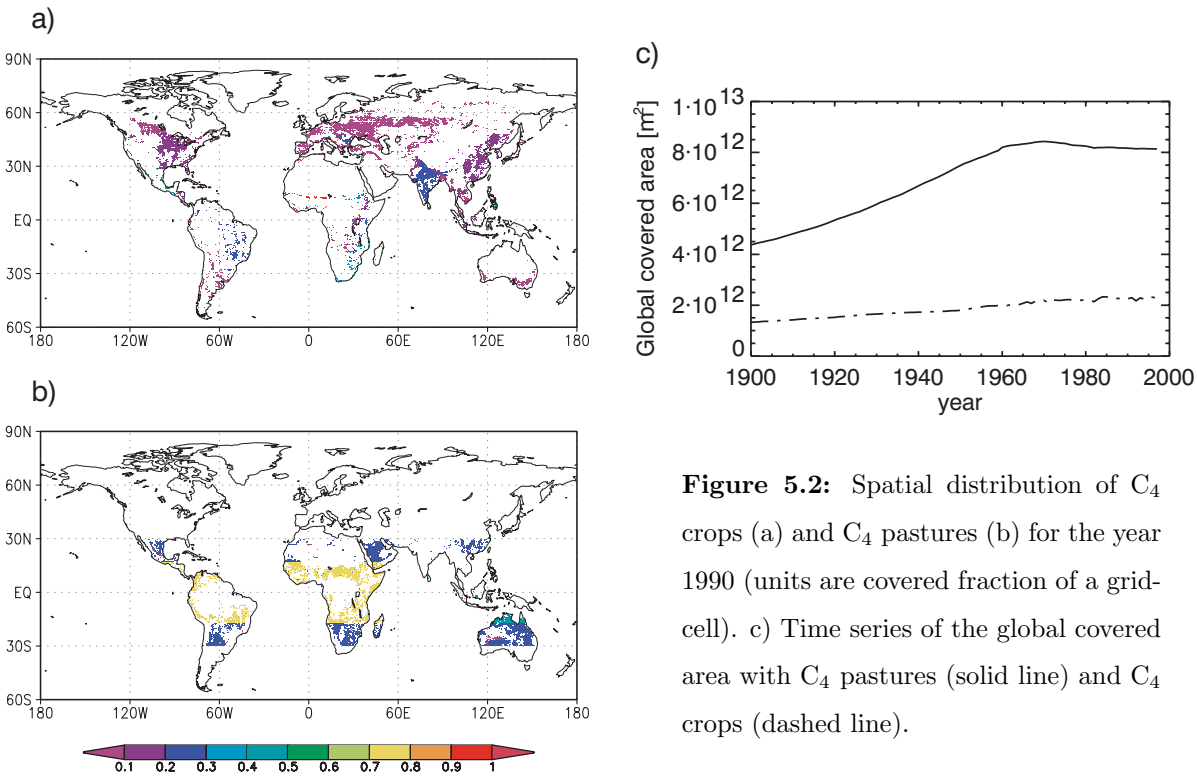

Figure 5.2: Spatial distribution of C_4 crops (a) and C_4 pastures (b) for the year 1990 (units are covered fraction of a grid-cell). c) Time series of the global covered area with C_4 pastures (solid line) and C_4 crops (dashed line).

and harvest at cultivated sites, and 3) the abandonment of cultivated sites. The flux associated with the conversion is simulated as a release of CO_2 due to the clearing (burning of slash, fuelwood). Harvested biomass from cultivated sites is decayed to the atmosphere from three product pools with different residence times based on their uses: 1 year (agricultural products), 10 years (paper products), and 100 years (lumber products). If a previously cultivated site has been abandoned the model is allowed to grow back natural vegetation and biomass from the current state at the time of abandonment. The locations of cultivated sites and their conversion and abandonment years are derived from the historical (1700 to 1992) fractional croplands dataset of Ramankutty and Foley [1999] which has been transformed to a boolean croplands data set preserving total cropland area at a 5° gridcell level. Thus, a 0.5° model gridcell is either agricultural or natural. Between 1993 and 1998 the agricultural state of 1992 has been used. The net primary productivity (NPP) of cultivated sites is estimated using the relative agricultural productivity (RAP) approach [Esser, 1995]. The RAP data set defines the agricultural productivity relative to the productivity of the natural vegetation on a country specific basis. Therefore, no changes are made to the simulated vegetation cover.

In addition to the general land use scheme applied in the ISOLU simulation, the temporal and spatial extent of C_4 crops (corn, sugar cane, millet, and sorghum) has been prescribed in the ISOLUC experiment in order to calculate the influence of C_4 crops on the terrestrial isotopic signature. A country specific dataset of the area covered with C_4 crops has been compiled from the FAO [2002] database for the years 1961 to 1998. This area in each country is then transformed into a fraction covered by C_4 crops of a 0.5° gridcell by dividing the C_4 crop area

with the total crop area given by Ramankutty and Foley [1999] for each country using a gridded (0.5° resolution) political map of the world. In a very few cases (less than 1% of the gridcells covered with C_4 crops) the C_4 crop fraction is higher than one because the Ramankutty and Foley [1999] map gets less area covered with crops than the FAO [2002] C_4 crop dataset (e.g. gridcells located in Eritrea, Congo or Benin). In these cases the C_4 crop fraction is then set to one. The mean ratio over the years 1961 to 1970 of C_4 crop area to total crop area per country has been used to calculate the fractional C_4 crop coverage for the years 1901 to 1960 using the Ramankutty and Foley [1999] dataset. Figure 5.2a displays a snapshot of C_4 crop extent in the year 1990 and Figure 5.2c shows the time series of the global area covered by C_4 crops. A similar map of C_4 vegetation including also the global C_4 crop distribution has been compiled by Still et al. [2003]. However, their map represents a static picture of the C_4 vegetation distribution, whereas for this study also the temporal evolution is of importance.

To analyse the impact of expanding tropical C_4 pastures on ecosystem isotope discrimination, tropical C_4 pastures as well as the above described C_4 crops have been specified in the ISOLUCP simulation. Global pasture area extent from 1700 to 1990 is taken from the HYDE database [Klein Goldewijk, 2001; Klein Goldewijk and Battjes, 1997] with a 0.5° spatial and 10 year temporal resolution. This dataset has been linearly interpolated between the 10 year steps to obtain a pasture dataset on a yearly time basis. In addition to the HYDE data, global pasture area per country from the FAO [2002] database covering the period 1961 to 1998 has been spatialized on a 0.5° grid using the same method as described above for the C_4 crops with the pasture maps from the HYDE database and keeping the spatial distribution constant after 1990. The amount of C_4 plants in tropical pastures is specified according to Townsend et al. [2002]: 80% of the pasture area is covered by C_4 plants in a zonal band from 17° S to 17° N in South America and Africa while only a value of 50% is assumed in this zonal band in Asia due to rice cultivation. In the area covered in the latitudinal band from 30°S to 17° S and 17° N to 30° N 30% of the pasture area is assumed to be covered by C_4 plants; south of 30° S and north of 30° N pastures are dominated by C_3 plants. A snapshot of the C_4 pasture extent from the year 1990 is shown in Figure 5.2b and the time series of the global area covered by C_4 pastures in Figure 5.2c.

In order to simulate C_4 land use in LPJ the fraction of the gridcell covered by C_4 crops and C_4 pastures is modelled using the C_4 grass PFT; in the remaining area of the gridcell LPJ simulates its own vegetation composition based on competition and the bioclimatic limits of the PFTs. Carbon 13 is treated the same way as total carbon in land-use gridcells, i.e. for each of the three total carbon land-use product pool exists a respective ^{13}C pool for separate accounting.

5.2.3 Isotopic disequilibrium

The isotopic disequilibrium flux from the terrestrial biosphere is given by [e.g., Joos and Bruno, 1998]

$$D_b = F_{ba}[(\delta^{13}C_a + \epsilon_{ab}) - \delta^{13}C_{resp}] \tag{5.1}$$

where F_{ba} is the CO_2 flux from the land biosphere to the atmosphere (ecosystem respiration R_{eco} which is the sum of the modelled heterotrophic respiration and fire emission or in case of the land use experiments also the agricultural decay fluxes), and $\delta^{13}C_{resp}$ is the isotopic ratio of this flux. $\delta^{13}C_a$ is the isotopic ratio of atmospheric CO_2 and ϵ_{ab} the fractionation factor during CO_2 assimilation. The isotopic disequilibrium is then given by the difference between the isotopic ratios of the uptake flux and of the ecosystem respiration:

$$\mathcal{D}_b = (\delta^{13}C_a + \epsilon_{ab}) - \delta^{13}C_{resp} = \delta^{13}C_{leaf} - \delta^{13}C_{resp} \tag{5.2}$$

The $\delta^{13}C_{resp}$ of the modelled ecosystem respiration is calculated as the flux-weighted mean of the isotopic ratios of the heterotrophic respiration and of the biomass burning flux:

$$\delta^{13}C_{resp} = \frac{\delta^{13}C_{R_h}R_h + \delta^{13}C_{fire}F_{fire}}{R_h + F_{fire}} \tag{5.3}$$

or in case of the land use experiments as:

$$\delta^{13}C_{resp} = \frac{\delta^{13}C_{R_h}R_h + \delta^{13}C_{fire}F_{fire} + \delta^{13}C_{prod}F_{prod} + \delta^{13}C_{conv}F_{conv}}{R_h + F_{fire} + F_{prod} + F_{conv}} \tag{5.4}$$

where F_{prod} and F_{conv} are the carbon fluxes due to the decay of the product pools and due to the conversion from natural vegetation to cultivation, respectively. $\delta^{13}C_{prod}$ and $\delta^{13}C_{conv}$ are the respective isotopic ratios of these fluxes. F_{fire} is the carbon flux to the atmosphere due to biomass burning and $\delta^{13}C_{fire}$ its isotopic ratio.

Fire emissions are calculated from the burnt biomass of leaf foliage, woody tissue and the above-ground litter pool. The isotopic signature of the biomass burning is computed as the flux-weighted mean of the isotopic ratios of the respective pools. These pools contain carbon which is younger than the carbon of the soil pools in the sense of the time past since assimilation. Due to the change in $\delta^{13}C_a$ from fossil fuel burning the fire flux is therefore more depleted in ^{13}C than the heterotrophic respiration flux and thus, reduces the isotopic disequilibrium. To quantify the influence of the fire flux on the isotopic disequilibrium $\delta^{13}C_{resp}$ is calculated by replacing $\delta^{13}C_{fire}$ with $\delta^{13}C_{R_h}$ in Equation 5.3. Thus, the amount of the total ecosystem respiration flux is not changed by assuming that the missing biomass burning flux is compensated by an increased heterotrophic respiration and therefore, changing the isotopic signature of the ecosystem respiration as $\delta^{13}C_{fire}$ and $\delta^{13}C_{R_h}$ usually have different values. These results are purely diagnostic and denoted under the 'ISOVAR without fire' experiment.

5.3 Results and Discussion

5.3.1 Net terrestrial carbon fluxes

Net carbon exchange (NCE) is calculated as:

$$NCE = R_h + F_{fire} - NPP \tag{5.5}$$

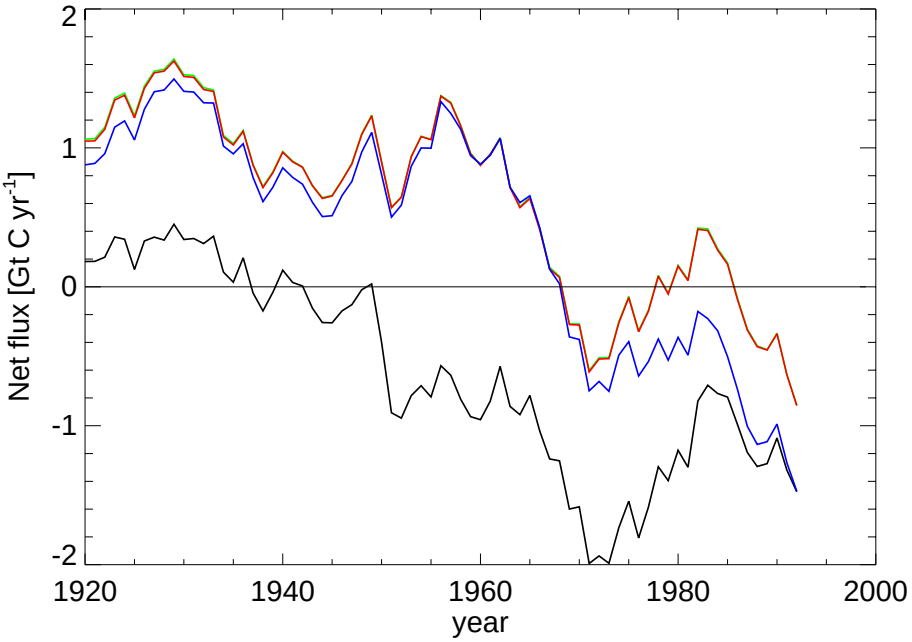

Figure 5.3: Simulated 10-year running means of the global terrestrial net carbon exchange between 1920 and 1992 (positive values indicate net release to the atmosphere). Colours represent: black ISOVAR, green ISOLU, red ISOLUC and blue ISOLUCP.

or in the case of the land use experiments as:

$$NCE = R_h + F_{fire} + F_{prod} + F_{conv} - NPP \tag{5.6}$$

The total terrestrial net carbon fluxes as simulated by the ISOVAR and ISOLU experiment have already been discussed in detail by McGuire et al. [2001] (the ISOVAR experiment corresponds to their S2 simulation and the ISOLU experiment to their S3 simulation). Results of the net fluxes presented here are slightly different than the values reported by McGuire et al. [2001] as the climate input data is not exactly the same. However, the relative differences among the various experiments of the two studies (McGuire et al. [2001] and this) are comparable. In Figure 5.3 smoothed global records of net carbon exchanges for the different experiments from this study are shown. As already discussed by McGuire et al. [2001] the net carbon exchange substantially changed from neutral (ISOVAR) or release (land use experiment) to storage of carbon after 1970. The storage seems to be associated with both the CO_2 fertilization effect (as seen in the ISOVAR experiment) and for the land use experiments also with the deceleration in the expansion of croplands and therefore the decline in the CO_2 release from land use conversion which peaked around 1950.

McGuire et al. [2001] estimated a mean annual release of carbon to the atmosphere between 1980 and 1989 of 0.9 petagrams (10^{15}g) of carbon per year (Pg C yr^{-1}) due to the inclusion of land use. Here, the effect of land use on the total (^{12}C+^{13}C) terrestrial carbon budget results into a slightly larger release of 0.96 Pg C yr^{-1} to the atmosphere (mean net carbon exchange of -0.7

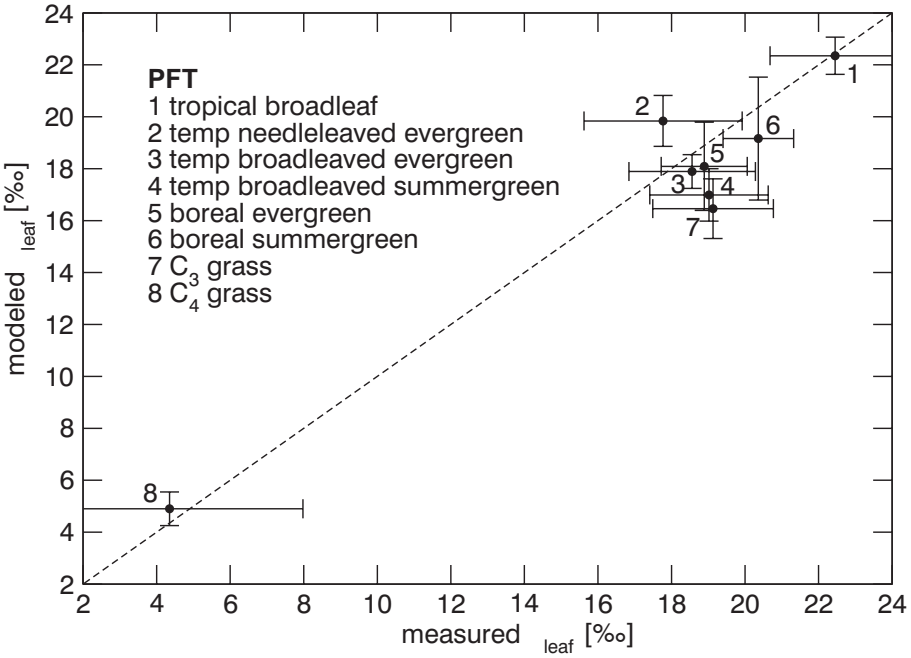

Figure 5.4: Modeled and measured leaf carbon isotope discrimination Δ_{leaf}. Error bars represent one standard deviation around the mean.

Pg C yr^{-1} for the ISOVAR experiment compared to 0.26 Pg C yr^{-1} for the ISOLU experiment, McGuire et al. [2001] report a total value of 0.3 Pg C yr^{-1} for their S3 simulation). The addition of C_4 crops to the land use scheme (ISOLUC simulation) yields a mean net carbon exchange of 0.25 Pg C yr^{-1} over the years 1980 to 1989 which is almost no change in the terrestrial carbon budget as compared to the ISOLU experiment. Including also tropical C_4 pastures leads to a mean storage of 0.65 Pg C yr^{-1} for the years 1980 to 1989 and thus, gives a total net carbon exchange of -0.4 Pg C yr^{-1} for this time period (ISOLUCP). However, the storage capacity in the ISOLUCP experiment is mainly apparent during the years 1970 until 1998, in the years before there is almost no difference to the ISOLU and ISOLUC experiment. Figure 5.2c shows that from 1970 onwards the global area of tropical C_4 pastures is slightly decreasing and therefore former grazing areas are reconverted to forests which leads to this additional terrestrial carbon storage.

5.3.2 Discrimination during photosynthesis

Comparison with measurements

Results from the ISOVAR simulation are compared with measurements of isotope discrimination at the leaf level during photosynthesis (denoted as Δ_{leaf}). Figure 5.4 displays simulated monthly mean ^{13}C discrimination values during photosynthesis versus measurements of leaf discrimination (data compiled by Buchmann and Kaplan [2001]) at PFT level. Agreement between simulated and measured values is good: results correspond for almost all PFTs within one stan-

dard deviation ($\approx 2‰$). Variations in Δ_{leaf} among the C_3 PFTs is of the order of 6‰ for the simulated and slightly less for the measured values. This variability reflects the diversity in discrimination among different plant types and is well captured by LPJ.

Impact of land use on leaf discrimination

The spatial pattern in annual leaf discrimination (mean over the years 1985 to 1995) is illustrated in Figure 5.5 for potential natural vegetation (ISOVAR), for vegetation including C_4 crops (ISOLUC) and for vegetation including both C_4 crops and C_4 pastures (ISOLUCP). There is almost no difference in the spatial distribution between the ISOVAR, ISOFIX and ISOLU experiments. The heterogeneity reflects the effect of arid environments and PFT distribution; lowest values in discrimination occur in very dry climatic regions (e.g. Central Asia) or in regions with a high amount of C_4 plants (Brazilian grasslands, subtropical Africa and northern Australia). High leaf discrimination values can be found in very humid environments such as the tropical rain forest or the boreal forest. In contrast to the natural vegetation the spatial distribution of Δ_{leaf} for land use vegetation shows the importance of specifying C_4 crops (the North American corn belt, south eastern Europe, the Indian subcontinent and Southeast Asia) and C_4 pastures (South America, Africa and also Australia) especially in regions where the natural vegetation is forest. Globally flux-weighted annual leaf discrimination averaged over the years 1982 to 1992 varies between 17.58‰ for the ISOVAR experiment and 17.04‰ for the ISOLUCP experiment (see Table 5.2), a reduction of more than 0.5‰ in the global value because of C_4 land use. These values lie well within the range of values from other studies: 14.8‰ [Lloyd and Farquhar, 1994] to 18.2‰ [Ito, 2003]. Lloyd and Farquhar [1994] probably over-emphasize the importance of C_4 photosynthesis and report therefore the lowest discrimination value. Still et al. [2003] found a global discrimination value of 16.5‰ considering also C_4 crops which is less than the 17.07‰ from the ISOLUCP simulation. Kaplan et al. [2002] (18.6‰) and Bakwin et al. [1998] (16.8‰) report global ecosystem discrimination (see Equation 5.7) values which are comparable to 17.8‰ from the ISOVAR experiment.

The impact of a climatic dependant discrimination during CO_2 assimilation on inverse methods to quantify terrestrial carbon fluxes has already been discussed by Scholze et al. [2003]. The interannual variability in the ISOFIX experiment is reduced by approximately a factor of three as compared to the ISOVAR simulation. As can be seen from Figure 5.6 the magnitude and the pattern of the interannual variability in the flux weighted global leaf discrimination does not change much in the land use experiments as compared to the ISOVAR experiment. However, the total magnitude of the discrimination is reduced substantially in the ISOLUCP experiments with prescribed C_4 crops and C_4 pastures. The long-term increasing trend which is apparent in the ISOVAR, ISOLU and ISOLUC simulations is due to climatic effects [Scholze et al., 2003]. The specification of C_4 pastures in the ISOLUCP simulation seems to compensate this trend by the higher amount of low C_4 plant discrimination values.

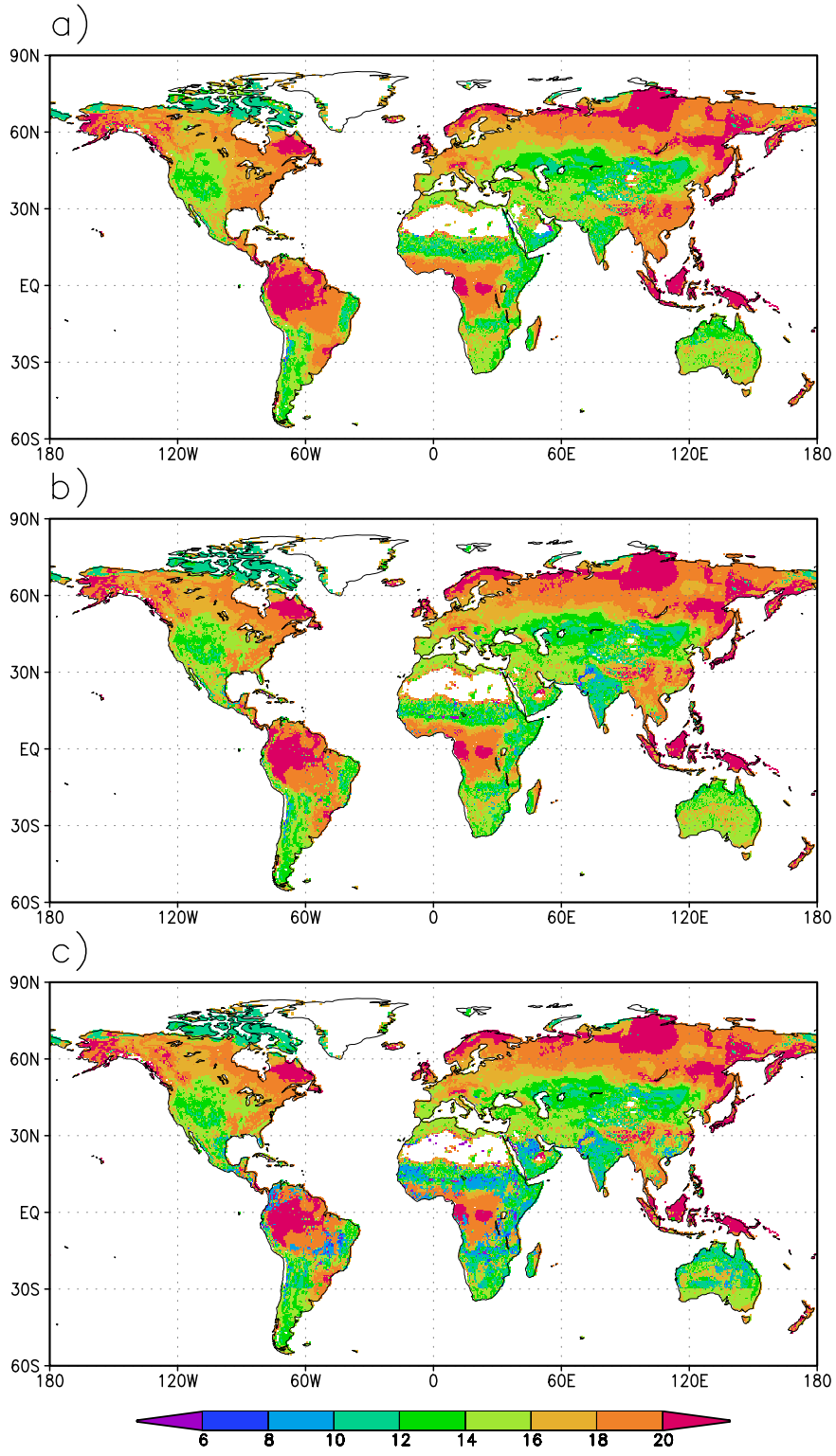

Figure 5.5: Modelled annual leaf discrimination for (a) potential natural vegetation (ISOVAR), (b) vegetation including C_4 crops (ISOLUC), and (c) including C_4 crops and C_4 pastures (ISOLUCP). Units are ‰.

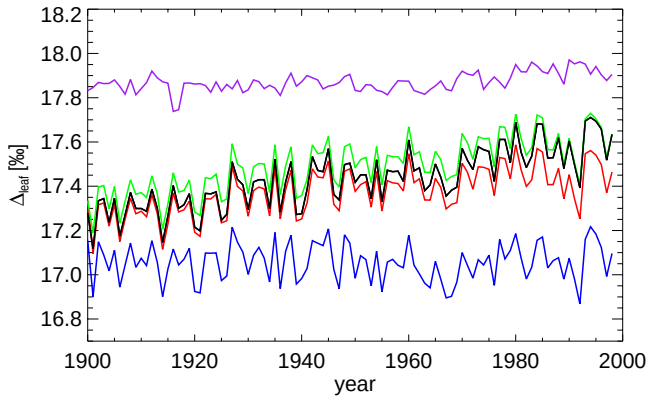

Figure 5.6: Time series of modeled carbon isotope discrimination Δ_{leaf}. Colours represent: black ISOVAR, purple ISOFIX, green ISOLU, red ISOLUC and blue ISOLUCP.

Spatial variance of leaf discrimination

The standard deviation of the spatially explicit modeled discrimination illustrates areas with high temporal variability in the discrimination. In order to account for areas with high variability in the fractionation factor due to changes in the presence and non-presence of PFTs in these regions (e.g., borders of deserts where gross CO_2 fluxes are also small), Figure 5.7 shows the product of the standard deviation with the mean NPP for the years 1950 to 1998. The displayed quantity is the standard deviation of an isoflux, but only with the variability of the discrimination contributing to it. Areas with high values in Figure 5.7a such as Central America, the subtropics in Africa, India, and parts of Southeast Asia are the transition zones between tropical and subtropical climate. This variability is mainly due to the interannual variations in the C_3/C_4 plant distribution and thus, the relative amount of C_4 productivity compared to C_3 productivity per gridcell. Figure 5.7b shows the difference between the ISOVAR and ISOFIX experiment in the standard deviation of this isoflux. This difference illustrates regions with a high variability in the fractionation factor of C_3 plants imposed by climate variability directly. The dominant areas here are mainly the temperate zones (North America, Europe, eastern Asia) and parts of the tropics. The rather low variance in the tropics is consistent with the low variance in modelled leaf discrimination for tropical PFTs (see Figure 5.4). However, as the measured variance for tropical PFTs is much higher it seems that the sensitivity of the ^{13}C discrimination during photosynthesis against climate is underestimated for the tropical PFTs in the model.

5.3.3 Ecosystem discrimination and isotopic disequilibrium

Comparison with measurements

In Figure 5.8 the simulated flux-weighted zonal mean ecosystem discrimination from the ISOVAR experiment is compared with measurements of ecosystem discrimination (Δ_e). Δ_e is an integrated signal of the ^{13}C signature of ecosystem CO_2 exchange with the atmosphere (see Buchmann et al. [1998] for the concept of ecosystem discrimination). Modeled ecosystem discrimination is calculated as the flux weighted difference (respecting the sign of the fluxes) in

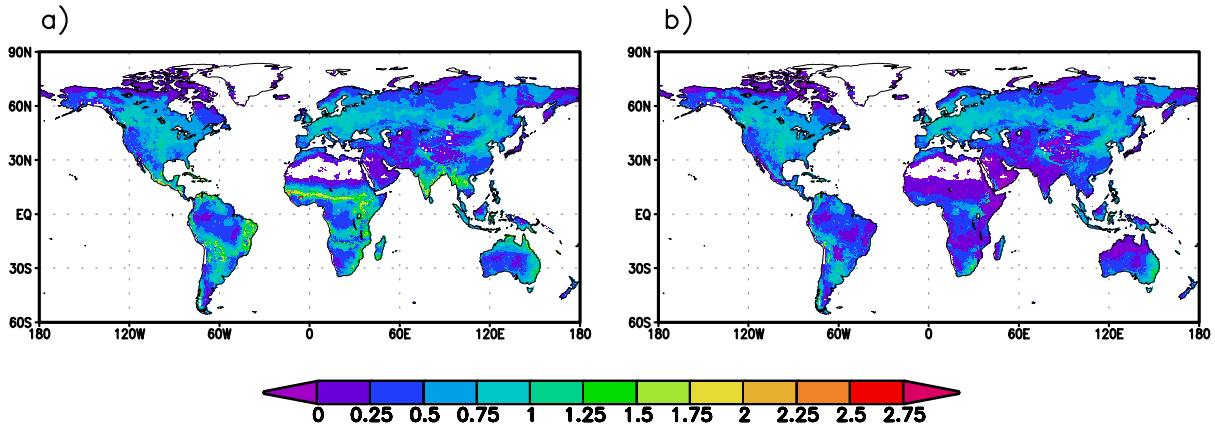

Figure 5.7: Standard deviation of Δ_{leaf} multiplied by the mean NPP (similar to an isoflux) for the years 1950 to 1998 (a) for the ISOVAR experiment and (b) for the difference between ISOVAR and ISOFIX. Units are kg C ‰ m^{-2} yr^{-1}.

isotopic discrimination from NPP and ecosystem respiration (R_{eco}):

$$\Delta_e = \frac{\Delta_{leaf} NPP - \Delta_{resp} R_{eco}}{NPP - R_{eco}} \tag{5.7}$$

Maximum Δ_e values can be found close to the equatorial tropics and the boreal regions due to the high photosynthetic ^{13}C discrimination values of tropical and boreal forests. The wide range of Δ_e values within areas dominated by C_3 vegetation (≈16‰ to 21‰) demonstrate the changing water availability for the plants and their adaptation to arid environments. The lowest values for modeled Δ_e can be found in the subtropics because of the relatively high amount of C_4 plants but also at latitudes around 40° N due to the rather arid climate there which leads to a reduced transpiration of C_3 plants. Measurements of ecosystem discrimination of natural vegetation (data also compiled by Buchmann and Kaplan [2001]) agree well with the simulated values of Δ_e at various latitudes and are almost always lying within the range of one standard deviation in the temporal variations around the simulated mean.

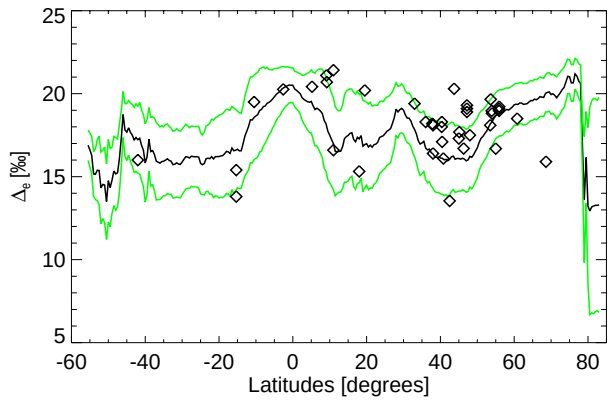

Figure 5.8: Simulated flux-weighted latitudinal ecosystem discrimination (line) from the ISOVAR simulation averaged over the years 1950 to 1998 and measured ecosystem discrimination (symbols). Green lines represent one temporal standard deviation around the simulated mean.

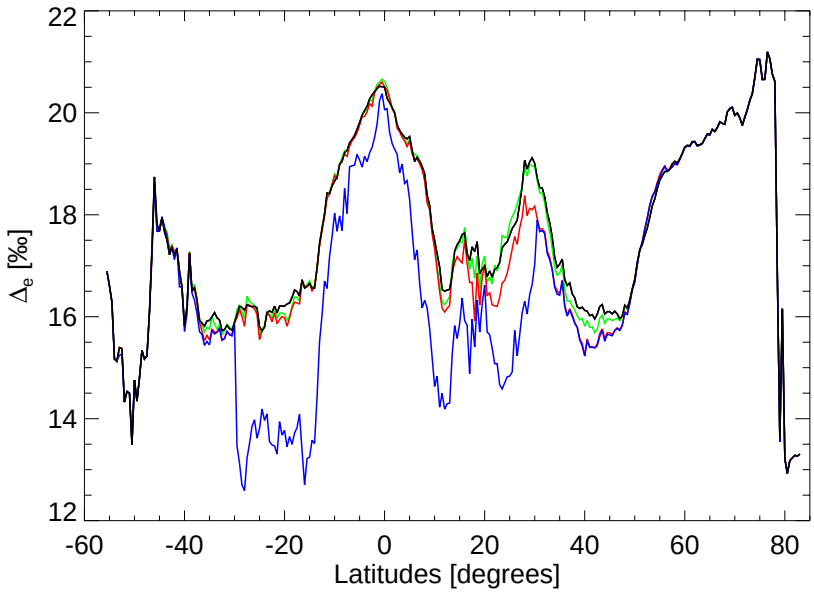

Figure 5.9: Simulated flux weighted latitudinal ecosystem discrimination averaged over the years 1950 to 1998. Colours represent: black ISOVAR, brown ISOVAR without fire, green ISOLU, red ISOLUC and blue ISOLUCP

Table 5.2: Simulated mean global flux-weighted leaf discrimination, isotopic disequilibrium $\mathcal{D}_b$, isotopic disequilibrium flux D_b, and total ecosystem respiration flux F_{resp} which is the sum of heterotrophic respiration and fire flux or in the case of the land use experiments the sum of heterotrophic respiration, fire, conversion and agricultural productivity flux for the period 1982-1992. The isotopic disequilibrium values for the ISOVAR without fire row are purely diagnostics and as fire has no influence on the leaf discrimination no values are diagnosed

Experiment	Δ_{leaf} [‰]	$\mathcal{D}_b$ [‰]	D_b [Pg C ‰ yr^{-1}]	F_{resp} [Pg C YR^{-1}]
ISOVAR	17.58	0.49	34.8	69.4
ISOVAR without fire		0.63	44.7	69.4
ISOFIX	17.93	0.45	31.5	69.4
ISOLU	17.58	0.46	29.1	64.3
ISOLUC	17.42	0.41	28.5	64.5
ISOLUCP	17.04	0.35	20.7	62.7

Impact of land use on ecosystem discrimination

The land use scheme without specifying C_4 crops and C_4 pastures (ISOLU simulation) has a negligible effect on the latitudinal variations in ecosystem discrimination (Figure 5.9). However, specifying C_4 crops (ISOLUC experiment) clearly reduces ecosystem discrimination in the northern hemisphere between 15° N to 50° N by about 1.5‰ (North American corn belt, European and Asian C_4 agriculture). The highest reduction of almost 3‰ in Δ_e occurs in a latitudinal band between 30° S and 17° S as modelled in the ISOLUCP experiment reflecting the influence of extensive grazing areas in South America, South Africa and Australia which here are assumed to consist only of 30% C_4 plants. Although the specified fraction of C_4 pastures for the inner tropics (17° S to 17° N) is much higher than for the outer tropics (80% compared to 30%, see Figure 5.2c), the reduction in ecosystem discrimination is significantly less (but still a reduction of ≈1‰ in Δ_e) because the higher discrimination values of the tropical forest PFTs and their greater productivity in comparison to the tropical C_4 pastures.

Modelled isotopic disequilibrium

In all experiments, the average flux-weighted isotopic disequilibrium ($\mathcal{D}_b$) over the years 1985 to 1995 exhibits a high spatial variability Figure 5.10). In general, $\mathcal{D}_b$ values are high, around 1‰ to 1.5‰, in regions where the turnover time of soil carbon is large (northern hemisphere boreal forests), whereas low $\mathcal{D}_b$ values, around 0‰, can be found in areas with a high amount of herbaceous vegetation as turnover times are usually higher for grasslands than for forests. This is in agreement with the findings of Fung et al. [1997], they report low values of ≈0.2‰ for grasslands and deserts and high values of more than 0.5‰ for boreal forests.

Fire has an important impact on the spatial pattern of the isotopic equilibrium; regions where LPJ simulates a high fire frequency, usually dry areas with enough biomass to sustain frequent fires such as the American grasslands, subtropical Africa, parts of India and Australia, have a much lower (a difference of ≈1‰) isotopic disequilibrium in the ISOVAR simulation than in the ISOVAR without fire experiment. Only natural fire events are modelled in LPJ, therefore areas with a high amount of anthropogenic biomass burning such as Southeast Asia are almost not effected.

C_4 land use both crops and pastures have a distinct influence on $\mathcal{D}_b$, especially in areas where forest is converted to C_4 crops or C_4 pastures. After the conversion the ecosystem respiration still carries the isotopic signal of the C_3 forest whereas the assimilation flux has the much lower isotopic signature of C_4 plants. Thus, a recently cleared grazing or crop area has a negative disequilibrium value as compared to an old pasture where the C_3 fraction of ecosystem respiration has already declined (Figure 5.11). Low isotopic discrimination values (around 0‰) due to C_4 land use can be found in the North American corn belt, South American grazing areas (Brazil and Argentina), South Africa and in parts of Europe and Southeast Asia.

Mean modelled values of the global flux-weighted isotopic disequilibrium and the disequilibrium flux and the corresponding ecosystem respiration fluxes averaged over 1982–1992 are

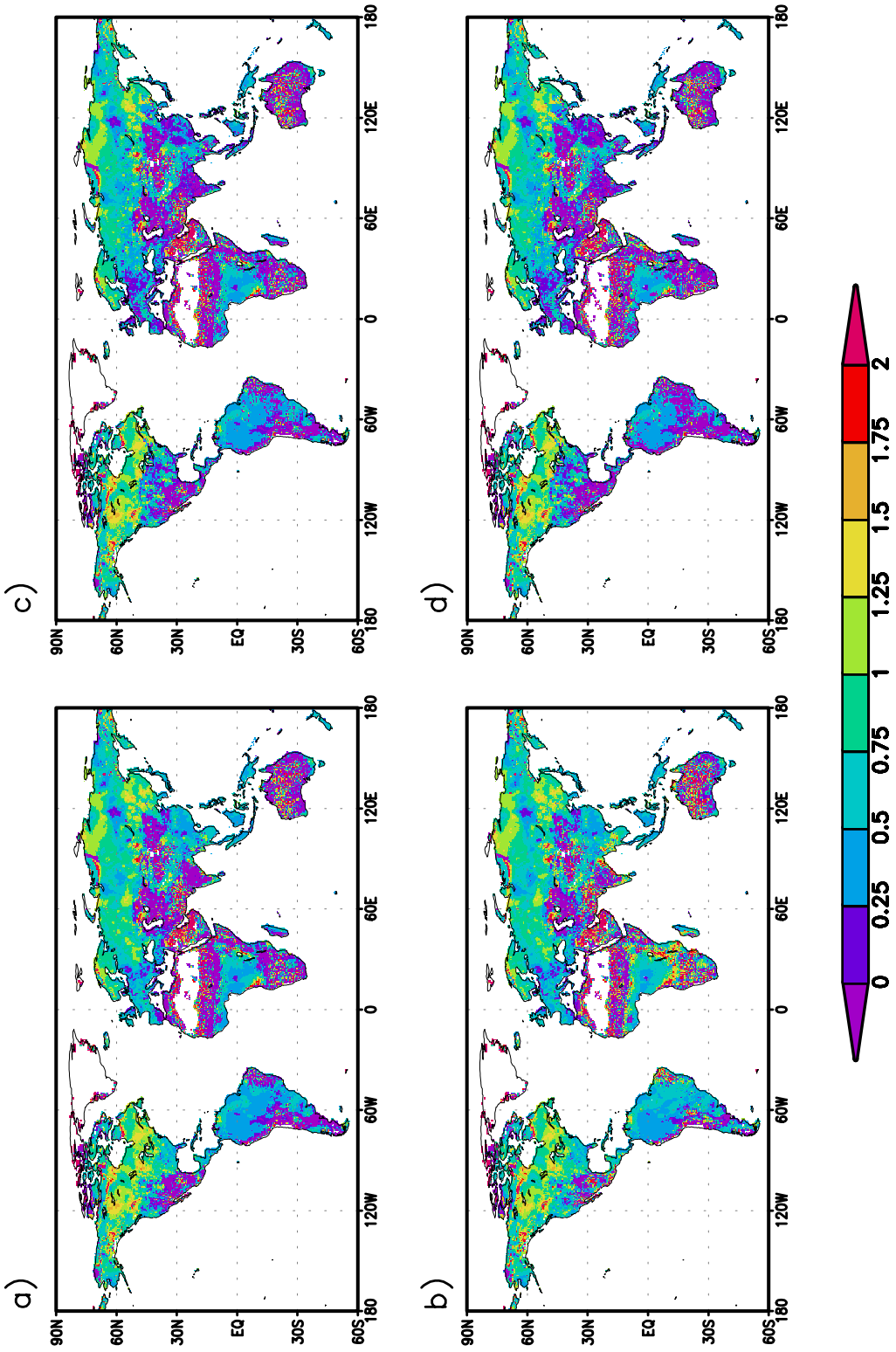

Figure 5.10: Spatial pattern of the mean flux-weighted isotopic disequilibrium over the years 1985 to 1995 for (a) ISOVAR, (b) ISOVAR without fire,(c) ISOLUC, and (d) ISOLUCP experiment.

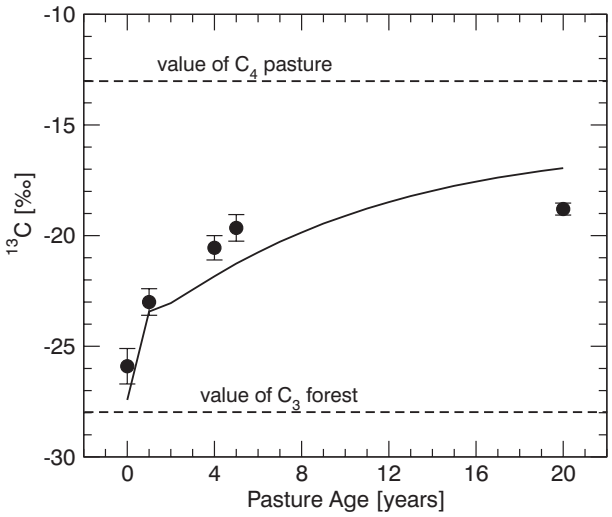

Figure 5.11: Modelled isotopic ratio of heterotrophic respiration after clearance of C_3 forest to C_4 pasture. Data points are from a field site in Costa Rica Townsend et al. [2002]. Note that the temporal resolution of modelled values is one year.

presented in Table 5.2. An increasing trend in $\mathcal{D}_b$ through time (see Figure 5.12) due to the change in the atmospheric isotopic ratio from intensified fossil fuel burning is clearly visible (0.34‰ for the period 1962–72 compared to 0.49 ‰ for the period 1982–92 as simulated in the ISOVAR experiment). These results lie well within values reported elsewhere (e.g., 0.56 ‰ by Ciais et al. [1999]), see Table 5.3 for a comparison with other studies. Furthermore, modelled global values of the isotopic disequilibrium differ considerably among the different experiments: while the ISOVAR without fire experiments yields the highest $\mathcal{D}_b$ mean value of 0.63‰ (for 1982–92), the ISOLUCP experiment estimates a mean value of only 0.35‰ for the same period. This decline in $\mathcal{D}_b$ is a result of several processes: first, δ^{13}C values of fire emissions are closer to the isotopic composition of newly formed biomass than the δ^{13}C values of soil emissions (see Section 5.2) and second, the highly reduced discrimination during C_4 photosynthesis compared to C_3 photosynthesis over-compensates the decrease in atmospheric δ^{13}C and therefore, largely reduces or even changes the sign in the difference of newly formed phytomass and ecosystem respiration at regions which have recently been converted from C_3 plants to C_4 plants. Together with calculations of the ecosystem respiration, the global isotopic disequilibrium flux ranges from 44.7 Pg C ‰ yr^{-1} (ISOVAR without fire) to 20.7 Pg C ‰ yr^{-1} (ISOLUCP). This is partly due to the slightly reduced total ecosystem respiration flux (69.4 Pg C yr^{-1} for the ISOVAR, ISOVAR without fire and ISOFIX experiments to 62.7 Pg C yr^{-1} for the ISOLUCP experiment) but mainly because of the highly reduced $\mathcal{D}_b$: 0.63‰ (ISOVAR without fire) compared to 0.35 ‰ (ISOLUCP). The ISOVAR without fire calculations yield a 'real' (meaning an isoflux without a flux in total carbon) additional isotopic disequilibrium flux as the total respiration flux does not change in the calculations, however only the isotopic signature of the fire flux is changed (Section 5.2.3). The effect of fire is an overall reduction of the residence time of carbon as, through the biomass burning not much 'old' soil and litter carbon is produced. Table 5.3 summarizes and compares results from this study with previous studies. In general, the agreement with values from previous studies is better with results from the ISOLUCP experiment than from the ISOVAR experiment.

Table 5.3: Comparison of terrestrial ^{13}C quantities

Period	Value	Source
	Isotopic Disequilibrium D_b	
1988	0.43‰	Joos and Bruno [1998]
	0.33‰	Fung et al. [1997]
	0.49‰	Morimoto et al. [2000]
	0.59‰	this study, ISOVAR
	0.42‰	this study, ISOLUCP
	Isotopic Disequilibrium Flux $\mathcal{D}_b$	
1970–1990	23.4 Pg C ‰ yr^{-1}	Heimann and Meier-Reimer [1996]
	22.5 Pg C ‰ yr^{-1}	Joos and Bruno [1998]
	33.4 Pg C ‰ yr^{-1}	this study, ISOVAR
	19.2 Pg C ‰ yr^{-1}	this study, ISOLUCP
1987	25.8 Pg C ‰ yr^{-1}	Francey et al. [1995]
	33.6 Pg C ‰ yr^{-1}	this study, ISOVAR
	22.2 Pg C ‰ yr^{-1}	this study, ISOLUCP
1988	27.2 Pg C ‰ yr^{-1}	Morimoto et al. [2000]
	41.8 Pg C ‰ yr^{-1}	this study, ISOVAR
	23.8 Pg C ‰ yr^{-1}	this study, ISOLUCP

Partitioning the reduction in the global disequilibrium flux to the various processes reveals that the modelling of natural biomass burning reduces D_b by around 10 Pg C ‰ yr^{-1}. The total amount of simulated fire emissions is relatively stable with a global value of around 8 Pg C yr^{-1}, whereas literature values of the biomass burning flux vary between only 2 and 5 Pg C yr^{-1} [Andreae, 1991; Malingreau and Zhuang, 1998]. Therefore, the impact of fire on the isotopic disequilibrium with a reduction of 10 Pg C ‰ yr^{-1} in D_b seems to be overestimated. Including a land use scheme into the modelling framework leads to another reduction of 6 Pg C ‰ yr^{-1} because of the different treatment of the agricultural product pools (independent of climate) compared to the litter and soil pools. Including C_4 crops has only a marginal effect on the global disequilibrium flux, however, including also tropical C_4 pastures decreases D_b by almost another 8 Pg C ‰ yr^{-1}. Townsend et al. [2002] specified this 'reversed' isotopic disequilibrium flux due to the conversion from tropical C_3 forests to C_4 pastures by using values of total conversion fluxes from Houghton and Hacker [1995] and estimates of the isotopic signature of the heterotrophic respiration from model studies at point sites. Depending on the time since clearing (10 to 30 years) of the forests their, average results for the 1990s lie between 8.8 and 15.8 Pg C ‰ yr^{-1}, respectively. However, for this study it is crucial to know the spatial and temporal distribution of tropical C_4 pastures as accurate as possible. With accurately a dataset of only 10 years temporal resolution it might be possible that the total amount of converted area is underestimated and therefore the calculated additional decrease of 8 Pg C ‰ yr^{-1} in the isotopic disequilibrium might be too low.

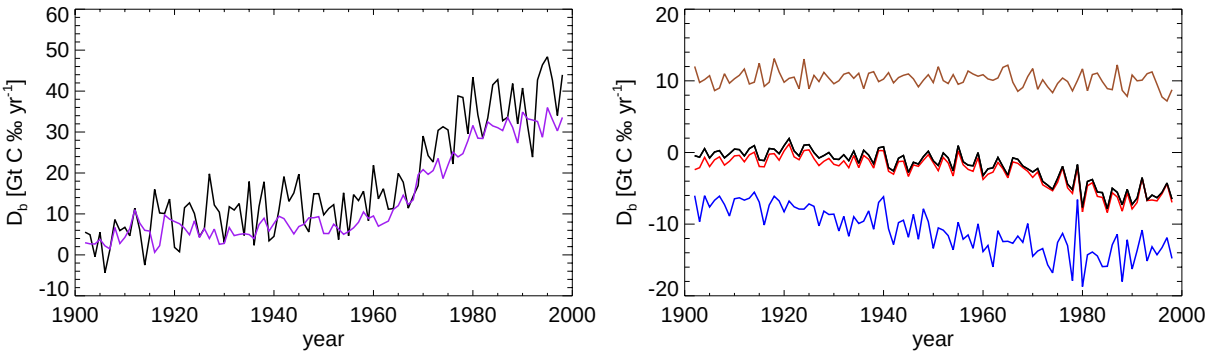

Figure 5.12: Global time series of the modelled isotopic disequilibrium flux D_b for the ISOVAR (black line) and ISOFIX (purple) simulations and time series of the differences in global isotopic disequilibrium: ISOVAR without fire - ISOVAR (brown), ISOLU - ISOVAR (black), ISOLUC - ISOVAR (red) and ISOLUCP - ISOVAR (blue).

As can be seen from Figure 5.12 the ISOVAR simulation exhibits a much higher amount of interannual variablity in the isotopic disequilibrium flux than the ISOFIX experiment. This large interannual variability is also apparent in the ISOVAR without fire and the land use experiments. The fluctuations are mainly induced by the variability of the ^{13}C discrimination during photosynthesis. High frequency variations in the isotopic ratio of the respiration flux are strongly damped because of the relatively long residence time of carbon in the terrestrial pools. However, biomass burning has a potentially high influence on the interannual variability of the isotopic disequilibrium flux because it is believed that in certain years (with strong El Niño events) the burning flux is much higher than in other years [Langenfelds et al., 2002; Page et al., 2002]. As this additionally released carbon is mainly due to anthropogenic fire events it is not simulated by LPJ's fire module which only models natural fire events. The simulated interannual variability in the natural carbon fire flux is rather low (less than 10% of the burning flux).

A secular increasing trend after 1960 due to the increased burning of fossil fuel which depletes atmospheric CO_2 in ^{13}C is clearly visible. However, as can be seen from the differences between the ISOVAR and the other experiments in the isotopic disequilibrium flux, this increasing trend is decelerated in the land use experiments. The specification of tropical C_4 pastures (ISOLUCP) has the strongest effect on this trend due to the higher amount of low discriminating C_4 plants. In addition, there is a peak value in the difference between the ISOVAR and ISOLUCP experiments around 1980, after that year the difference is decreasing again. This is in agreement with the findings in the net carbon exchange in Section 5.3.1 and results also from the decrease in the global area covered with tropical C_4 pastures.

Heimann and Meier-Reimer [1996] concluded from a sensitivity study that the value of the isotopic disequilibrium is one of the most crucial quantities in double deconvolution studies. The standard deviation of the global isotopic disequilibrium flux induced only by climate variability

(i.e. the difference of D_b between experiments with a variable discrimination during photosynthesis and the ISOFIX experiment) is larger than 5 Pg C ‰ yr^{-1} for all experiments. This value is in good agreement with the standard deviation in D_b of 5.8 Pg C ‰ yr^{-1} reported by Ito [2003]. Because variations in the isotopic disequilibrium are mainly due to the variability in the leaf discrimination (as stated above) the spatial pattern of the variance in isotopic disequilibrium resembles very much the patterns of the variance in Δ_{leaf} (see Figure 5.7).

5.4 Conclusions

This study presents a process-based modelling framework for simulating terrestrial carbon and carbon 13 cycling. The influence of various quantities (climate, fire, land use and C_4 land use) on the temporal and spatial patterns of the isotopic composition of the terrestrial biosphere has been analysed. Variability in the atmosphere-biosphere ^{13}C exchange (both leaf discrimination and isotopic disequilibrium) on an interannual time scale is mainly influenced by climate variability and vegetation composition (fluctuations between C_3 and C_4 plants), whereas processes such as fire, land use and C_4 land use effect primarily the spatial distribution and the global mean values. The history of conversion from natural vegetation to cultivation is an important boundary condition for estimating the effect of land conversion on the terrestrial isotopic composition. Therefore, more information on the temporal and spatial distribution of land use, especially of C_4 crops and C_4 pastures distribution would help to quantify the impact of land use on atmospheric $\delta^{13}C$ and thus, strengthen the results of observationally analyses of the global carbon budget.

References

Andreae, M. O., 1991. Biomass burning: its history, use, and distribution and its impact on environmental quality and global change. In: Levine, J. S. (Ed.), Global biomass burning: atmospheric, climatic, and biospheric implications. MIT Press, Cambridge, USA, pp. 3–21.

Bakwin, P. S., Tans, P. P., White, J. W. C., Andres, R. J., 1998. Determination of the isotopic ($^{13}C/^{12}C$) discrimination by terrestrial biology from a global network of observations. Glob. Biogeochem. Cycles 12 (3), 555–562.

Battle, M., Bender, M. L., Tans, P. P., White, J. W. C., Ellis, J. T., Conway, T., Francey, R. J., 2000. Global carbon sinks and their variability inferred from atmospheric O_2 and $\delta^{13}C$. Science 287, 2467–2470.

Buchmann, N., Brooks, R. J., Flanagan, L. B., Ehleringer, J. R., 1998. Carbon isotope discriminiation of terrestiral ecosystems. In: Griffiths, H. (Ed.), Stable Isotopes. BIOS Sci., Oxford, pp. 203–222.

Buchmann, N., Kaplan, J. O., 2001. Carbon isotope discrimination of terrestrial ecosystems - How well do observed and modeled results match? In: Schulze, E.-D., Heimann, M., Harrison, S., Holland, E., Lloyd, J., Prentice, I. C. (Eds.), Global biogeochemical cycles in the climate system. Academic Press, San Diego, pp. 253–266.

Ciais, P., Friedlingstein, P., Schimel, D. S., Tans, P. P., 1999. A global calculation of the δ^{13}C of soil respired carbon: Implications for the biospheric uptake of anthropogenic CO_2. Glob. Biogeochem. Cycles 13 (2), 519–530.

Ciais, P., Tans, P. P., Trolier, M., White, J. W. C., Francey, R. J., 1995. A large northern hemisphere terrestrial CO_2 sink indicated by the $^{13}C/^{12}C$ ratio of atmospheric CO_2. Science 269 (1098-1102).

Ekblad, A., Högberg, P., 2001. Natural abundance of ^{13}C in CO_2 respired from forest soils reveals speed of link between tree photosynthesis and root respiration. Oecologia 127, 305–308.

Esser, G., 1995. Contribution of monsoon Asia to the carbon budget of the biosphere, past and future. Vegetatio 121 (1-2), 175–188.

FAO, 2002. FAOSTAT, internet version (http://apps.fao.org/). Food and Agricultural Organization of the United Nations, Rome.

Foley, J., 1995. An equilibrium model of the terrestrial carbon budget. Tellus 47B, 310–319.

Francey, R. J., Allison, C. E., Etheridge, D. M., Trudinger, C. M., Enting, I. G., Leuenberger, M., Langenfelds, R. L., Michel, E., Steele, L. P., 1999. A 1000-year high precision record of δ^{13}C in atmospheric CO_2. Tellus 51B, 170–193.

Francey, R. J., Tans, P. P., Allison, C. E., Enting, I. G., White, J. W. C., Trolier, M., 1995. Changes in oceanic and terrestrial carbon uptake since 1982. Nature 373, 326–330.

Fung, I., Field, C. B., Berry, J. A., Thompson, M. V., Randerson, J. T., Malmström, C. M., Vitousek, P. M., Collatz, G. J., Sellers, P. J., Randall, D. A., Denning, A. S., Badeck, F., John, J., 1997. Carbon 13 exchanges between the atmosphere and biosphere. Glob. Biogeochem. Cycles 11, 507–533.

Heimann, M., Meier-Reimer, E., 1996. On the relations between the oceanic uptake of CO_2 and its carbon isotopes. Glob. Biogeochem. Cycles 10 (1), 89–110.

Houghton, R. A., Hacker, J. L., 1995. ORNL/CDIAC data set NDP-050.

Ito, A., 2003. A global-scale simulation of the CO_2 exchange between the atmosphere and the terrestrial biosphere with a mechanistic model including stable carbon isotopes, 1953-1999. In press, Tellus .

Joos, F., Bruno, M., 1998. Long-trem variability of the terrestrial and oceanic carbon sinks and the budgets of the carbon isotopes ^{13}C and ^{14}C. Glob. Biogeochem. Cycles 12, 277–295.

Kaplan, J. O., Prentice, I. C., Buchmann, N., 2002. The stable carbon isotope composition of the terrestrial biosphere. Glob. Biogeochem. Cycles 16, 8–1–8–11.

Keeling, C. D., Bacastow, R. B., Carter, A. F., Piper, S. C., Whorf, T. P., Heimann, M., Mook, W. G., Roeloffzen, H., 1989. A three-dimensional model of the atmospheric CO_2 transport based on observed winds: 1. Analysis of observational data. In: Peterson, D. H. (Ed.), Aspects of Climate Variability in the Pacific and the Western Americas. Vol. 55. AGU, Washington, D.C., pp. 165–236.

Klein Goldewijk, C. G. M., Battjes, J. J., 1997. A hundred year (1890 - 1990) database for integrated environmental assessments (HYDE, version 1.1). Tech. Rep. 422514002, National Institute of Public Health and the Environment (RIVM), Bilthoven, The Netherlands.

Klein Goldewijk, K., 2001. Estimating global land use change over the past 300 years: the HYDE database. Glob. Biogeochem. Cycles 15, 417–434.

Langenfelds, R. L., Francey, R. J., Pak, B. C., Steele, L. P., Lloyd, J., Trudinger, C. M., Allison, C. E., 2002. Interannual growth rate variations of atmospheric CO_2 and its $\delta^{13}C$, H_2, CH_4 and CO between 1992 and 1999 linked to biomass burning. Glob. Biogeochem. Cycles 16, doi:10.1029/2001GB001466.

Lloyd, J., Farquhar, G., 1994. ^{13}C discrimination during CO_2 assimilation by the terrestrial biosphere. Oecologia 99, 201–215.

Lloyd, J., Taylor, J. A., 1994. On the temperature-dependence of soil respiration. Funct. Ecol. 8 (3), 315–323.

Malingreau, J.-P., Zhuang, Y. H., 1998. Biomass burning: an ecosystem process of global significance. In: Galloway, J., Mellilo, J. (Eds.), Asian change in the context of global climate change. Cambridge University Press, Cambridge, U.K., pp. 101–127.

McGuire, A. D., Sitch, S., Clein, J., Dargaville, R., Esser, G., Foley, J., Heimann, M., Joos, F., Kaplan, J., Kicklighter, D. W., Meier, R. A., Melillo, J. M., III, B. M., Prentice, I. C., Ramankutty, N., Reichenau, T., Schloss, A., Tian, H., Wittenberg, U., 2001. Carbon balance of the terrestrial biosphere in the twentieth century: Analyses of CO_2, climate and land use effects with four process-based ecosystem models. Glob. Biogeochem. Cycles 15, 183–206.

Morimoto, S., Nakazawa, T., Higuchi, K., Aoki, S., 2000. Latitudinal distribution of atmospheric CO_2 sources and sinks inferred by $\delta^{13}C$ measurements from 1985 to 1991. J. Geophys. Res. 105 (D19), 24315–24326.

New, M., Hulme, M., Jones, P., 2000. Representing twentieth-century space-time climate variability. Part II: Development of 1901-96 monthly grids of terrestrial surface climate. Journal of Climate 13, 2217–2238.

Page, S., Siegert, F., Rieley, J. O., Boehm, H.-D. V., Jaya, A., Limin, S., 2002. The amount of carbon released from peat and forest fires in Indonesia during 1997. Nature 420, 61–65.

Prentice, I. C., Farquhar, G. D., Fasham, M. J. R., Goulden, M. L., Heimann, M., Jaramillo, V. J., Kheshgi, H. S., Le Quéré, C., Scholes, R. J., Wallace, D. W. R., 2001. The carbon cycle and atmospheric carbon dioxide. In: Houghton, J. T., Ding, Y., Griggs, D. J., Noguer, M., van der Linden, P. J., Dai, X., Maskell, K., Johnson, C. A. (Eds.), Climate Change 2001: The Scientific basis. Cambridge University Press, Cambridge, U.K., pp. 183–237.

Ramankutty, N., Foley, J., 1999. Estimating historical changes in global land cover: Croplands from 1700 to 1992. Glob. Biogeochem. Cycles 13 (4), 997–1027.

Rayner, P., Enting, I., Francey, R., Langenfelds, R., 1999. Reconstructing the recent carbon cycle from atmospheric CO_2, $\delta^{13}C$ and O_2/N_2 observations. Tellus B51 (2), 213–232.

Scholze, M., Kaplan, J. O., Knorr, W., Heimann, M., 2003. Climate and interannual variability of the atmosphere-biosphere $^{13}CO_2$ flux. Geophys. Res. Lett 30 (2), 1097, doi:10.1029/2002GL015631.

Sitch, S., Prentice, I. C., Smith, B., Arneth, A., Bondeau, A., Cramer, W., Kaplan, J. O., Levis, S., Lucht, W., Sykes, M. T., Thonicke, K., Venevsky, S., 2003. Evaluation of ecosystem dynamics, plant geography and terrestrial carbon cycling in the LPJ dynamic global vegetation model. Global Change Biology 9, 161–185.

Still, C. J., Berry, J. A., Collatz, G. J., DeFries, R. S., 2003. Global distribution of C_3 and C_4 vegetation: Carbon cycle implications. Glob. Biogeochem. Cycles 17 (1), doi:10.1029/2001GB001807.

Thonicke, K., Venevsky, S., Sitch, S., Cramer, W., 2001. The role of fire disturbance for global vegetation dynamics: Coupling fire into a dynamic global vegetation model. Glob. Ecol. Biogeogr. 10 (6), 661–677.

Townsend, A., Asner, G., White, J., Tans, P., 2002. Land use effects on atmospheric ^{13}C imply a sizable terrestrial CO_2 sink in tropical latitudes. Geophys. Res. Lett. 29 (10), 68–1–68–4.

Wittenberg, U., Esser, G., 1997. Evaluation of the isotopic disequilibrium in the terrestrial biosphere by a global carbon isotope model. Tellus 49B, 263–269.

Chapter 6

First results from a prototype Carbon Cycle Data Assimilation System (CCDAS)

6.1 Introduction

The rising concentration of CO_2 in the atmosphere and the attendant potential for climate change has stimulated substantial scientific and policy scrutiny. Two scientific foci have been to map the current fluxes of the gas to the atmosphere and to predict the evolution of these fluxes into the future. Generally, the tools used to perform these two tasks have been different. One tool commonly employed to deduce current fluxes is atmospheric transport inversions [e.g., Keeling et al., 1989; Enting et al., 1995; Rayner et al., 1999; Bousquet et al., 2000]. This method infers space-time patterns of fluxes which, when subject to atmospheric transport, produces a set of concentrations close to those observed. The sparsity of the observing network and the continuous nature of the flux field make this a poorly conditioned inverse problem which manifests itself as large uncertainties on the inferred space-time pattern [e.g., Kaminski et al., 1999b]. Approaches to solving this problem usually involve some kind of regularization such as the use of prior information as a constraint on the available solution or solving for fluxes only in a highly restricted subspace [e.g., Fan et al., 1998]. These approaches contain their own pitfalls as demonstrated by Kaminski and Heimann [2001] and Kaminski et al. [2001]. A more fundamental problem is that the solution, no matter how good, contains no information on the processes responsible for the inferred flux pattern. Thus, it has no inherent predictive power.

The other approach is the traditional one of forward modelling of the most important processes. This approach can allow one to make predictions and can include process understanding. Most forward models will be checked ad hoc against various data sources or, in the worst case, an ensemble of other models but unfortunately, there is no mechanism built into the model to incorporate such testing data formally. That task is usually known as data assimilation and is, necessarily, the operational procedure when best guess predictions must be made on the basis of current knowledge. This chapter applies the concepts of data assimilation to a model of the

terrestrial carbon cycle.

The basic approach has been applied previously to a highly simplified model by Kaminski et al. [2002], hereafter denoted as K02. Briefly, they optimised the controlling parameters (light-use efficiency of the incoming radiation and temperature dependency of heterotrophic respiration) of the Simple Diagnostic Biosphere Model (SDBM, Knorr and Heimann [1995]) with respect to a set of observations, in their case a seasonal cycle of atmospheric CO_2 concentrations. Parameter uncertainties were inferred from uncertainties in observed concentrations. The model, driven by these optimised parameters, was then run to predict a range of quantities of interest. These quantities included net terrestrial carbon fluxes and their uncertainties arising from the optimised parameters and their uncertainties.

Here, SDBM is replaced with the "Biosphere-Energy-Transfer-HYdrology" (BETHY) model described by Knorr [2000]. BETHY is a fully prognostic model of the terrestrial carbon cycle and can, if model-generated driving fields are available, be run for future scenarios. Therefore, knowledge about the current terrestrial carbon cycle can be predicted to its evolution into the future. Furthermore, the formal uncertainty estimates gained during the parameter optimisation step can be propagated to calculate uncertainties of any of the predicted quantities, including the future evolution of the model.

Less formal versions of the same approach have been used previously for estimating parameters in other terrestrial biosphere models. Vukićević et al. [2001] estimated model parameters for a simple, globally averaged terrestrial model by inversion of the model against global temperature and CO_2 anomaly data using a variational method. However, they did not derive uncertainties for the model parameters. Randerson et al. [2002] used a direct mapping of the probability distribution to estimate the seasonal exchanges and isotopic discrimination of the terrestrial high latitudes. Finally Barrett [2002] used a genetic algorithm, and a model of primary production and soil and litter decomposition to predict the turn-over time of soil carbon within Australia. Although these studies apply the same basic approach, they do so to different data using quite different optimisation techniques. Both the model and optimisation procedure used in this study are more complex than those cited above. The model includes both the photosynthesis and soil biogeochemistry process models and signals are mixed and transported from the various source gridpoints to the atmospheric observing sites by an atmospheric transport model, capable of simulating the independent impact of fluxes from every gridpoint. However this study is by no means comprehensive and only describes first results of a prototype: all the data sources used by these previous studies can also be brought to bear on the processes in BETHY and will be a subject for further model development.

This approach can be used, among others, to probe the behaviour of the current carbon cycle. Here again the aim is to combine the forward and inverse modelling procedures which have usually remained separate. Several inverse studies, [e.g., Rayner et al., 1999; Bousquet et al., 2000] have produced space-time distributions of fluxes and attempted to make comment on the underlying processes. Conversely, forward modelling studies of the recent past [e.g., Dargaville et al., 2002] have compared output from process models against observations. These models,

coupled with an apparently reasonable atmospheric transport model, generally underestimate both the seasonal cycle and interannual variability in atmospheric CO_2 concentrations. Most studies either of observed interannual variability of ocean fluxes [e.g., Feely et al., 1999] or ocean models capable of simulating such interannual variability [e.g. Le Quéré et al., 2000] suggest ocean flux variability is insufficient to bring simulated atmospheric CO_2 concentrations close to observed. Similarly recent inverse studies, [e.g., Bousquet et al., 2000] suggest terrestrial fluxes dominate interannual variability. Thus we have reason to suspect either the model formulation or controlling parameters in the models used by Dargaville et al. [2002]. While the formulation of the BETHY model cannot be corrected in this study, it is valuable to consider the simulation of fluxes from a model which is optimally adjusted to match the observed concentrations.

In particular questions such as what processes are responsible for the apparently large interannual variations in terrestrial carbon uptake and how do they relate to anomalous climate events (such as e.g., El Niño) can be asked. Furthermore, which are the regions mostly influenced by such climatic events. Understanding the sensitivity of the carbon cycle to interannual climate variability may be one of the few observational clues we have of the evolution of the carbon cycle during the 21st century.

This chapter presents the Carbon Cycle Data Assimilation System (CCDAS) around BETHY Version 11, together with a set of preliminary results from a control experiment. These results have to be digested with care, however, as this CCDAS is still a prototype in a development and test stage. Errors in this version have been identified and removed.

6.2 Methodology

The observed data used here is assimilated in two steps: first the full BETHY model is used to assimilate remote sensing data for optimising parameters controlling soil moisture and phenology. Second a reduced version of BETHY is used to assimilate atmospheric CO_2 concentration observations. This simplified form of the model uses then the optimised leaf area index (LAI) and plant available soil moisture fields from the first assimilation step as input data. The setup of the system is sketched in Figure 6.1.

6.2.1 Assimilating remote sensing data

The method of assimilating space-borne remote sensing data into the BETHY model has already been described in detail by Knorr and Schulz [2001]. In brief, they defined a cost function by the squared deviation between global monthly fields of the fraction of Absorbed Photosynthetically Active Radiation (fAPAR) derived from satellite data and monthly fields of fAPAR as predicted by BETHY as well as initial and adjusted model parameters, both are normalized by their assumed error variances. Model parameters are then adjusted until the cost function reaches a minimum using the downhill simplex method [Press et al., 1992]. The chosen parameters represent the phenology and hydrology part of the BETHY model and affect LAI and maximum

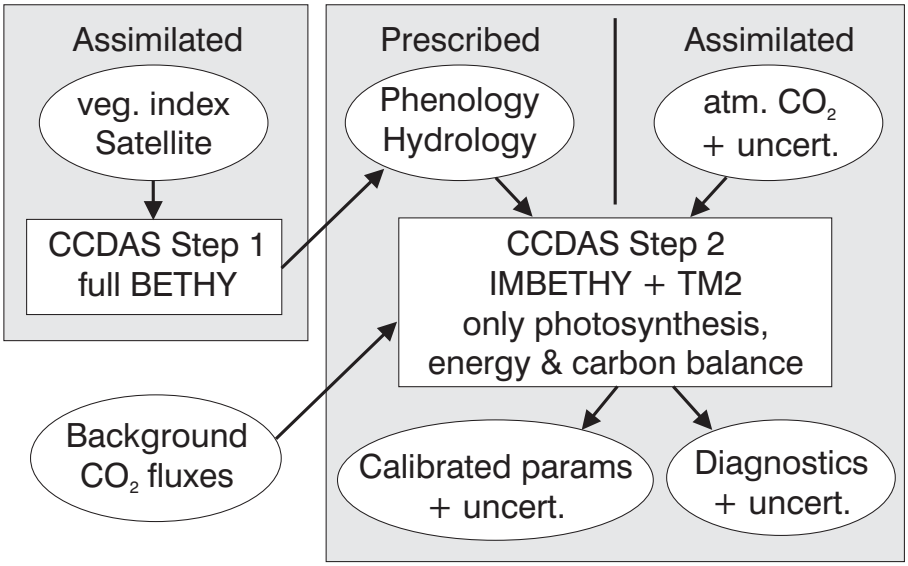

Figure 6.1: Sketch of the CCDAS setup: ovals represent input and output data, boxes represent calculation steps.

plant available soil moisture (ω_{max}).

6.2.2 Assimilating atmospheric CO_2 data

The method of assimilating atmospheric CO_2 data into BETHY follows closely the method as described by K02. Therefore it is only briefly sketched with emphasis put on differences between K02 and this study here. The assimilation system is operated first in a calibration mode and then in a prognostic mode. The calibration step of deriving an optimal parameter set $\mathbf{x}$ from atmospheric concentration observations $\mathbf{c}$ involves propagation of information in an inverse sense through a chain of models. In the forward direction, the flow of information is sketched in Figure 6.2. In the prognostic mode various quantities of interest (e.g., terrestrial carbon fluxes or atmospheric CO_2 concentrations) and their uncertainties can be calculated from the optimised parameter vector and its uncertainty as derived in the calibration mode. Figure 6.3 shows the model set-up for the prognostic mode.

First, a terrestrial biosphere model B produces from a parameter vector $\mathbf{x}$ among other quantities a space-time distribution of modelled fluxes $\mathbf{f}_M$ on a $2°\times2°$ grid. These fluxes are then mapped via an aggregation routine onto the $7.8°\times10°$ grid of an atmospheric transport model, denoted as $\mathbf{A}$. Thus, small-scale forcing of the biosphere can propagate through to the atmospheric concentrations. The atmospheric transport model, denoted as $\mathbf{T}$, finally maps fluxes onto atmospheric concentrations. The use of the adjoint approach described by Kaminski et al. [1999a] means that $\mathbf{T}$ can take fluxes at the full resolution of the underlying transport model and map them onto a predetermined set of observed concentrations. In fact, Kaminski

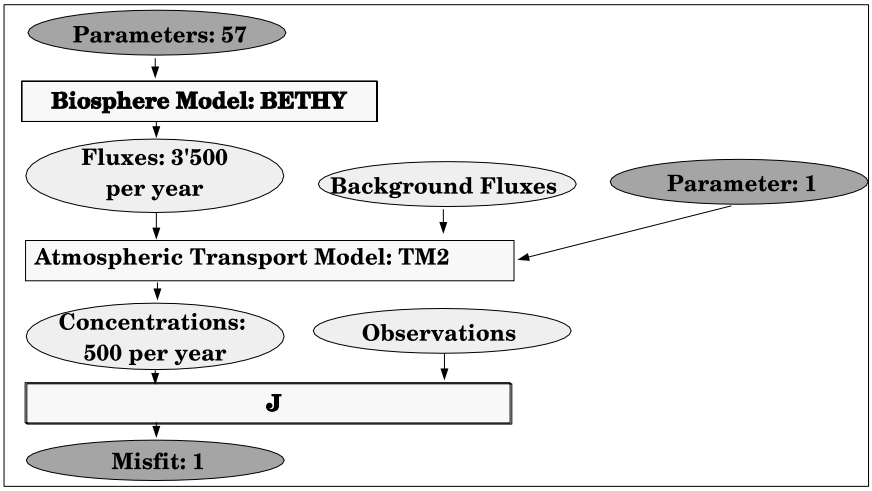

Figure 6.2: Model setup for the calibration mode. Oval boxes show the various quantities, dependent and independent variables are dark grey, intermediate fields are light grey. Rectangular boxes denote the mappings between these fields.

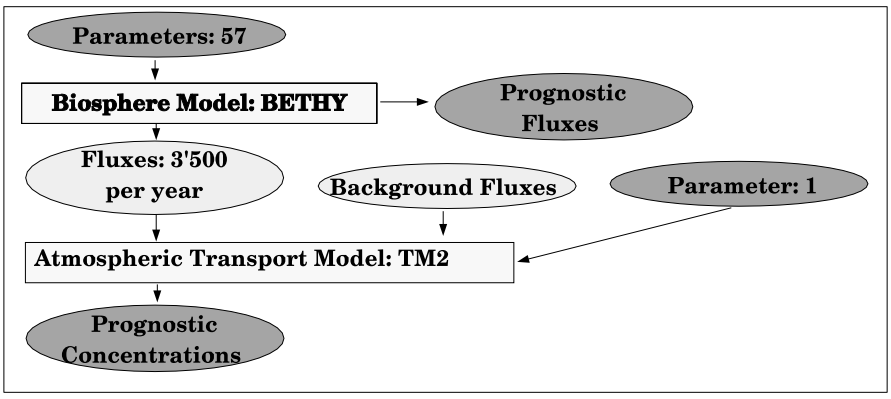

Figure 6.3: Model set-up for the prognostic mode. Oval boxes show the various quantities, dependent and independent variables are dark grey, intermediate fields are light grey. Rectangular boxes denote the mappings between these fields.

et al. [1999a] demonstrated that, if only modelled concentrations at selected sites and times are needed, the transport model can be included as a simple matrix multiplication without loosing the required generality of flux fields.

Combining the three steps yields a mapping from biosphere model parameters to modelled concentrations $\mathbf{c}_M$

$$\mathbf{c}_M = M(\mathbf{x}) = \mathbf{T} \times \mathbf{A} \times B(\mathbf{x}) \tag{6.1}$$

The above equation represents a composition of functions. However, $\mathbf{T}$ and $\mathbf{A}$ are linear functions and therefore, can also be considered as matrix multiplication.

The Bayesian approach is used here to formulate the optimisation problem [Tarantola, 1987; Enting, 2002]. Thus, a term embodying a priori knowledge $\mathbf{p}$ on the parameter vector is combined with the observational information to define an overall mismatch of an optimised parameter vector $\mathbf{x}$. This mismatch is calculated by a cost function

$$J(\mathbf{x}) = \frac{1}{2}((M(\mathbf{x}) - \mathbf{c})^T \, {\mathbf{C_c}}^{-1} \, (M(\mathbf{x}) - \mathbf{c}) + (\mathbf{x} - \mathbf{p})^T \, {\mathbf{C_p}}^{-1} \, (\mathbf{x} - \mathbf{p})) \ , \tag{6.2}$$

where $\mathbf{C_c}$ expresses the uncertainty for the observations $\mathbf{c}$ and $\mathbf{C_p}$ the uncertainty for the priors $\mathbf{p}$ in the form of covariance matrices. This definition of the cost function reflects the assumption of Gaussian probability distributions for the observed concentrations and the a priori information about the parameters (the Gaussian assumption).

Optimisation of $\mathbf{x}$ in the nonlinear composite model M is done by minimizing J. Powerful minimization algorithms for functions like J rely on the availability of the gradient of J with respect to the parameters. Thus, the optimisation step uses the derivative of the cost function with respect to input parameters, which is provided by the adjoint of the composite model, M. All derivative code is generated by the tool Transformation of Algorithms in Fortran (TAF, [Giering and Kaminski, 1998; Giering et al., 2003]), which applies automatic differentiation [Griewank, 2000] to the source code of the model. Hence, TAF is applied in reverse mode to generate a subroutine to calculate $\nabla_{\mathbf{x}} J(\mathbf{x})$ for any $\mathbf{x}$. A more detailed description of the use of TAF is given by Kaminski et al. [2003], also Appendix A. The adjoint of J evaluates the derivative of a scalar valued function. This derivative is a fairly compact expression, mapping a few dozen parameters onto their impact on the cost function. The cost function minimization allows the calculation of an optimal parameter set $\mathbf{x_{opt}}$.

The dependency of the cost function on the inhomogeneous set of BETHY-parameters is highly nonlinear, which renders the minimisation a complex task. Fortunately, in a few tens of iterations, the optimisation can absorb the large scale information from the observations, which is reflected by reduction in the value of the cost function by several orders of magnitude and a good fit to observations. However, even in a stage, where the decrease in the function values has almost stopped and a further reduction appears to be driven by noise in the observations, the optimisation does not achieve a zero gradient, the necessary condition for a minimum.

6.2.3 Calculation of uncertainties

The curvature of the cost function is described by the Hessian, a matrix containing all the second and cross-derivatives at a point $\mathbf{x}$ in the parameter space. At a minimum in the cost function, the Hessian approximates the inverse covariance in the uncertainty of the parameters [Tarantola, 1987]. The Hessian matrix is calculated by differentiating the gradient vector with respect to all parameters by applying TAF a second time to the function which calculates the gradient itself. Because the numbers of inputs and outputs for the gradient calculation are equal, this second differentiation is most efficiently carried out in forward mode, i.e. by the tangent linear model.

In general one cannot expect that a given observational network is capable of constraining every direction in the space of control variables. For example, in the time dependent flux inversion of Rayner et al. [1999] a network that is similar to the one used in the present study has observed only a small subset of about 10-20 dimensions. In the present system, well observed directions exhibit high curvature of the cost function at its minimum, while the curvature in the unobserved directions is determined by the prior uncertainties on parameters.

As mentioned above, the optimisation has absorbed only the large scale information in the observations. The lack of absorbing the small scale noise is reflected not only in a non zero gradient but also in a Hessian, which is not positive definite. The following procedure is used to extract the large scale curvature and approximate the covariance in the uncertainty of the parameters.

1. Calculate the eigen-spectrum for the Hessian as

$$\mathbf{H} = \mathbf{V_H} \mathbf{\Lambda_H} \mathbf{V_H^T} \tag{6.3}$$

   where $\mathbf{H}$ is the Hessian, $\mathbf{V_H}$ is a matrix composed of the eigen-vectors of $\mathbf{H}$ (one per column) and $\mathbf{\Lambda_H}$ is the diagonal matrix of eigen-values of $\mathbf{H}$ arranged in the same order as $\mathbf{V_H}$, in other words the usual diagonalization of $\mathbf{H}$.

2. Replace $\mathbf{\Lambda_H}$ in Equation 6.3 by

$$\begin{aligned} \mathbf{\Lambda_H^*} = &\quad \mathbf{\Lambda_H} \quad |\mathbf{\Lambda_H} > \text{th} \\ = &\quad \mathbf{I} \quad |\mathbf{\Lambda_H} < \text{th} \end{aligned} \tag{6.4}$$

   where the threshold value th is the order of $\text{th} = -\min(\mathbf{\Lambda_H})$.

3. Define the covariance of parameter uncertainties by $\mathbf{V_H} \mathbf{\Lambda_H^*}^{-1} \mathbf{V_H^T}$.

6.3 Models and Data

6.3.1 Terrestrial carbon cycle model

BETHY is a process-based model of the terrestrial biosphere [Knorr, 1997, 2000]. It simulates carbon assimilation and plant and soil respiration embedded within a full energy and water

Table 6.1: PFTs defined in BETHY and their abbreviations.

PFT No.	PFT Name	Abbreviation
1	Trop. broadleaved evergreen tree	TrEv
2	Trop. broadleaved deciduous tree	TrDec
3	Temp. broadleaved evergreen tree	TmpEv
4	Temp. broadleaved deciduous tree	TmpDec
5	Evergreen coniferous tree	EvCn
6	Deciduous coniferous tree	DecCn
7	Evergreen shrub	EvShr
8	Deciduous shrub	DecShr
9	C3 grass	C3Gr
10	C4 grass	C4Gr
11	Tundra vegetation	Tund
12	Swamp vegetation	Wetl
13	Crops	Crop

balance. Hence, it is structured into four compartments, energy and water balance (1), photosynthesis (2), phenology (3), and carbon balance (4). BETHY is driven by observed climate data for the period 1979 to 2000 (Nijssen et al. [2001] which have been extended to the year 2000 [R. Schnur, personal communication]). It is run on a $2^\circ \times 2^\circ$ grid resolution. Global vegetation is mapped onto 13 plant functional types (PFT) based on Wilson and Henderson-Sellers [1985]. A gridcell can contain up to three different PFTs, with the amount specified by their fractional coverage. Table 6.1 lists the PFTs and the map in Figure 6.4 shows, in each grid cell, its dominant PFT.

The model is used in two forms. In its full form it assimilates AVHRR data for the years 1989–90 following the method of Knorr and Schulz [2001] as mentioned earlier. This first assimilation step provides monthly time-series of LAI and w_{max} for later use in the simplified form of the model to assimilate atmospheric concentration observations. In this simplified form BETHY is slightly reduced by leaving out the water balance from compartment one and the phenology compartment (3) completely. Therefore it can be run "off-line" with prescribed LAI and plant available soil moisture ω from the full model. Time steps for the photosynthesis and autotrophic respiration part are one hour, and for the heterotrophic respiration part one day. To speed up computation only one mean day is calculated per month preserving diurnal variations, the daily fluxes are then multipied by the month length to generate monthly fluxes. Control parameters affect the photosynthesis scheme, and both the autotrophic and heterotrophic respiration schemes. The parameters are described in the following (marked by an underlying bar in the equations) and listed with their a priori values and uncertainties in Table 6.2.

At each model grid cell photosynthesis is simulated following a Farquhar/Collatz scheme [Farquhar et al., 1980; Collatz et al., 1992] which distinguishes between C_3 and C_4 metabolism. In the case of C_3 photosynthesis gross primary productivity (GPP) is calculated as the minimum of an electron transport limited rate, J_E, and a rate, J_C, limited by the carboxylation enzyme

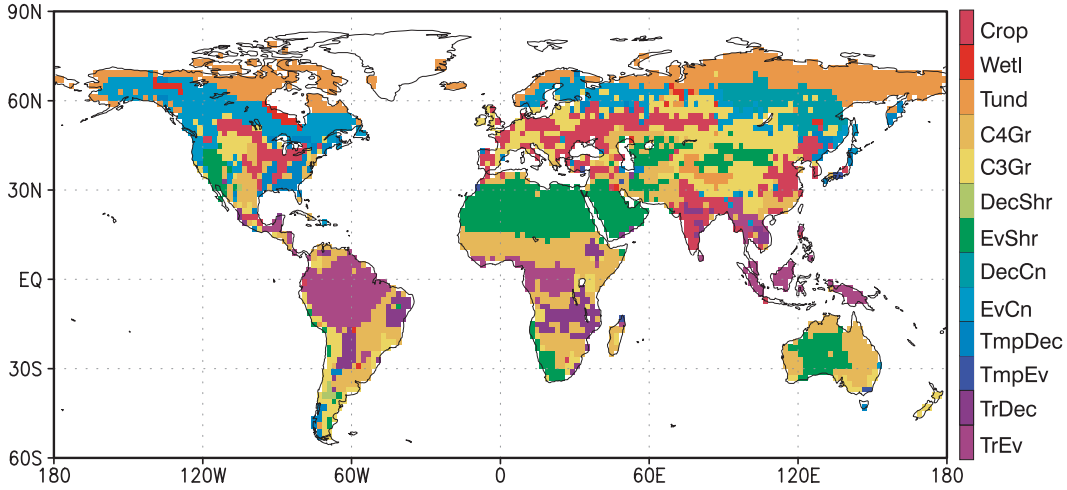

Figure 6.4: Distribution of the dominant PFT per gridcell, PFT labels are given in Table 6.1.

Rubisco from which the leaf or dark respiration, R_d, is subtracted:

$$\text{GPP} = \min[J_C; J_E] - R_d \tag{6.5}$$

with

$$J_C = V_{max}\frac{C_i - \Gamma_*}{C_i + K_C(1 + O_x/K_O)} \tag{6.6}$$

$$J_E = J\frac{C_i - \Gamma_*}{4(C_i + 2\Gamma_*)} \tag{6.7}$$

where

$$J = \frac{\underline{\alpha_q} I J_{max}}{\sqrt{J_{max}^2 + \underline{\alpha_q^2} I^2}} \tag{6.8}$$

with the parameter α_q the quantum efficiency, C_i the leaf-internal CO_2 concentration, I the photosynthetically active radiation (PAR) absorption rate, and O_x the O_2 partial pressure. The temperature dependence of the maximum electron transport, J_{max}, is calculated from the vegetation temperature, T_v in °C, the respective rate at 25°C and, as one of the parameters the proportionality factor jmt [Farquhar, 1988]:

$$J_{max}(T_v) = J_{max}(25°\text{C}) \times \underline{jmt} \times T_v \tag{6.9}$$

with

$$J_{max}(25°\text{C}) = \underline{jtv} \times \underline{V_{max}}(25°\text{C}) \tag{6.10}$$

Here, the ratio $jtv = J_{max}/V_{max}$, calculated from the a priori values of J_{max} and V_{max} at 25°C, which is then multiplied by V_{max} to obtain J_{max}, is taken as a parameter instead of J_{max} directly. The CO_2 compensation point, Γ_*, depends linearly on the vegetation temperature with the parameter gt being the dependency factor [Farquhar, 1988]:

$$\Gamma_* = \underline{gt} \times T_v \tag{6.11}$$

The temperature dependency of further enzyme kinetic rates such as the Michaelis-Menten constants K_O and K_C and the maximum carboxylation rate, V_{max}, are computed from the following equation with E the respective activation energy (with T_v in °C):

$$k(T_v) = \underline{k}(25°\mathrm{C}) \exp\left\{\frac{(T_v - 25°\mathrm{C})\underline{E}}{298\mathrm{K}R(T_v + 273°\mathrm{C})}\right\} \tag{6.12}$$

where k stands for the rate in question and R is the general gas constant in $\mathrm{JK}^{-1}\mathrm{mol}^{-1}$. The values of K_O, K_C and V_{max} at 25°C and the respective activation energies are taken as parameters in this study. For C_4 photosynthesis there are three limiting rates [Collatz et al., 1992]:

$$\begin{aligned} \mathrm{GPP} &= \min[J_e; J_c; J_i] - R_d \\ J_e &= V_{max} \\ J_c &= \underline{jtv} \times V_{max} \times C_i \\ J_i &= \underline{\alpha_i} I \end{aligned} \tag{6.13}$$

where in the case of C_4 photosynthesis

$$\underline{jtv} = k/V_{max} \tag{6.14}$$

with k the PEPcase CO_2 specificity. α_i is the integrated C_4 quantum efficiency, and jtv and α_i are both parameters. The dark respiration R_d is calculated as [Farquhar et al., 1980; Knorr, 1997]:

$$R_d(25°C) = \begin{cases} 0.011\ \underline{V_{max}}(25°C) & (C_3) \\ 0.042\ \underline{V_{max}}(25°C) & (C_4) \end{cases} \tag{6.15}$$

The temperature dependency of R_d is also given by Equation 6.12 with the activation energy E_R as a controlling parameter.

The net primary productivity (NPP) is calculated as gross uptake of CO_2 by the leaves (GPP) minus total autotrophic respiration which includes plant maintenance respiration R_M and growth respiration R_G. Following Knorr [2000], R_M is calculated from the leaf respiration as

$$R_M = R_d/\underline{f_{R,leaf}} \tag{6.16}$$

with $f_{R,leaf}$ the leaf fraction of the maintenance respiration. Growth respiration is itself proportional to NPP and calculated as follows:

$$R_G = (\underline{f_{R,growth}} - 1)\mathrm{NPP} = (\underline{f_{R,growth}} - 1)(\mathrm{GPP} - R_M - R_G) \tag{6.17}$$

where $f_{R,growth}$ is the amount of carbon to be produced for a unit gain in vegetation biomass. Both $f_{R,leaf}$ and $f_{R,growth}$ are taken as parameters.

The net ecosystem productivity (NEP) is now defined as

$$\mathrm{NEP} = \mathrm{NPP} - \mathrm{SR} = \mathrm{NPP} - R_{SR,f} - R_{SR,s} \tag{6.18}$$

where the heterotrophic soil respiration (SR) is composed of respiration from a short-lived litter pool with time-varying size and a long-lived soil organic matter pool [Knorr, 2000]. Soil respiration is assumed to be temperature and soil moisture dependent and calculated from the following equations:

$$\mathrm{SR} = (1 - \underline{f_S}) k_f C_f + k_s C_s \tag{6.19}$$

with the sizes of the fast or litter pool, C_f, and the slow pool, C_s, the rate constants

$$k_f = \omega^{\underline{\kappa}} \underline{Q}_{10,f}^{T_a/10} / \underline{\tau_f} \tag{6.20}$$

and

$$k_s = \omega^{\underline{\kappa}} \underline{Q}_{10,s}^{T_a/10} / \tau_s \tag{6.21}$$

f_S is the fraction of litter loss that goes to the long-lived soil carbon pool, T_a the air temperature, κ the soil moisture dependence parameter, $Q_{10,f}$ and $Q_{10,s}$ temperature dependence parameters, and τ_f and τ_s the pool turnover times. f_S, κ, $Q_{10,f}$, $Q_{10,s}$ and τ_f are controlling parameters, whereas the turnover time of the slow carbon pool, τ_s, is set to infinity as described in the following.

In a normal forward run the carbon pools must be spun up until respiration from these pools comes into equilibrium with material entering the pools. In fact, this is done for the fast litter pool by spinning up the model for five years. The slow carbon pool is treated differently as the spin-up can take centuries of simulation, thereby dominating the computational cost. One cannot neglect the process however, since the relationship between this respiration flux and long-term mean NPP will determine the overall carbon balance. The size of the slow carbon pool is held constant through the simulation time of 21 years and is determined by the time averages of NPP and SR (denoted by an overlying bar) at each gridcell and a scaling parameter β:

$$C_s = \frac{\overline{\mathrm{NPP}} / \underline{\beta} - (1 - \underline{f_S}) \overline{k_f C_f}}{\overline{k_s}} \tag{6.22}$$

Substituting into Equations 6.19 and 6.18 yields

$$\overline{\mathrm{NEP}} = \overline{\mathrm{NPP}} \left(1 - \frac{1}{\underline{\beta}} \right) \tag{6.23}$$

From Equation 6.23 it follows that $\overline{\mathrm{NEP}}$ is zero for $\beta = 1$ and is positive (net uptake) for $\beta > 1$.

Parameters and spatial discretization

A choice one always faces when setting up a parameter estimation problem such as this is the level of detail or the resolution of the parameter set. BETHY has 21 controlling parameters for each PFT, there are 13 PFTs and 3462 gridpoints. Thus, there is a range of choices from a single global description (21 controlling parameters) to an independent parameter set for every gridpoint (21×3462 controlling parameters). In this study 18 of the 21 parameters are applied globally, mainly those concerning the soil model or general plant physiology. Two of the key

photosynthetic parameters, V_{max} and the ratio $jtv = J_{max}/V_{max}$ are explicit for each PFT. Finally the key carbon storage parameter β also varies with PFT. Some of these parameters, mainly those controlling the heterotrophic respiration part (except for β) have been transformed by a logarithmic scale to resemble a Gaussian probability distribution for the optimisation routine. This holds especially true for the Q_{10} values as they exhibit a log-normal probability density [Holland et al., 2000]. In addition to these 57 parameters within BETHY an initial value of the atmospheric concentration (offset) is added as an unknown. The full list of parameters with their initial values and uncertainties is given in Table 6.2 as mentioned earlier.

6.3.2 Transport model

The transport model used here is the TM2 as described in Heimann [1995]. The model is an off-line tracer transport model with a 7.8° latitude × 10° longitude grid and nine vertical levels. It is driven by analyzed winds from the European Centre for Medium Range Weather Forecasts (ECMWF). The model features vertical transport by convection and turbulent eddy transport following the schemes of Louis [1979] and Tiedtke [1989] respectively. TM2 has been a participant throughout the series of experiments in the Transport Model Comparison (TRANSCOM) studies [Law et al., 1996; Gurney et al., 2002].

The adjoint form of TM2 as discussed in K02 is used in this study. This form of the model was constructed by Kaminski et al. [1999a] and used in a previous flux inversion by Kaminski et al. [1999b]. As required by the shift to interannual rather than cyclostationary concentration fields, the pulse response form of the adjoint is used so that the decay of emissions back towards a uniform background can be captured. A limitation of this study is the use of meteorological driving data from a single year, in this case 1987. Thus interannual variations in measured concentration caused by interannual variations in transport will be misinterpreted as arising from interannual variations of sources. This may, in turn, corrupt estimates of parameters constrained by interannual source variations. Dargaville et al. [2000] considered the impact of interannual variations in transport on their mass-balance inversion and found them to be small.

6.3.3 Background fluxes

A prerequisite in making any inferences about the terrestrial biosphere from atmospheric observations is the contribution of other CO_2 fluxes. In this study, these contributions are accounted as fixed fluxes, i.e. they do not depend on additional parameters. Three contributions (fossil fuel emissions, ocean fluxes and land-use change) to this background flux are considered using prior estimates of these fluxes.

Combined emissions from fossil fuel burning and cement production are known to have increased over the study period and changed in spatial structure. Flux magnitudes from Marland et al. [2001] for the years 1979 to 1995 have been extended by a constant magnitude of 6.5 Pg C yr^{-1} for the years 1995 to 2000. The spatial patterns of this flux are taken from Andres

Table 6.2: Controlling parameters and their initial and optimised values and uncertainties. Units are V_{max}: μmol(CO_2)$m^{-2}s^{-1}$, jmt: $(°C)^{-1}$, gt: μmol(CO_2)mol(air)$^{-1}(°C)^{-1}$, activation energies E: J/mol, τ_f: years, offset: ppm, all others unitless. Uncertainties are in percentage unless a range is given and represent one standard deviation.

Parameter	initial value	optimised value	init. uncertainty	opt. uncertainty
V_{max}(TrEv)	60	43.2	20	10.5
V_{max}(TrDec)	90	153.6	20	19.0
V_{max}(TmpEv)	41	41.0	20	20.0
V_{max}(TmpDec)	35	40.8	20	19.9
V_{max}(EvCn)	29	32.5	20	16.3
V_{max}(DecCn)	53	94.2	20	19.9
V_{max}(EvShr)	52	108.0	20	19.9
V_{max}(DecShr)	160	218.5	20	19.4
V_{max}(C3Gr)	42	18.0	20	16.9
V_{max}(C4Gr)	8	0.2	20	12.8
V_{max}(Tund)	20	27.2	20	19.3
V_{max}(Wetl)	20	19.4	20	20.0
V_{max}(Crop)	117	45.4	20	17.9
jtv(TrEv)	1.96	1.97	5	5.0
jtv(TrDec)	1.99	1.98	5	5.0
jtv(TmpEv)	2.0	2.0	5	5.0
jtv(TmpDec)	2.0	2.0	5	5.0
jtv(EvCn)	1.79	1.81	5	5.0
jtv(DecCn)	1.79	1.80	5	5.0
jtv(EvShr)	1.96	1.97	5	5.0
jtv(DecShr)	1.66	1.66	5	5.0
jtv(C3Gr)	1.9	1.89	5	5.0
jtv(C4Gr)	17.5	17.5	5	5.0
jtv(Tund)	1.85	1.84	5	5.0
jtv(Wetl)	1.85	1.85	5	5.0
jtv(Crop)	1.88	1.88	5	5.0
α_q	0.28	0.39	5	4.9
α_i	0.04	0.04	5	5.0
K_C	460×10^{-6}	351×10^{-6}	5	4.9
K_O	0.33	0.34	5	5.0
jmt	0.04	0.04	5	5.0
gt	1.7	1.0	5	5.0
E_{K_O}	35948	36117	5	5.0
E_{K_C}	59356	59266	5	4.9
$E_{V_{max}}$	58520	67657	5	4.8
E_k	50967	50806	5	5.0
E_{R_d}	45000	45799	5	4.9
$f_{R,leaf}$	0.4	0.27	25	14.9
$f_{R,growth}$	1.25	0.53	5	4.9
f_S	0.2	0.7	-0.1; +0.2	-0.1; +0.11
κ	1.0	0.7	-0.9; +9	-0.29; +0.51
$Q_{10,f}$	1.5	2.7	-0.5; +0.75	-0.38; +0.43
$Q_{10,s}$	1.5	1.2	-0.5; +0.75	-0.11; +0.12
τ_f	1.5	3.2	-1.; +3.	-0.7; +0.9
β(TrEv)	1	1.11	25	15.0
β(TrDec)	1	1.03	25	24.2
β(TmpEv)	1	1.13	25	25.0
β(TmpDec)	1	1.90	25	24.9
β(EvCn)	1	0.75	25	9.0
β(DecCn)	1	2.26	25	25.0
β(EvShr)	1	2.43	25	25.0
β(DecShr)	1	1.55	25	9.8
β(C3Gr)	1	1.05	25	23.6
β(C4Gr)	1	1.08	25	23.9
β(Tund)	1	1.25	25	20.1
β(Wetl)	1	0.81	25	25.0
β(Crop)	1	2.82	25	24.9
offset	338	338.0	0.3	0.1

et al. [1996] for the years up to 1990 and then kept constant through the 1990s. There is no seasonality in the fossil fuel flux.

The specified ocean fluxes are taken from two sources. As in K02, the flux pattern and magnitude from Takahashi et al. [1999] are used to describe the monthly flux climatology. An estimate of interannual variability in ocean flux taken from the study of Le Quéré et al. [2000] is added by first removing the seasonal climatology from this field and then adding the anomalies for each month to the Takahashi et al. [1999] climatology. Interannual variability in ocean flux is generally believed to be small [Prentice et al., 2001]. This is also true for the Le Quéré et al. [2000] study. So, even if relative errors in that flux are large, the impact on the present study will be small. More important is the long-term trend in this flux with gradually increasing uptake in response to increasing atmospheric CO_2 concentrations. This trend is captured by the model with decadal average ocean uptake in the 1990s 0.3 Pg C yr^{-1} greater than for the 1980s.

Land-use change induced carbon fluxes are undoubtedly the most problematic background fluxes for this study as it is even not perfectly clear which quantity is exactly needed for such a study. Processes which are not captured by the terrestrial model must be included. These might well be different in different models. BETHY has no treatment of land-use induced disturbance and so land-use change has to be specified as an external flux. As in K02 estimates of Houghton et al. [1990] for the flux caused by land-use change are used. Importantly, this flux compilation contains no information about either seasonality or interannual variability.

6.3.4 Data

As already mentioned, the model is optimised in two stages and against two different datasets. The first dataset is of daily AVHRR fields from the NOAA Global Vegetation Index (GVI) satellite data archive for the years 1989 and 1990 with a resolution of 1/7° latitude by longitude [Gutman et al., 1995]. From this field the Global Environment Monitoring Index (GEMI, Pinty and Verstraete [1992]) is computed and then averaged to 1° latitude by longitude over space and to monthly values over time. The annual average data coverage is almost 75% of the global land areas. Values of GEMI are then translated into fAPAR following a regression derived by Gobron et al. [1997]. The error in fAPAR is estimated to lie between 0.05 and 0.1.

The second dataset is of monthly mean atmospheric concentration data from GLOBALVIEW-CO_2 [2001]. This data consists of pseudo-weekly interpolation of spatial and temporal fits to flask and continuous in situ CO_2 concentration data measured at approximately 100 sites globally. Data are only used for years, where the number of measurements was sufficient to avoid data which are synthesized by the gap-filling procedures in the GLOBALVIEW-CO_2 [2001] compilation. The uncertainty is derived from compilation's residual standard deviation (RSD) values by adding a floor of 0.5 ppm, which accounts for model error:

$$\mathrm{unc} = \sqrt{0.25 + \mathrm{RSD}^2} \tag{6.24}$$

The choice of CO_2 monitoring stations to use in a study such as this is also a trade-off among competing requirements. The more data one can include the lower the predicted uncertainty

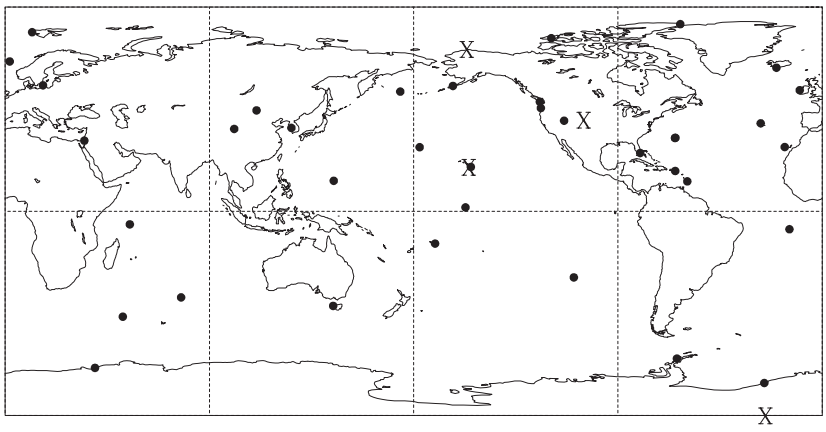

Figure 6.5: CO_2 observing network used for this study. Crosses denote station for which simulated concentrations are shown.

on parameters will be and, correspondingly, the better the constraint on predicted quantities. However, changes in station density throughout the study period may be misinterpreted by the optimisation procedure as interannual variability in concentration whereas it may be only the observation of previously undetected phenomena. Further stations with unrealistically large responses to the background fluxes will bias estimates of the mean concentration climatology. This climatology also helps constrain parameters. In summary the observing network has to be sufficiently dense for a good constraint, sufficiently invariant to allow realistic estimates of interannual variability and containing monitoring stations which give a reasonable simulation by the transport model. Most of these criteria also held for K02, therefore the same observing network as used in this study is adopted here. The network is shown in Figure 6.5 and listed in Table 6.3.

6.4 Results and Discussion

This section presents first CCDAS results derived from a control experiment based on BETHY 11 and the set of assumptions listed in the previous sections. However, as this CCDAS is still a prototype in a development and test stage bugs have been identified and removed. For example, an error in BETHY 11 related to the spin-up in the fast soil carbon pool has been identified in the course of this analysis. Hence, the results have to interpreted with care, with the influence of this error in mind.

As might be expected, there is a rich suite of possible results to explore from such a calculation. The results can be grouped into three major topics: (1) the fit of the simulated concentrations to the measured atmospheric CO_2 concentrations, (2) the optimised parameter set, and (3) the simulated terrestrial carbon fluxes using the optimised parameters. Nevertheless having mentioned the above drawbacks, it is still valuable to compare anomalies in the net

Table 6.3: List of station codes and names along with their residual standard deviation (RSD) for the year 1998 (if not available then for the year given in brackets after the value).

Code	Descriptive Name	RSD exemplarily for 1998 (ppmv)
ALT	Alert, N.W.T., Canada	0.91
AMS	Amsterdam Island	0.38 (1990)
ASC	Ascension Island	0.76
AVI	St. Croix, Virgin Islands	0.69 (1990)
AZR	Terceira Island, Azores	1.12
BAL	Baltic Sea	4.72
BME	St. David's Head, Bermuda	1.26
BMW	Southhampton, Bermuda	1.87
BRW	Barrow, Alaska	1.17
CBA	Cold Bay, Alaska	1.42
CGO	Cape Grim, Tasmania	0.52
CHR	Christmas Island, Kiribati	0.51
CMO	Cape Meares, Oregon	1.71
CRZ	Crozet, Indian Ocean	0.55
EIC	Easter Island	0.75
GMI	Guam, Mariana Islands	0.85
HBA	Halley Bay, Antarctica	0.51
ICE	Storhofdi, Heimaey, Iceland	0.72
IZO	Tenerife, Canary Islands	0.79
KEY	Key Biscayne, Florida	1.09
KUM	Cape Kumukahi, Hawaii	1.06
MBC	Mould Bay, N.W.T., Canada	0.92
MHD	Mace Head, Ireland	1.20
MID	Sand Island, Midway	0.95
MLO	Mauna Loa, Hawaii	0.64
NWR	Niwot Ridge, Colorado	1.06
OPW	Olympic Peninsula, Washington	0.82 (1990)
PSA	Palmer Station, Antarctica	0.53
RPB	Ragged Point, Barbados	0.73
SEY	Mahe Island, Seychelles	0.75
SHM	Shemya Island, Alaska	1.10
SMO	Tutuila, American Samoa	0.68
SPO	South Pole, Antarctica	0.51
STM	Atlantic Ocean (Polarfront)	1.09
SYO	Syowa Station, Antarctica	0.50
TAP	Tae-ahn Peninsula, Korea	2.44
UTA	Wendover, Utah	1.85
UUM	Ulaan Uul, Mongolia	1.45
WIS	Sede Boker, Israel	1.67
WLG	Mt. Waliguan, China	1.18
ZEP	Zeppelin Station, Svalbard	1.26

terrestrial carbon flux with climate anomalies to demonstrate the principal usefulness.

6.4.1 Fit to Data

The overall quality of the fit to the data is embodied in the final value of the cost function. Strictly there is also a contribution from the mismatch between initial and predicted parameter values but this is much smaller than the data contribution. This is hardly surprising given the 10332 data points in the concentration dataset versus only 58 parameters. The final value of the cost function is 12316, with a value of 11766 resulting from the concentration mismatch. This suggests an adequate fit to the data, however only from years in which measurements were made at a site are attempt to fit in the extended dataset of GLOBALVIEW-CO_2 [2001]. The real number of observations is hence 6936 observations with any real input into the cost function.

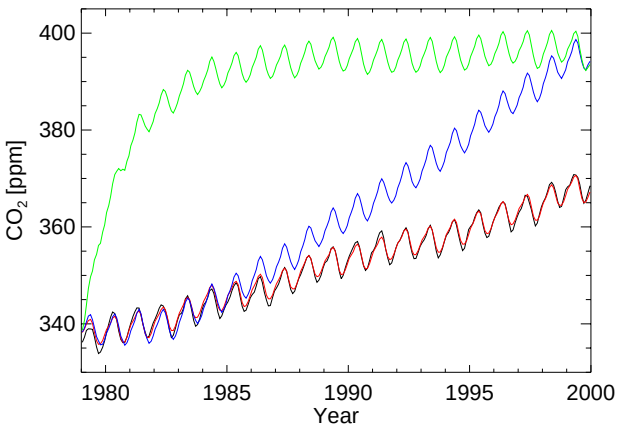

Figure 6.6: Time-series of atmospheric CO_2 concentration at Mauna Loa, Hawaii. The black line denotes the measured values, the red line the prognosed concentration with the optimised parameter vector, the green line the simulated concentration as derived from the first guess parameter values including the erroneous spin-up procedure and the blue line the first guess concentrations with a corrected spin-up.

The average squared mismatch or reduced χ^2 statistic is the most common measure of the quality of a fit. In this case it is 1.69. In general a statistical consistent fit to the data would give a χ^2 of ≈ 1. The larger value here suggests that the model is incapable of fitting the data as well as the data uncertainties demand. Enlarged data uncertainties would propagate through the calibration algorithms to enlarged parameter uncertainties. Therefore, the uncertainty estimates on parameters should be regarded as slightly optimistic.

Figure 6.6 shows besides the observed and prognosed times-series of atmospheric CO_2 concentration also two simulated time-series using the a priori parameter values from two different BETHY versions. The green line represents concentrations as simulated by BETHY 11 and shows a rather strange behaviour with a rapid increase of CO_2 during the first three simulation years. This is because the fast decomposing soil carbon pool was not in equilibrium at the beginning of the simulation period due to an error in the spin-up procedure. This error has been removed in BETHY 12 which can be seen by the blue line. The dramatic rise of simulated atmospheric CO_2 concentrations to almost 400 ppm is a consequence of the a priori assumption of a neutral biosphere over the simulation period ($\beta = 1$) and is apparent in both simulations as this is a fixed point determined by the background fluxes. However, all results presented here are derived from BETHY 11 and therefore, as mentioned above, are only preliminary. The optimal fit to the data seems to be rather good (as also discussed in the following) although it is derived from the erroneous BETHY 11 version.

Simulated time-series of CO_2 concentrations at a station can be decomposed into a climatological seasonal cycle and interannual variability, the latter often filtered to emphasize signals of key scientific interest. Here, the procedure of Thoning et al. [1989] is used for this decomposition and the fits are displayed exemplarily for four selected stations. Figure 6.7 shows seasonal cycles fitted to the simulated and observed concentration time-series at Point Barrow, Alaska and Niwot Ridge, Colorado. The uncertainties indicated by the dotted lines are the one standard deviation uncertainties averaged over the whole record. For both stations Niwot Ridge and Point Barrow the simulated seasonal cycle fits the observed data well. This is not entirely surprising as the full BETHY model itself constrained only by satellite data (here, the first assimilation

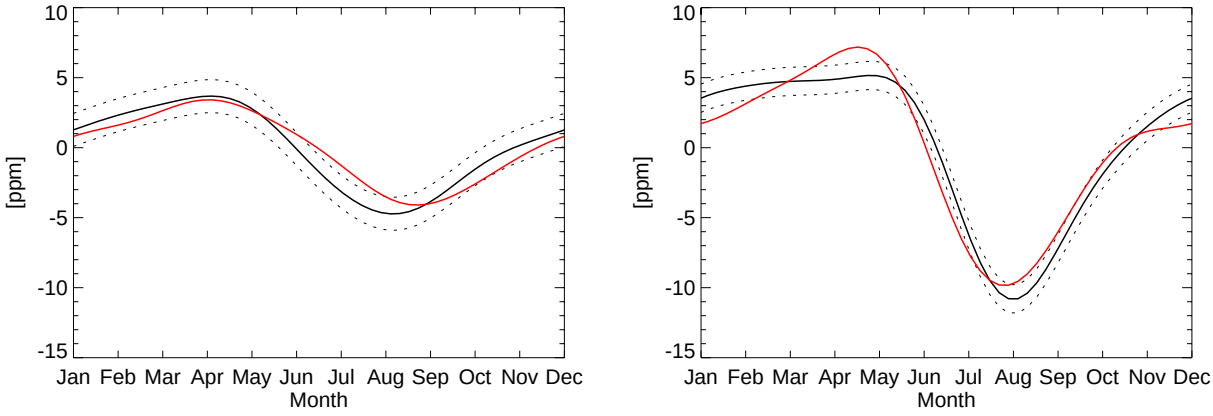

Figure 6.7: Simulated (red) and observed (black, with mean uncertainty) seasonal cycle of atm. CO_2 for two sites: Niwot Ridge, Colorado (left) and Point Barrow, Alaska (right).

step) shows already a modelled seasonal cycle consistent with CO_2 measurements [Knorr, 1997]. There is a striking mismatch between simulated and observed concentrations in spring at Point Barrow station which is also already apparent in the original BETHY model [Knorr, 1997] and thus, seems to be a model inherent problem although the magnitude of the mismatch is largely reduced in this study here.

Figure 6.8 shows errors (simulated − observed) concentration time-series for Mauna Loa, Hawaii and South Pole filtered to retain periods greater than 80 days [Thoning et al., 1989]. The constant uncertainties are the averages over the yearly values used in the optimisation. The first thing to note is that, for both records, the mismatch in the first year (1979) is much bigger than the uncertainty which is clearly a result of the erroneous spin-up procedure. However, for the rest of the simulation period (1980 to 2000) differences are generally smaller than observational uncertainties, suggesting a good fit to the observations. There are periods (mainly the years 1984 and 1986) when trends in the observed and simulated time-series at Mauna Loa are clearly different. This mismatch seems most likely to indicate errors in sources which impact the measured concentrations as opposed to transport errors. The south Pole record shows a very good fit between the model and observations (neglecting the year 1979). This is encouraging for interpretations made at a global scale since South Pole, remote as it is from local sources, is probably the best available record of globally integrated concentrations at interannual timescales.

6.4.2 Optimised Parameters

Recall from Section 6.3 that there is a division between globally uniform and spatially explicit parameters in our set-up according to the PFT distribution. Table 6.2 lists besides the prior values and uncertainties also the posterior values and uncertainties for all parameters.

As mentioned already in Section 6.2.3 only a subset of the space of control variables can be constrained. In this study 17 out of the 58 dimensions could be observed from the chosen CO_2 concentration network, i.e. 17 eigen-values are larger than the absolute value of the largest

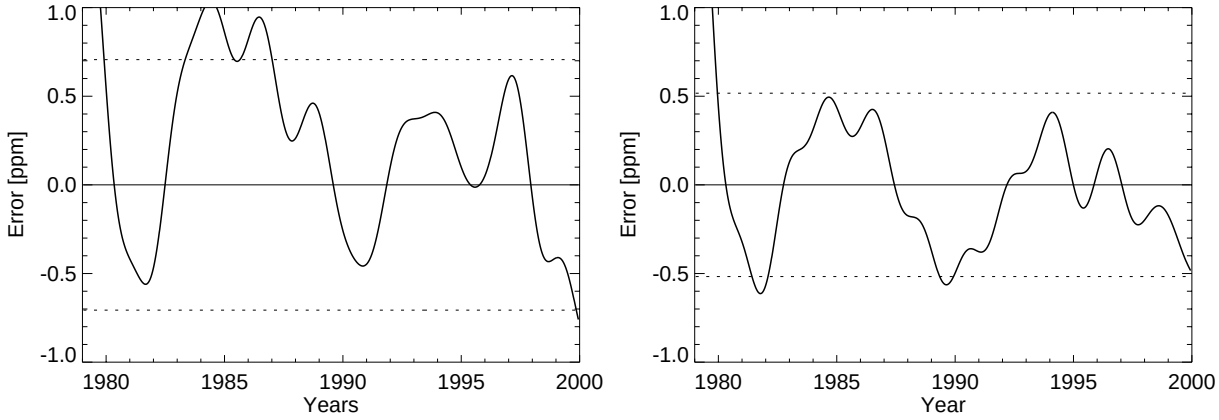

Figure 6.8: Time-series of errors (simulated − observed) in the interannual variability of concentrations for two observing sites: left panel Mauna Loa, Hawaii and right panel South Pole. Dotted lines are the averaged uncertainties over the simulation period in the observed records.

negative eigen-value of **H** (see Equation 6.4). This is also reflected in the reduction of the parameter uncertainties; for about 16 parameters initial uncertainties are reduced by more than 10% (among them some of the PFT specific V_{max} and β parameters, the offset, the leaf fraction of the maintenance respiration and parameters controlling the heterotrophic respiration).

One of the most important parameters to derive a good fit to the data is the spatially explicit β parameter. As noted in Section 6.3.1 the β parameter controls the carbon storage efficiency of a given ecosystem. This parameter, along with NPP, defines the net carbon uptake of the terrestrial biosphere (Equation 6.23) and therefore strongly influences modelled CO_2 concentrations. Figure 6.9 shows a map of the mean β parameter weighted by the fractional coverage of the respective PFTs per gridcell and the mean weighted relative reduction in the uncertainty. It is interesting to note that the terrestrial biosphere is almost everywhere a carbon sink except the North American boreal region and a small band from Scandinavia to Central Siberia which also is mainly covered by boreal vegetation. In these regions the biosphere is a carbon source to the atmosphere. These areas also seem to be the best constraint areas by atmospheric CO_2 observations as there the uncertainty reduction for β is the highest by more than 50%. The mid latitudinal areas but also the main desert regions (Sahara, Arabian peninsula and central Australia) exhibit the highest β_{opt} values of ≈2 due to the high values for crops, deciduous conifers and evergreen shrubs which are the dominant PFTs in these regions. The high storage capacity for crops is plausible as it is reinforced by the harvest of agricultural products. Throughout this whole area of high carbon sink capacity the uncertainty in β is almost unchanged to the initial uncertainty. Besides, the desert areas are the regions with the lowest productivity. However, the highly productive tropical areas show only a small carbon storage capacity with a β_{opt} value of ≈1.1 but are fairly well constrained (uncertainty reduced by ≈30%).

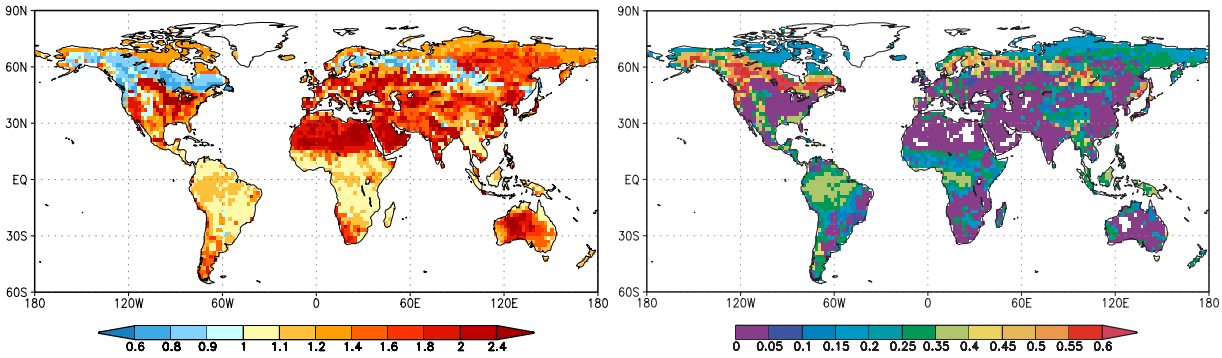

Figure 6.9: Map of the mean optimised β parameter weighted by the fractional coverage of the PFTs per gridcell (left panel) and accordingly the relative reduction in the uncertainty of the β parameter (right panel), white areas over land denote no reduction.

Besides the β parameter, V_{max} and the ratio $jtv = J_{max}/V_{max}$ are both spatially explicit parameters. For eight out of the thirteen PFTs, V_{max} shows optimised values which are more than two standard deviation higher or lower than the initial value. The $V_{max,opt}$ value for C_4 grass reveals the highest change from an initial value of 8 μmol(CO_2)$m^{-2}s^{-1}$ to only 0.2 μmol(CO_2)$m^{-2}s^{-1}$ suggesting a drastic reduction in the carbon assimilation of C_4 grass. Uncertainties of V_{max} values for C_4 grass and tropical evergreen trees are substantially reduced whereas uncertainties for the other V_{max} values are only slightly reduced. This holds even more so for the jtv parameter with optimised values very close to the initial values and also no reduction in their uncertainties. This suggests that the sensitivity of this parameter is highly colinear with the V_{max} parameter which mainly reflects prior knowledge as the ratio J_{max}/V_{max} was chosen as a parameter instead of J_{max} directly.

Of major interest are the parameters controlling the heterotrophic respiration and here especially the optimised Q_{10} values as the temperature dependency of the soil carbon decomposition has recently been under debate because of contradicting observations [Trumbore et al., 1996; Giardina and Ryan, 2000]. Unfortunately, the error in the spin-up procedure in BETHY 11 led to an unrealistic high amount of carbon in the fast soil carbon pool at the beginning of the simulation period which was also not in equilibrium with the plants productivity after the spin-up. Therfore the optimisation procedure had to chose parameter values which compensate for this artefact as can be seen by the somewhat unexpected high litter fraction transformed into slow decomposing soil carbon, $f_{S,opt} = 0.7$, the relatively high $Q_{10,f,opt}$ value of 2.7 suggesting high litter decomposition rates at already moderate temperatures and a low $Q_{10,s,opt}$ value of 1.2 reducing the decomposition rates of the slow soil carbon pool with temperature. The optimised turnover time of the litter pool has a relatively large value, $\tau_{f,opt} = 3.2$, which partly counteracts against the fast decomposition of the oversized litter pool at the beginning of the simulation period.

Of course this error in the BETHY 11 version finally affects all parameters, therefore, no final conclusions should be drawn from their reported optimised values here. A parameter

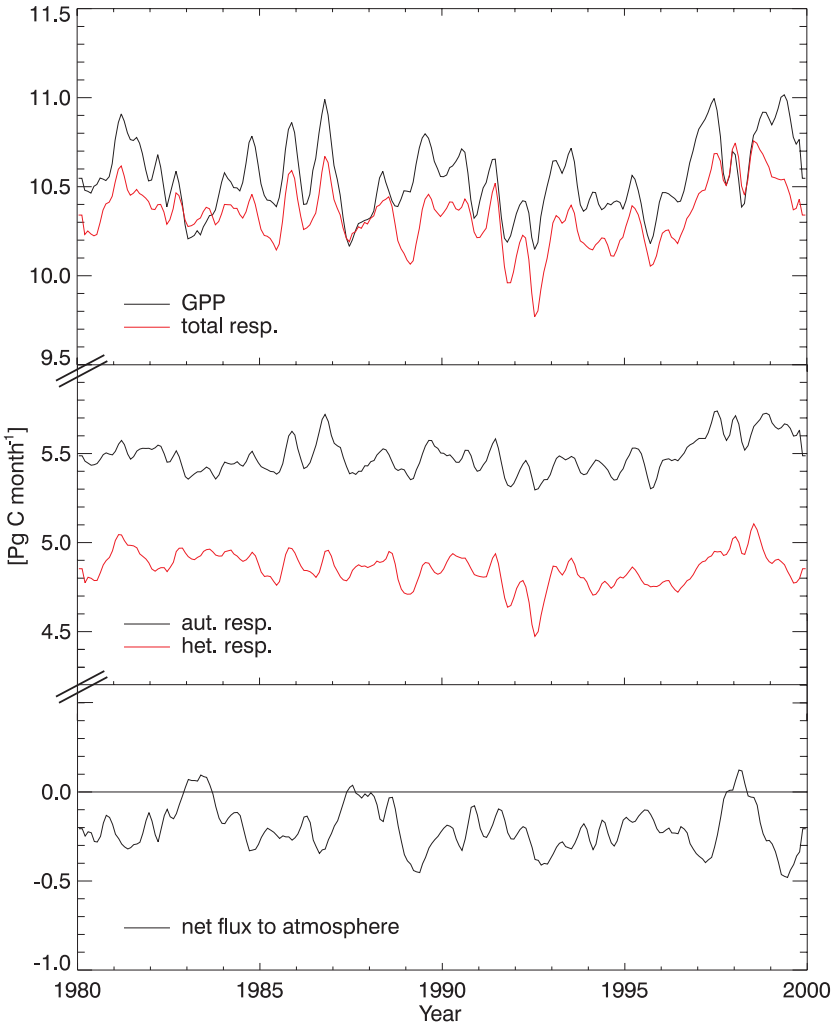

Figure 6.10: Time-series of global monthly fluxes prognosed from CCDAS smoothed with a five month running mean filter.

optimisation using the corrected BETHY 12 version is currently running and showing some very different parameter values, however, this optimisation has not found a cost function minimum yet and still exhibits a large gradient to the current cost function value.

6.4.3 Derived Fluxes

Although the optimised parameters which control the ecosystem processes in BETHY are most likely to be unrealistic as explained above it is still worthwhile to analyze the prognosed fluxes because these fluxes lead if transported by an atmospheric transport model to simulated CO_2 concentrations consistent with observations as shown in Section 6.4.1.

Figure 6.10 displays time-series of the relevant global fluxes (GPP, autotrophic and heterotrophic respiration, and the net flux to the atmosphere). Throughout almost the entire

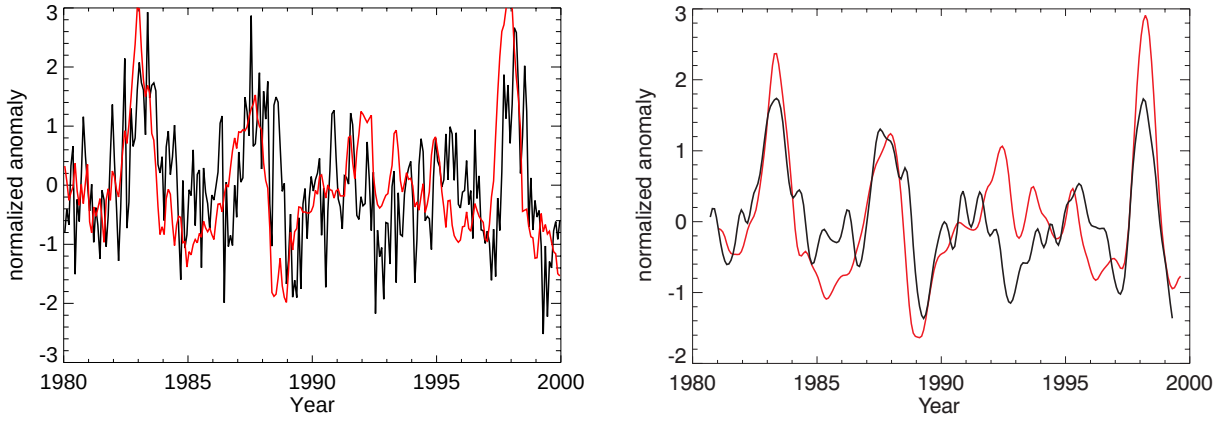

Figure 6.11: Time-series of normalized anomalies of the Niño-3 SST index (red line) and the net terrestrial CO_2 flux (black line): the left panel shows unfiltered monthly values and the right panel shows low-pass filtered records with the Niño-3 SST record shifted forward by 4 months.

simulation period GPP slightly exceeds total respiration making the terrestrial biosphere a carbon sink. However, there are three distinct events (1983, 1987, and 1998) where a reduction in GPP exceeds a reduction in the respiration flux leading to an anomalous terrestrial carbon source as can be seen from the net flux. Terrestrial carbon sink anomalies are not as distinct as the source anomalies except for the year 1989 where the decrease in respiration is much stronger than the decrease in GPP and also for the year 1992 showing rather a heterotrophic respiration anomaly with the lowest respiration values around this year in the entire record. The carbon source anomalies strongly correlate with pronounced EL Niño events whereas the sink anomalies correlate with a strong La Niña event for the case of 1989 or the Mount Pinatubo eruption for the year 1992.

The left panel in Figure 6.11 shows time-series of the monthly Niño-3 SST anomalies (from Climate Prediction Center [2002]) and the monthly net CO_2 flux anomalies (with the seasonal cycle being subtracted) as prognosed by CCDAS both normalized by the respective standard deviation. The correlation between these two time-series shows a maximum with a correlation coefficient of 0.8 at a four months lag of the terrestrial net flux as can be seen from the right panel of Figure 6.11 displaying the records smoothed by a 6-month low-pass filter and the Niño-3 SST time-series shifted forward by four months. It is worthwhile to stress that the correlation between ENSO and the net CO_2 flux is strong for both El Niño and La Niña events. A response lag of four months of the terrestrial biosphere to climate anomalies such as ENSO seems reasonable as the response is mainly triggered by a change in plant available soil moisture which can have a buffer capacity of several months in responding to ENSO induced changes in precipitation. This buffer capacity is especially pronounced in tropical regions as plants can have very deep roots there [Kleidon and Heimann, 1998].

The largest deviation in the positive correlation between ENSO (as presented by the Niño-3

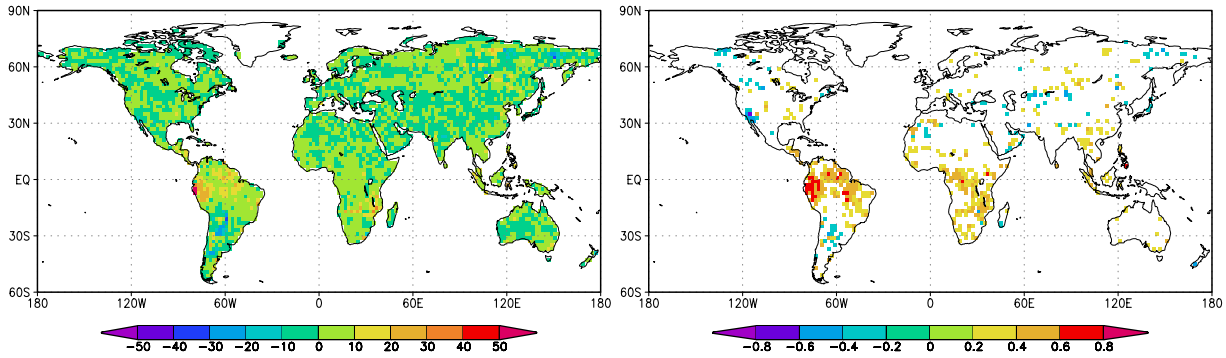

Figure 6.12: Monthly net CO_2 flux averaged over the months during which the Niño-3 SST > 1σ (left map, units: g C $m^{-2}month^{-1}$, positive: flux to the atmosphere). Correlation coefficient of each gridcell with the normalized Niño-3 index at a 99% significance level (right map).

index) and the net terrestrial CO_2 flux occurs during 1992 and is most likely a response to the Mount Pinatubo eruption which lead to a global surface cooling during the early 1990s [Robock, 2002].

The left map of Figure 6.12 displays the pattern of the monthly net CO_2 flux averaged over the months during which the normalized Niño-3 SST index is larger than one considering the four months lag between the two records. The magnitude of this mean monthly net flux lies almost over the entire land area in an interval between -10 to 10 g C $m^{-2}month^{-1}$ except for larger net fluxes to the atmosphere around Ecuador, the northern border of Brasil and also in Africa around the area of Moçambique. Argentina is the only area where somewhat higher net terrestrial uptake fluxes are shown. The right map of Figure 6.12 shows a map of the 4-months lagged correlation coefficient of each gridcell with the normalized Niño-3 SST index; shown are only gridcells at a 99% significance level derived from a Student's t-test. The areas with a large net CO_2 flux to the atmosphere (Ecuador, north Brazil, and Moçambique) show in general a positive correlation of around 0.6. Anti-correlated gridcells can be found in Argentina and also in California, both regions are affected with an increase in precipitation during strong El Niño events [Diaz and Kiladis, 1992].

6.5 Conclusions

A carbon cycle data assimilation system is presented capable of assimilating both remote sensing data as well as atmospheric CO_2 concentration measurements into a process-based model of the terrestrial biosphere in order to (1) calibrate the model parameters, (2) derive terrestrial CO_2 fluxes consistent with the atmospheric observations, and (3) present uncertainties on both model parameters and derived quantities such as fluxes. This system heavily relies on the availability of the derivative (adjoint, tangent linear, and Hessian) code of the underlying model which is derived by the technique of automatic differentiation. The model system is still under

development and the results presented in this chapter are preliminary especially since errors in the underlying model version have recently been detected. Based on a corrected model version, a new set of experiments is currently being carried out.

The preliminary results are promising as they demonstrate that the method works and is capable of fitting 20 years of monthly CO_2 concentration data with a set of 58 parameters. The assimilation of the concentration data substantially reduced the a priori uncertainties of some key parameters. In addition to the estimation of uncertainties this method also provides uncertainty covariances, which allows to define observed and unobserved directions in the 58 dimensional parameter space. The current set of observations illuminates about 17 directions in that space.

As the design of CCDAS is flexible to include further streams of data (eddy flux measurements, stable carbon isotope measurement), these data should be exploited to enlarge the observed subset of the parameter space. K02 have demonstrated this effect for eddy flux measurements in regions, which are sparsely covered by the atmospheric network.

It is interesting to note that these preliminary results contradict the recently discussed theories that attribute anomalous large growth rates in atmospheric CO_2 during the strong El Niño years 1994/1995 and 1997/1998 to biomass burning [Langenfelds et al., 2002; Page et al., 2002]. The present study suggests that these observed anomalous growth rates are a direct response of the terrestrial biosphere to El Niño induced climate fluctuations, which results in a net flux to the atmosphere. This net flux is caused by small perturbations of the large gross photosynthesis and respiration fluxes. A future CCDAS version should include a fire module which can allow for large, non-linear singular respiration events.

Each CCDAS calibration run uses a set of ingredients which reflect prior assumptions. In the described control experiment some of these ingredients such as the values of the background fluxes, the prior uncertainties or the chosen parameter set reflect a particular choice. Experiments based on combinations of alternative choices should be used to quantify the influence of particular assumptions.

References

Andres, R. J., Marland, G., Fung, I., Matthews, E., 1996. A $1^\circ \times 1^\circ$ distribution of carbon dioxide emissions from fossil fuel consumption and cement manufacture, 1950-1990. Glob. Biogeochem. Cycles 10 (3), 419–429.

Barrett, D. J., 2002. Steady state turnover time of carbon in the Australian terrestrial biosphere. Glob. Biogeochem. Cycles 16 (4), doi:10.1029/2002GB001860.

Bousquet, P., Peylin, P., Ciais, P., Le Quéré, C., Friedlingstein, P., Tans, P. P., 2000. Regional changes in carbon dioxide fluxes of land and oceans since 1980. Science 290 (5495), 1342–1346.

Climate Prediction Center, 2002. National Centers for Environmental Prediction.

NOAA/National weather service, Camp Springs, MD, USA, Available online via http://www.cpc.ncep.noaa.gov/data/indices/index.html.

Collatz, G. J., Ribascarbo, M., Berry, J. A., 1992. Coupled photosynthesis-stomatal conductance model for leaves of C_4 plants. Aust. J. Plant Physiol. 19 (5), 519–538.

Dargaville, R. J., Heimann, M., Mcguire, A. D., Prentice, I. C., Kicklighter, D. W., Joos, F., Clein, J. S., Esser, G., Foley, J., Kaplan, J., Meier, R. A., Melillo, J. M., Moore, B., Ramankuty, N., Reichenau, T., Schloss, A., Sitch, S., Tian, H., Williams, L. J., Wittenberg, U., 2002. Evaluation of terrestrial carbon cycle models with atmospheric CO_2 measurements: Results from transient simulations considering increasing CO_2, climate, and land-use effects. Glob. Biogeochem. Cycles 16 (4), doi:10.1029/2001GB001426.

Dargaville, R. J., Law, R. M., Pribac, F., 2000. Implications of interannual variability in atmospheric circulation on modeled CO_2 concentrations and source estimates. Glob. Biogeochem. Cycles 14 (3), 931–943.

Diaz, H. F., Kiladis, G. N., 1992. Atmospheric teleconnections associated with the extreme phases of the Southern Oscillation. In: Diaz, H. F., Markgraf, V. (Eds.), El Niño: Historical and paleoclimatic aspects of the Southern Oscillation. Cambridge University Press, Cambridge, UK, pp. 7–28.

Enting, I. G., 2002. Inverse Problems in Atmospheric Constituent Transport. Cambridge University Press, Cambridge, U.K.

Enting, I. G., Trudinger, C. M., Francey, R. J., 1995. A synthesis inversion of the concentration and $\delta^{13}C$ of atmospheric CO_2. Tellus 47B (1-2), 35–52.

Fan, S., Gloor, M., Mahlman, J., Pacala, S., Sarmiento, J., Takahashi, T., Tans, P., 1998. A large terrestrial carbon sink in North America implied by atmospheric and oceanic carbon dioxide data and models. Science 282 (5388), 442–446.

Farquhar, G. D., 1988. Models relating subcellular effects of temperature to whole plant response. Symposium of the society for Experimental Biology 42, 395–409.

Farquhar, G. D., Caemmerer, S. V., Berry, J. A., 1980. A biochemical-model of photosynthetic CO_2 assimilation in leaves of C_3 species. Planta 149 (1), 78–90.

Feely, R. A., Wanninkhof, R., Takahashi, T., Tans, P. P., 1999. Influence of El Niño on the equatorial pacific contribution to atmospheric CO_2 accumulation. Nature 398 (6728), 597–601.

Giardina, C., Ryan, M., 2000. Evidence that decomposition rates of organic carbon in mineral soil do not vary with temperature. Nature 404 (6780), 858–861.

Giering, R., Kaminski, T., 1998. Recipes for adjoint code construction. ACM Trans. Math. Software 24, 437–474.

Giering, R., Kaminski, T., Slawig, T., 2003. Applying TAF to a Navier-Stokes solver that simulates an Euler flow around an airfoil. to appear in Future Generation Computer Systems.

GLOBALVIEW-CO_2, 2001. Cooperative Atmospheric Data Integration Project - Carbon Dioxide. CD-ROM, NOAA CMDL, Boulder, Colorado, [Also available on Internet via anonymous FTP to ftp.cmdl.noaa.gov, Path: ccg/co2/GLOBALVIEW].

Gobron, N., Pinty, B., Verstraete, M. M., Govaerts, Y., 1997. A semidiscrete model for the scattering of light by vegetation. J. Geophys. Res. 102 (D8), 9431–9446.

Griewank, A., 2000. Evaluating Derivatives: Principles and Techniques of Algorithmic Differentiation. No. 19 in Frontiers in Appl. Math. SIAM, Philadelphia, Penn.

Gurney, K. R., Law, R. M., Denning, A. S., Rayner, P. J., Baker, D., Bousquet, P., Bruhwiler, L., Chen, Y. H., Ciais, P., Fan, S., Fung, I. Y., Gloor, M., Heimann, M., Higuchi, K., John, J., Maki, T., Maksyutov, S., Masarie, K., Peylin, P., Prather, M., Pak, B. C., Randerson, J., Sarmiento, J., Taguchi, S., Takahashi, T., Yuen, C. W., 2002. Towards robust regional estimates of CO_2 sources and sinks using atmospheric transport models. Nature 415 (6872), 626–630.

Gutman, G., Tarpley, D., Ignatov, A., Olson, S., 1995. The enhanced NOAA global land dataset from the Advanced Very High-Resolution Radiometer. Bull. Amer. Meteorol. Soc. 76 (7), 1141–1156.

Heimann, M., 1995. The global atmospheric tracer model TM2. Technical Report No. 10, Max-Planck-Institut für Meteorologie, Hamburg, Germany.

Holland, E. A., Neff, J. C., Townsend, A. R., Mckeown, B., 2000. Uncertainties in the temperature sensitivity of decomposition in tropical and subtropical ecosystems: Implications for models. Glob. Biogeochem. Cycle 14 (4), 1137–1151.

Houghton, J. T., Jenkins, G. J., Ephraums, J. J. (Eds.), 1990. Climate change: The IPCC assessment. Cambridge University Press, Cambridge, U.K.

Kaminski, T., Giering, R., Scholze, M., Rayner, P., Knorr, W., 2003. An example of an automatic differentiation-based modelling system. In: Gavrilova, L., Kumar, V., L'Ecuyer, P., Tan, C. J. K. (Eds.), to appear in Computational Science – ICCSA 2003, Proceedings of the International Conference on Computational Science, Montreal, Canada, May 18-21, 2003. Lecture Notes in Computer Science. Springer, Berlin.

Kaminski, T., Heimann, M., 2001. Inverse modeling of atmospheric carbon dioxide fluxes. Science 294 (5541), U1–U1.

Kaminski, T., Heimann, M., Giering, R., 1999a. A coarse grid three-dimensional global inverse model of the atmospheric transport, 1, Adjoint model and Jacobian matrix. J. Geophys. Res. 104, 18,535–18,553.

Kaminski, T., Heimann, M., Giering, R., 1999b. A coarse grid three-dimensional global inverse model of the atmospheric transport, 2, Inversion of the transport of CO_2 in the 1980. J. Geophys. Res. 104, 18,555–18,581.

Kaminski, T., Knorr, W., Rayner, P. J., Heimann, M., 2002. Assimilating atmospheric data into a terrestrial biosphere model: A case study of the seasonal cycle. Glob. Biogeochem. Cycles 16 (4), doi:10.1029/2001GB001463.

Kaminski, T., Rayner, P., Heimann, M., Enting, I., 2001. On aggregation errors in atmospheric transport inversions. J. Geophys. Res. 106 (D5), 4703–4716.

Keeling, C. D., Bacastow, R. B., Carter, A. F., Piper, S. C., Whorf, T. P., Heimann, M., Mook, W. G., Roeloffzen, H., 1989. A three-dimensional model of the atmospheric CO_2 transport based on observed winds: 1. Analysis of observational data. In: Peterson, D. H. (Ed.), Aspects of Climate Variability in the Pacific and the Western Americas. Vol. 55. AGU, Washington, D.C., pp. 165–236.

Kleidon, A., Heimann, M., 1998. A method of determining rooting depth from a terrestrial biosphere model and its impacts on the global water and carbon cycle. Glob. Change Biol. 4 (3), 275–286.

Knorr, W., 1997. Satellitengestützte Fernerkundung und Modellierung des globalen CO_2-Austauschs der Landvegetation: Eine Synthese. Ph.D. thesis, Max-Planck-Institut für Meteorologie, Hamburg, Germany.

Knorr, W., 2000. Annual and interannual CO_2 exchanges of the terrestrial biosphere: Process-based simulations and uncertainties. Glob. Ecol. Biogeogr. 9 (3), 225–252.

Knorr, W., Heimann, M., 1995. Impact of drought stress and other factors on seasonal land biosphere CO_2 exchange studied through an atmospheric tracer transport model. Tellus 47B (4), 471–489.

Knorr, W., Schulz, J.-P., 2001. Using satellite data assimilation to infer global soil moisture status and vegetation feedback to climate. In: Beniston, M., Verstraete, M. M. (Eds.), Remote Sensing and Climate Modelling: Synergies and Limitations. Vol. 7 of Advances in Global Change Research. Kluwer Academic Publisher, Dordrecht and Boston, pp. 273–306.

Langenfelds, R. L., Francey, R. J., Pak, B. C., Steele, L. P., Lloyd, J., Trudinger, C. M., Allison, C. E., 2002. Interannual growth rate variations of atmospheric CO_2 and its $\delta^{13}C$, H_2, CH_4 and CO between 1992 and 1999 linked to biomass burning. Glob. Biogeochem. Cycles 16, doi:10.1029/2001GB001466.

Law, R. M., Rayner, P. J., Denning, A. S., Erickson, D., Fung, I. Y., Heimann, M., Piper, S. C., Ramonet, M., Taguchi, S., Taylor, J. A., Trudinger, C. M., Watterson, I. G., 1996. Variations in modeled atmospheric transport of carbon dioxide and the consequences for co2 inversions. Glob. Biogeochem. Cycles 10 (4), 783–796.

Le Quéré, C., Orr, J. C., Monfray, P., Aumont, O., Madec, G., 2000. Interannual variability of the oceanic sink of CO_2 from 1979 through 1997. Global Biogeochem. Cycles 14, 1247–1265.

Louis, J. F., 1979. A parametric model of vertical eddy fluxes in the atmosphere. Boundary Layer Meteorology 17, 187–202.

Marland, G., Boden, T. A., Andres, R. J., 2001. Global, regional, and national CO_2 emissions. In: Trends: A Compendium of Data on Global Change. Carbon Dioxide Information Analysis Center, Oak Ridge National Laboratory, U.S. Department of Energy, Oak Ridge, USA.

Nijssen, B., Schnur, R., Lettenmaier, D., 2001. Retrospective estimation of soil moisture using the vic land surface model, 1980-1993. J. Climate 14 (8), 1790–1808.

Page, S., Siegert, F., Rieley, J. O., Boehm, H.-D. V., Jaya, A., Limin, S., 2002. The amount of carbon released from peat and forest fires in Indonesia during 1997. Nature 420, 61–65.

Pinty, B., Verstraete, M. M., 1992. GEMI - a nonlinear index to monitor global vegetation from satellites. Vegetatio 101 (1), 15–20.

Prentice, I. C., Farquhar, G. D., Fasham, M. J. R., Goulden, M. L., Heimann, M., Jaramillo, V. J., Kheshgi, H. S., Le Quéré, C., Scholes, R. J., Wallace, D. W. R., 2001. The carbon cycle and atmospheric carbon dioxide. In: Houghton, J. T., Ding, Y., Griggs, D. J., Noguer, M., van der Linden, P. J., Dai, X., Maskell, K., Johnson, C. A. (Eds.), Climate Change 2001: The Scientific basis. Cambridge University Press, Cambridge, U.K., pp. 183–237.

Press, W. H., Teukolsky, S. A., Vetterling, W. T., Flannery, B. P., 1992. Numerical recipes in Fortran. Cambridge University Press, Cambridge, U.K.

Randerson, J. T., Still, C. J., Balle, J. J., Fung, I. Y., Doney, S. C., Tans, P. P., Conway, T. J., White, J. W. C., Vaughn, B., Suits, N., Denning, A. S., 2002. Carbon isotope discrimination of arctic and boreal biomes inferred from remote atmospheric measurements and a biosphere-atmosphere model. Glob. Biogeochem. Cycles 16 (3), doi:10.1029/2001GB001435.

Rayner, P. J., Enting, I. G., Francey, R. J., Langenfelds, R., 1999. Reconstructing the recent carbon cycle from atmospheric CO_2, $\delta^{13}C$ and O_2/N_2 observations. Tellus 51B (2), 213–232.

Robock, A., 2002. Pinatube eruption: The climatic aftermath. Science 295, 1242–1244.

Takahashi, T., Wanninkhof, R. H., Feely, R. A., Weiss, R. F., Chipman, D. W., Bates, N., Olafsson, J., Sabine, C., Sutherland, S. C., 1999. Net sea-air CO_2 flux over the global oceans: An improved estimate based on the sea-air pCO_2 difference. In: Nojiri, Y. (Ed.), Extended

abstracts of the 2nd International CO_2 in the Oceans Symposium, Tsukuba, Japan, January 18-22, 1999. pp. 9–15.

Tarantola, A., 1987. Inverse problem theroy - Methods for data fitting and model parameter estimation. Elsevier Science, New York, USA.

Thoning, K. W., Tans, P. P., Komhyr, W. D., 1989. Atmospheric carbon-dioxide at Mauna Loa Observatory: 2. Analysis of the NOAA GMCC data, 1974-1985. J. Geophys. Res. 94 (D6), 8549–8565.

Tiedtke, M., 1989. A comprehensive mass flux scheme for cumulus parameterization in large-scale models. Mon. Weath. Rev 117, 1779–1800.

Trumbore, S. E., Chadwick, O. A., Amundson, R., 1996. Rapid exchange between soil carbon and atmospheric carbon dioxide driven by temperature change. Science 272 (5260), 393–396.

Vukićević, T., Braswell, B. H., Schimel, D., 2001. A diagnostic study of temperature controls on global terrestrial carbon exchange. Tellus 53B (2), 150–170.

Wilson, M. F., Henderson-Sellers, A., 1985. A global archive of land cover and soils data for use in general-circulation climate models. Journal of Climatology 5 (2), 119–143.

Chapter 7

Summary and Perspectives

7.1 Summary of results

In the first part of this thesis (Chapter 2–5) the aim has been the investigation of the spatio-temporal pattern of the stable carbon isotopic composition of the land biosphere for the recent past as well as the understanding of the behaviour of terrestrial ecosystems, including atmosphere-biosphere $^{13}CO_2$ exchange for an abrupt climate change event. In addition to the conclusions given at the end of Chapter 2–5, the different results are in the following summarized in order to answer the questions raised in the introduction (Section 1.2):

1. *Does LPJ capture the main shifts in vegetation distribution for an abrupt climate change event such as the Younger Dryas cold period (≈12000 years BP)? Does this cold event which is believed to have happened mainly in the northern hemisphere have an impact on vegetation cover in the tropics or the southern hemisphere according to the LPJ simulation?*

   The main shifts in vegetation cover during an abrupt climate change event such as the Younger Dryas are well captured in the LPJ simulations as demonstrated in Chapter 2 and therefore, supports the usefulness of dynamic vegetation models for simulating terrestrial ecosystems for a transient climate regime. The fractional PFT coverage averaged over larger areas in Europe and North America reflect major pattern in vegetation distribution in these areas as shown by paleo-vegetation maps reconstructed from pollen records. However, the spatial resolution of the LPJ simulations is rather course (3.75° x 2.5°) and a more direct comparison of time series of the fractional PFT coverage per grid cell with pollen records is, due to site-specific effects in the pollen records rather difficult.

   Simulated changes in vegetation cover outside northern middle and high latitudes were rather small. Significant changes were only simulated for parts of the tropical forests which have been replaced by grasslands in the simulations as has been shown in Section 3.3. However, palynological evidence for a shift in vegetation distribution due to a Younger Dryas cold event in regions outside Europe and North America is not certain [Peteet,

1995].

2. *How does the terrestrial carbon cycle change under an abrupt climate change event and what are the characteristic time scales? How does the release of terrestrial carbon during a Younger Dryas like event agree with atmospheric CO_2 measurements from ice cores? How robust is the terrestrial signal towards changes in boundary conditions or model parameterizations? Can simulations of the terrestrial carbon 13 cycling during an abrupt climate change event help to clarify the origins of the modulations in atmospheric CO_2 during the last glacial transition (Figure 1.1).*

   The results of Chapter 2 and Chapter 3 clearly show that the terrestrial carbon cycle undergoes major changes during an abrupt climate change event. Chapter 2 shows that both changes in the vegetation distribution due to different climate conditions but also the direct effect of climate on the productivity of the plants have an impact on the land carbon storage capacity. Response time scales vary largely depending on the considered carbon stock: living biomass pools react rather fast to climate whereas the soil pools have much larger response times. It also seems that the time scales depend on the direction of climate change: for the cooling event the terrestrial biosphere reacts by a factor of approximately two faster than for the following warming (Chapter 2).

   Atmospheric CO_2 concentrations are strongly influenced by the vegetation dieback during the Younger Dryas and could possibly explain the accelerated increase in atmospheric CO_2 during the Younger Dryas as found in measurements from ice cores. This result is fairly robust against the sensitivity experiments carried out in Chapter 3. Furthermore, as suggested in Chapter 3, changes in the terrestrial carbon cycling may have even contributed to a large amount to the modulations of the atmospheric CO_2 concentration during the entire last transition from the glacial to the current warm phase which is apparent from the ice core measurements. The usefulness of stable carbon isotopes in clarifying the concurrent roles of ocean and land biota is limited by the rather large temporal resolution of the measurements, nevertheless the simulated atmospheric δ^{13}C values exhibit a strong signal for all sensitivity experiments and reflect the findings from measurements.

3. *Does the fractionation of carbon 13 during photosynthesis vary with climate fluctuations on a global scale and where are the regions exhibiting high variability in fractionation? To what extent is the variability of the fractionation factor caused by changes in the vegetation composition (shifts in C_3/C_4 plants)? What would be the impact of an interannually varying fractionation factor on carbon fluxes derived by double deconvolution?*

   The spatially resolved simulations of ^{13}C discrimination during photosynthesis reveal large interannual variations in the globally integrated terrestrial fractionation factor. These variations are mainly caused by anomalous climate events such as El Niño/Southern Oscillation. The two described experiments in Chapter 4 allow to distinguish between the variability in discrimination during photosynthesis caused by plant physiological responses

directly to climate (about two third of the variations) and by shifts from C_3 to C_4 plants (about one third). Regionally high variability is limited to areas where there are large fluctuations between C_3 and C_4 photosynthesis. Variability caused by physiological responses is dominated in the simulations in temperate regions (Chapter 5). The corrections in the derived terrestrial sink terms by double deconvolution studies using a climate dependant fractionation factor could be of the order of 0.8 Pg C yr^{-1} in certain years.

4. *Which are the main processes effecting the terrestrial isotopic disequilibrium during the last century and to what extent does the isotopic disequilibrium vary?*

   The results of Chapter 5 suggest that mainly two processes (in addition to the continuing depletion in ^{13}C of atmospheric CO_2 due to fossil fuel burning) effect the value of the isotopic disequilibrium: ecosystem disturbances by fire and the conversion of tropical forests into C_4 pastures. Land use itself, through the different treatment of agricultural products decreases also the absolute value of the isotopic disequilibrium, whereas cultivation of C_4 crops has only a minor influence on a global scale. Temporal and spatial variations in the isotopic disequilibrium mainly resemble the variations in the fractionation during photosynthesis. In addition, regions with a high natural fire frequency have a strong impact on the spatio-temporal pattern of the isotopic disequilibrium whereas the fractionation factor during photosynthesis is hardly influenced by fire events.

The results of this first part of the thesis demonstrate that a process-based forward modelling approach using a dynamic global vegetation model is a valuable tool for investigating aspects of the past and present carbon cycle which are not directly accessible by field or laboratory studies. The performed experiments clearly help to understand several aspects of the spatial and temporal pattern of the isotopic composition of the terrestrial biosphere which are useful for specifying terrestrial carbon sources and sinks. The results also demonstrate the potentially large impact of a rapid climate change event on the atmospheric CO_2 through the terrestrial response. Thus, studying the past carbon cycle gives valuable information for possible future climate change scenarios as an abrupt collapse of the thermohaline circulation due to increased atmospheric CO_2 concentrations might occur [Manabe and Stouffer, 1994] and could have a large effect on the terrestrial biosphere which would further increase atmospheric CO_2 concentrations.

The second part of the thesis (Chapter 6 and Appendix A) outlines the development of a formal data assimilation scheme for use in process-based terrestrial carbon cycle modelling (CCDAS: carbon cycle data assimilation system). Further, CCDAS is applied to derive calibrated model parameters and from which then in a so-called prognostic step terrestrial carbon fluxes optimally adjusted to observed atmospheric CO_2 concentrations are calculated for the period 1980 – 2000. Results presented here are calculated from an erroneous model version which has already been corrected but unfortunately corrected results are not available yet However, these results here already suggest that this method works and is capable of deriving a range of quantities of interest constrained by observational data: calibrated model parameter and their uncertainties, and terrestrial fluxes and their uncertainties. Appendix A gives a more detailed

description of the technical basis (automatic differentiation) and computational requirements for this system.

The simulated atmospheric CO_2 concentrations, besides terrestrial carbon fluxes one of the quantities calculated in the prognostic step of CCDAS, exhibit an excellent fit to the observational data on seasonal and interannual time-scales and underlines the usefulness of such a system. As explained in Chapter 6 it is also still worthwhile to analyze the simulated fluxes. The net terrestrial flux to the atmosphere shows a remarkable correlation with ENSO related climate anomalies. From the spatially explicit calculated fluxes ($2°\times2°$ resolution) the main regions (mainly parts of tropical South America and Africa) contributing to an anomalous terrestrial carbon source during strong El Niño years could be identified. The main process in this CCDAS set-up responsible for the anomalous source is a drop in the global primary productivity related to increased water stress at the corresponding regions. These results contradict the findings of Langenfelds et al. [2002] and Page et al. [2002] that during strong El Niño years the terrestrial carbon source anomaly is mainly coming from biomass burning.

7.2 Perspectives

One of the most interesting perspectives would certainly be the application of the modelled spatial and temporal pattern of the terrestrial isotopic composition in a double deconvolution study [e.g., Keeling et al., 1989; Joos and Bruno, 1998] to assess its usefulness. This would then probably lead to revisions in the derived carbon budgets but more importantly, it would certainly lead to a reduction in the uncertainties of the derived sources and sinks because (as already stated in Chapter 1) results of double deconvolution studies are particularly sensitive to the isotopic disequilibrium [Heimann and Meier-Reimer, 1996].

In this sense, the assessment of anthropogenic induced biomass burning on the terrestrial isotopic disequilibrium is of particular interest. There has been evidence that for specific periods, usually for years with a strong El Niño, a large part of the released carbon by terrestrial ecosystems is due to human made fires [Langenfelds et al., 2002; Page et al., 2002]. During these periods the isotopic disequilibrium is expected to be largely influenced by these fire events as it has been shown in Chapter 5 that fire is the most influential parameter on the value of the isotopic disequilibrium. To specify anthropogenic biomass burning in LPJ an inventory of the released carbon through human fire events would be necessary.

Further research should also be focused on the atmosphere-biosphere $^{13}CO_2$ exchange on shorter time scales such as monthly to daily. This would be very helpful in quantifying the magnitude of an isotopic disequilibrium induced by the difference in the isotopic ratios of photosynthesis and autotrophic respiration. Ekblad and Högberg [2001] have shown that more than half of the recently assimilated carbon becomes available for autotrophic root respiration within a few days. However, for the remaining carbon it can take several months before it is respired by the plant. In certain regions, preferable continental areas with a large seasonal hub in atmospheric $\delta^{13}C$ this may lead to large short term isotopic disequilibrium fluxes. The total values

and the relevance of this additional isotopic disequilibrium are still unresolved on a global scale.

In a dense canopy or also in a stable boundary layer condition respired CO_2 from plants and soils is partly assimilated by the plants again and thus, increasing the isotopic ratio of the photosynthate compared to assimilated carbon from free tropospheric CO_2. This mechanism is called the canopy recycling effect [Keeling, 1961]. So far, only site specific measurements exist which suggest that up to 39% of the respired CO_2 can be assimilated again [Sternberg et al., 1997]. The relevance of this recycling effect for the atmosphere biosphere $^{13}CO_2$ exchange on a global scale is still unknown. The isotope LPJ framework coupled to an atmospheric transport model would lead to new insights in the role of the recycling effect and could also quantitatively assess its magnitude for the isotopic composition of the terrestrial biosphere on a global scale.

Another promising and valuable perspective, especially for understanding the paleo carbon cycle is the development of a simply coupled biogeochemical ocean-land model system. The components themselves already exists: the isotope LPJ framework as the terrestrial model and the Hamburg ocean carbon model (HAMOCC, [Maier-Reimer and Heinze, 1992]). This would further enlighten the question of the concurrent roles of ocean and land biota in the modulations of the atmospheric CO_2 concentration and its $\delta^{13}C$ during the transition from the last glacial to the present warm phase.

As already mentioned in Section 6.5 the perspectives for CCDAS are rather straight forward: first, results from the currently being optimized CCDAS version have to be analyzed. A special focus in this analysis will be given to the processes responsible for the anomalous terrestial carbon source during strong El Niño years if it also is apparent in these new results. In addition, a simple fire module will be added in order to confirm the hypothesis of Langenfelds et al. [2002] and Page et al. [2002] that this source is mainly caused by biomass burning with such a data assimilation system. Besides, there is a range of possible applications of such a system,e.g.:

- explore different parameter configurations (which parameters are globally valid and which have to be spatially explicit),
- include fire as an additional process (as mentioned above),
- investigate which are the processes responsible for the apparent increase in terrestrial carbon uptake during the 1990s compared to the 1980s, and probably related to this,
- analyze the aspect of CO_2 fertilization (there is a substantial increase of almost 30 ppm in the atmospheric CO_2 concentration from 1980 until today),
- predict the future evolution of the terrestrial carbon cycle using data from IPPC climate scenario experiments.

Eventually this system will of course be further developed in a way that more data such as ecological site specific data, eddy flux measurements, and atmospheric isotope concentrations can be assimilated to add more various constraints on the terrestrial biosphere model. The inclusion of stable carbon isotope data seems to be especially promising as this would strongly constrain

the role of C_4 photosynthesis in the global terrestrial productivity, which is as discussed in Chapter 4 and Chapter 5 an important quantity. In the current CCDAS set-up C_4 photosynthesis is strongly reduced, and thus, somewhat contradicting findings from Chapters 4 and 5.

7.3 Concluding remark

Stabilization of the atmospheric CO_2 concentration and of course also other greenhouse gases is a primary goal of the United Nations Convention on Climate Change. As outlined in Section 1.1 CO_2 is the most important anthropogenic greenhouse gas in terms of radiative forcing. To stabilize atmospheric CO_2 is a major challenge to our society and requires an understanding of both the unperturbed natural carbon cycle and the by human intervention perturbed (through e.g., land use change) carbon cycle.

Two recently compiled studies [Cox et al., 2000; Dufresne et al., 2002] used a coupled carbon cycle climate general circulation model with predefined CO_2 emission scenarios to project future climate and atmospheric CO_2. Both found out that today's sink capacity of the terrestrial biosphere is reversed over this century. In the simulation from Cox et al. [2000] the land biosphere releases 170 Pg C during the 21^{st} century resulting in an atmospheric CO_2 concentration of 980 ppmv. This increased atmospheric CO_2 has a large impact on climate in this model simulation: a global warming of 8 °C over land. However, Dufresne et al. [2002] report an atmospheric CO_2 concentration of only 770 ppmv by 2100 and a global temperature increase of 4.4 °C over the continents. These large differences in the results are mainly caused by the different behaviour of the carbon cycle components and thus, reflect our still limited knowledge of the underlying processes. This is mostly true for the terrestrial processes as they are much more complex than the processes governing the ocean carbon cycle. A promising strategy to investigate the global carbon cycle consists besides of process studies and global observations also of model development and model studies. This thesis evaluated the importance of vegetation dynamics in studying the terrestrial carbon cycle and demonstrated the usefulness of process-based modelling of plant photosynthesis discrimination against ^{13}C in interpreting changes in $\delta^{13}C$ of atmospheric CO_2. In addition, it elucidated the development and application of a carbon cycle data assimilation system as a powerful tool in analyzing and predicting the terrestrial carbon cycle.

References

Cox, P. M., Betts, R. A., Jones, C. D., Spall, S. A., Totterdell, I. J., 2000. Acceleration of global warming due to carbon-cycle feedbacks in a coupled climate model. Nature 408 (6809), 184–187.

Dufresne, J. L., Friedlingstein, P., Berthelot, M., Bopp, L., Ciais, P., Fairhead, L., Le Treut, H., Monfray, P., 2002. On the magnitude of positive feedback between future climate change and the carbon cycle. Geophys. Res. Lett. 29 (10), doi:10.1029/2001GL013777.

Ekblad, A., Högberg, P., 2001. Natural abundance of ^{13}C in CO_2 respired from forest soils reveals speed of link between tree photosynthesis and root respiration. Oecologia 127, 305–308.

Heimann, M., Meier-Reimer, E., 1996. On the relations between the oceanic uptake of CO_2 and its carbon isotopes. Glob. Biogeochem. Cycles 10 (1), 89–110.

Joos, F., Bruno, M., 1998. Long-trem variability of the terrestrial and oceanic carbon sinks and the budgets of the carbon isotopes ^{13}C and ^{14}C. Glob. Biogeochem. Cycles 12, 277–295.

Keeling, C. D., 1961. A mechanism for cyclic enrichment of carbon-12 by terrestrial plants. Geochim. Cosmochim. Acta 24 (3-4), 299–313.

Keeling, C. D., Bacastow, R. B., Carter, A. F., Piper, S. C., Whorf, T. P., Heimann, M., Mook, W. G., Roeloffzen, H., 1989. A three-dimensional model of the atmospheric CO_2 transport based on observed winds: 1. Analysis of observational data. In: Peterson, D. H. (Ed.), Aspects of Climate Variability in the Pacific and the Western Americas. Vol. 55. AGU, Washington, D.C., pp. 165–236.

Langenfelds, R. L., Francey, R. J., Pak, B. C., Steele, L. P., Lloyd, J., Trudinger, C. M., Allison, C. E., 2002. Interannual growth rate variations of atmospheric CO_2 and its $\delta^{13}C$, H_2, CH_4 and CO between 1992 and 1999 linked to biomass burning. Glob. Biogeochem. Cycles 16, doi:10.1029/2001GB001466.

Maier-Reimer, E., Heinze, C., 1992. The Hamburg Ocean Carbon Ccyle model. Tech. Rep. 5, DKRZ, Hamburg.

Manabe, S., Stouffer, R. J., 1994. Multiple-century response of a coupled ocean-atmosphere model to an increase of atmospheric carbon-dioxide. J. Clim. 7 (1), 5–23.

Page, S., Siegert, F., Rieley, J. O., Boehm, H.-D. V., Jaya, A., Limin, S., 2002. The amount of carbon released from peat and forest fires in Indonesia during 1997. Nature 420, 61–65.

Peteet, D., 1995. Global Younger-Dryas? Quat. Int. 28, 93–104.

Sternberg, L. D. S., Moreira, M. Z., Martinelli, L. A., Victoria, R. L., Barbosa, E. M., Bonates, L. C. M., Nepstad, D. C., 1997. Carbon dioxide recycling in two Amazonian tropical forests. Agric. For. Meteorol. 88 (1-4), 259–268.

Appendix A

An example of an automatic differentiation-based modelling system

Abstract. We present a prototype of a Carbon Cycle Data Assimilation System (CCDAS), which is composed of a terrestrial biosphere model (BETHY) coupled to an atmospheric transport model (TM2), corresponding derivative codes and a derivative-based optimisation routine. In calibration mode, we use first and second derivatives to estimate model parameters and their uncertainties from atmospheric observations and their uncertainties. In prognostic mode, we use first derivatives to map model parameters and their uncertainties onto prognostic quantities and their uncertainties. For the initial version of BETHY the corresponding derivative codes have been generated automatically by FastOpt's automatic differentiation (AD) tool Transformation of Algorithms in Fortran (TAF). From this point on, BETHY has been developed further within CCDAS, allowing immediate update of the derivative code by TAF. This yields, at each development step, both sensitivity information and systematic comparison with observational data meaning that CCDAS is supporting model development. The data assimilation activities, in turn, benefit from using the current model version. We describe generation and performance of the various derivative codes in CCDAS, i.e. reverse scalar (adjoint), forward over reverse (Hessian) as well as forward and reverse Jacobian plus detection of the Jacobian's sparsity.

A.1 Introduction

In the past decades, numerical simulation models have become indispensable tools for earth system research. Component models describe parts of the system such as atmosphere, ocean, cryosphere, terrestrial and oceanic biosphere, or atmospheric chemistry. As there are important feedbacks between the dynamics of the individual components, coupling of component models is becoming more and more important. The steady increase in available computer resources allows an increase of the complexity of these models in terms of the level of component-detail, the number of components, and the numerical resolution.

A typical model formulation is based on a discretised set of equations and includes a number

of parameters, initial and boundary conditions, all of which are subject to uncertainties. The subset regarded most uncertain are usually specified as unknowns (or tunable parameters). In addition there are observable quantities that can be diagnosed by the model and are subject to observational uncertainties. The data assimilation (inverse modelling) community is concerned with combining models and observational data. Usually, on the basis of a given validated model rather sophisticated mathematical techniques are applied to infer information on the model's unknowns. A subset of these techniques are based on first- or higher-order derivative information.

In the model development community, the sensitivity of a given model formulation to values of the unknowns is usually assessed by multiple model runs. Validation is often carried out in a qualitative way, e.g. by plotting observational data against model simulations. Calibration of the models is usually guided by intuition rather than a mathematical algorithm. The advanced tools of the data assimilation community are rarely used. One of the reasons for this is the usually long delay from the release of a new model version to its integration in a data assimilation system. For derivative based data assimilation systems that rely on hand coding of, say, the adjoint of a complex model, this delay is often in the order of years. The ocean modelling community has started to reduce significantly this delay by employing an automatic differentiation (AD) tool to generate and maintain the derivative code of their data assimilation systems. FastOpt's AD tool Transformation of Algorithms in Fortran (TAF,Giering and Kaminski [1998a]; Giering et al. [2003]) has become an integral component of the ocean state estimation tool [Stammer et al., 2002a,b], a data assimilation system based on the MIT general circulation model (MITgcm, Marshall et al. [1995]; Adcroft et al. [2002]) built by the ECCO consortium. Within ECCO, model development and data assimilation go hand in hand and benefit from each other. TAF is also integrated in a similar system, which is currently being built around the Modular Ocean Model (MOM, Griffies et al. [2002], see also Galanti et al. [2002]) by the Geophysical Fluid Dynamics Laboratory at Princeton.

In this paper we present a prototype of a Carbon Cycle Data Assimilation System, CCDAS [Rayner et al., 2001], based on the terrestrial biosphere model BETHY [Knorr, 2000] coupled to the atmospheric transport model TM2 [Heimann, 1995]. CCDAS has been set up and is being used by a group of model development and data assimilation experts. For the initial version of BETHY, the corresponding derivative codes have been generated automatically by TAF. From this point on, BETHY has been developed within CCDAS, allowing immediate update of the derivative code by TAF. At each development step, rather than testing the current model formulation at a few subjectively selected points in parameter space, we explore that space algorithmically. In Section A.2 we give a brief description of the model underlying CCDAS, and Section A.3 presents the system as a whole. Section A.4 addresses the AD component including performance, and Section A.5 draws some conclusions.

A.2 BETHY and TM2

BETHY [Knorr, 1997, 2000] is a model of the terrestrial biosphere. For the initial version of CCDAS, the model has been restricted to the simulation of photosynthesis, carbon and energy balance (see also Rayner et al. [2001]). Global vegetation is mapped onto 13 plant functional types (PFTs) based on Wilson and Henderson-Sellers [1985]. The reduced BETHY can be driven by observed climate and radiation data (Nijssen et al. [2001] which have been extended to the year 2000 [Schnur, 2002]) or by climate model output. Hydrology and phenology are provided by an integration of the full BETHY version. For a given integration period (typically a number of years), the model simulates the diurnal cycle of a representative day for each month. This diurnal cycle is resolved at an hourly time step. BETHY computes carbon dioxide exchange fluxes with the atmosphere. To constrain the model with atmospheric concentrations observed at a global sampling network [GLOBALVIEW-CO_2, 2001], BETHY is coupled to the atmospheric transport model TM2 [Heimann, 1995]. For a passive tracer such as carbon dioxide, in our setup, TM2 acts as a linear function, mapping monthly mean fluxes across its about 9'000 surface grid cells onto monthly mean concentrations at 40–100 observational sites. Hence, we represent the model by its Jacobian matrix derived by reverse mode AD of TM2, in a similar way as Kaminski et al. [1999]. Coupling is realised on the Fortran code level, rather than on the level of the operating system. The same strategy has been applied previously for coupling a much simpler biosphere model, the Simple Diagnostic Biosphere Model (SDBM, Knorr and Heimann [1995]), to TM2. We refer to Kaminski et al. [2002] for details.

A.3 Two Modes of CCDAS

CCDAS has two modes of operation. We give a brief description here, for details consult Rayner et al. [2003]. In its calibration or assimilation mode, CCDAS employs observations plus their uncertainties to infer information on unknowns in the model. These unknowns include, for example, rate constants or asymptotic values of functional forms used to describe plant or soil behaviour. In our current setup, we have 57 parameters within BETHY plus an initial value of the atmospheric concentration as an additional unknown. The observations of 41 sites are provided by a global atmospheric flask sampling network [GLOBALVIEW-CO_2, 2001]. The atmospheric concentration is also affected by fluxes from components other than those simulated by BETHY. Our model accounts for these components as prescribed contributions (background fluxes) from ocean [Takahashi et al., 1999; Le Quéré et al., 2000], land use change [Houghton et al., 1987], and fossil fuel emissions [Andres et al., 2000; Marland et al., 2001]. Figure A.1 depicts the model setup for the calibration mode. Additional streams of observational data can be accessed by coupling further models. The model is currently calibrated at a global resolution of 2×2 degrees using 21 years of observations and a spin up period of 5 years in order to achieve a quasi-equilibrium state for its litter carbon pool.

The calibration problem is formulated in a Bayesian way (see e.g. Tarantola [1987]; Enting

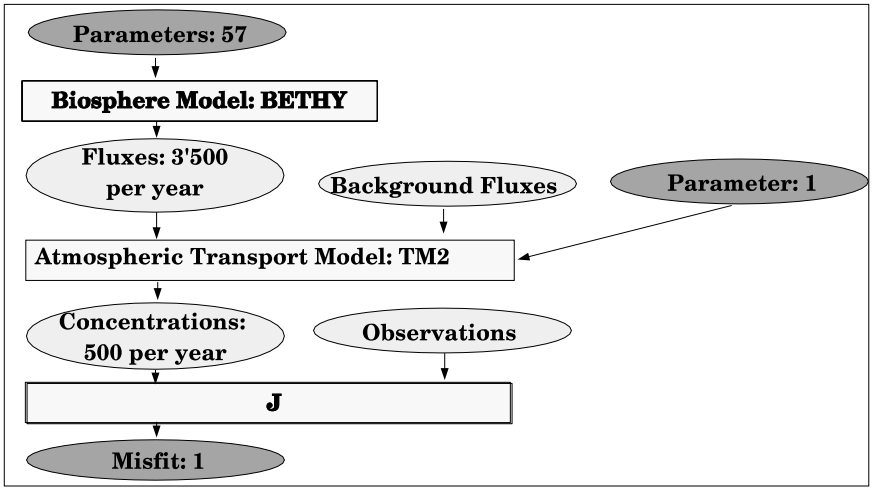

Figure A.1: Flow of information in the coupled model. Oval boxes show the various quantities, dependent and independent variables are dark grey, intermediate fields are light grey. Rectangular boxes denote the mappings between these fields.

[2002]): The observational information is combined with a priori knowledge on the unknowns and the constraint provided by the model. Observations and priors ($\mathbf{d}$ and $\mathbf{p}$, respectively) are assumed to have Gaussian probability distributions, i.e. they are represented by their mean values and covariance matrices ($\mathbf{C_d}$ and $\mathbf{C_p}$, respectively). Model error is reflected by a contribution to the observational covariance matrix. Currently we are using diagonal covariance matrices for observations and priors. Combining observed and prior information to the model yields a posterior probability distribution for the unknowns, which is highest at the minimum of the misfit function J

$$J(\mathbf{x}) = \frac{1}{2}((M(\mathbf{x}) - \mathbf{d})^T \, {\mathbf{C_d}}^{-1} \, (M(\mathbf{x}) - \mathbf{d}) + (\mathbf{x} - \mathbf{p})^T \, {\mathbf{C_p}}^{-1} \, (\mathbf{x} - \mathbf{p})) \ , \tag{A.1}$$

where M denotes our model and ^{T} the transpose. The calibration thus yields an optimisation problem with $\mathbf{x}$ as control variables. The problem is solved with a BFGS algorithm similar to Gilbert and Lemaréchal [1989], which iteratively evaluates both J and its gradient with respect to $\mathbf{x}$. The optimiser works off-line: at each iteration the values from function and gradient evaluations plus some internal information are recorded. This allows interruptions and restarts, which is convenient, e.g. for switching computing platforms. The optimisation is preconditioned with the prior covariance matrix, i.e control variables are normalised by their prior uncertainties.

The posterior uncertainty on the unknowns is approximated by the inverse Hessian of J at the minimum. We invert the Hessian in the subspace of unknowns which is constrained by the observations, in the orthogonal complement we keep the prior uncertainties.

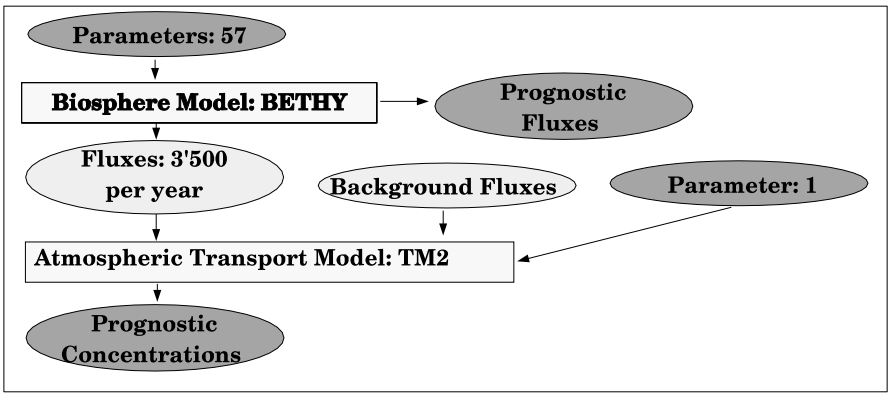

Figure A.2: Model set-up for the prognostic mode. Oval boxes show the various quantities, dependent and independent variables are dark grey, intermediate fields are light grey. Rectangular boxes denote the mappings between these fields.

In its prognostic mode, CCDAS computes selected target quantities and their uncertainties from the calibrated values and their uncertainties. The underlying modelling chain is shown in Figure A.2. Current target quantities are spatial and temporal means of exchange fluxes. Their uncertainties are approximated by

$$\mathbf{C_f} = \mathbf{D}M^T \mathbf{C_x} \mathbf{D}M \ , \tag{A.2}$$

where $\mathbf{D}M$ denotes the Jacobian of the model. By coupling further models, additional quantities can be predicted.

As mentioned above, a new version of BETHY was prepared for CCDAS. Attention has been paid to formulate the model in a differentiable way. As a consequence, the model formulation was improved and so was the approximation capability of the derivatives. This is beneficial for both the optimisation and the prognostic uncertainty approximation. From the initial version which was used to build up CCDAS, the model has been developed further within the system. This proved beneficial for model development in many cases. At an early stage, a sensitivity of zero to a particular parameter helped to detect and remove a bug in the model code. The first calibration of the model showed a poor fit to atmospheric observations. The model formulation was then revised to allow up to 3 PFTs per grid cell, rather than a single PFT as in the initial version. A calibration of model version 11 resulted in a good fit however a bug related to the model's spin up period was detected. To compensate for this bug, the calibration yielded a surprising value of a related parameter. Calibration of model version 12 (with the bug removed),

yields an improved fit to the observations compared to version 11. We refer to Scholze et al. [2002] for results based on version 11 and to Rayner et al. [2003] for results based on version 12.

A.4 Automatic Differentiation

All of the derivative codes mentioned in the foregoing sections are generated fully automatically by FastOpt's AD-tool Transformation of Algorithms in Fortran (TAF) [Giering and Kaminski, 1998a; Giering et al., 2003]. BETHY is implemented in Fortran-90. It uses features such as modules, allocation/deallocation of arrays, assumed shape arrays, derived types, and array expressions. Without comments, model version 12 comprises about 5'500 lines of source code. Both, initialisation of the model and postprocessing of the results are carried out in subroutines separate from the core of the model. For each derivative code generation there is a top-level subroutine that defines independent and dependent variables and invokes the core of the model.

The model's adjoint evaluates the gradient of the scalar-valued misfit function Equation A.1 with respect to the control variables and provides it to the optimiser. The most challenging task of adjoint coding is to provide values computed during the function evaluation (required values [Giering and Kaminski, 1998a]) to the derivative evaluation. For providing these required values, the adjoint uses a mixed strategy of recomputation and storing/reading [Giering and Kaminski, 1998a; Giering et al., 2003], which includes a two level checkpointing scheme [Griewank, 1992, 2000] as described by Giering et al. [2003]. In the inner checkpointing loop, values are stored in core memory, in the outer loop on hard disk. The entire store/read scheme is triggered by 8 TAF INIT directives, which create a tape in memory/disk each, plus 23 TAF store directives, which indicate the values to be stored. To support TAF's data flow analysis, there are 38 TAF loop directives, which indicate loops that can be executed in parallel, 5 TAF flow directives (see Giering et al. [2003]) trigger inclusion of the deallocation of model variables at the end of the adjoint integration. This deallocation is useful to allow multiple consecutive runs of the adjoint. Running the adjoint takes the time of about 3.4 function evaluations. For shorter integrations, without the need of the checkpointing scheme, this number would reduce to 2.4. Generation of the tangent linear code involves no particular complications. Its run times is that of 1.5 function evaluations.

Efficient code to provide the Hessian of the misfit function Equation A.1 is generated by redifferentiating the adjoint code in forward mode, which is known as forward over reverse mode of AD (see also Giering and Kaminski [1998b]; Giering et al. [2003]). Unfortunately the evaluation of the entire Hessian does not fit into the memory available on our production machine, a Linux PC, with 2 XEON 2GHz processors and 2 GByte core memory. Evaluating the Hessian in groups of 12 columns, however, just fits. Such an evaluation takes the time of about 50 function evaluations.

To provide the Jacobian needed in Equation A.2 we differentiate a function that maps the unknowns onto the prognostic quantities, which are currently simple diagnostics of the field of carbon fluxes into the atmosphere. Depending on the ratio of number of diagnostics to number

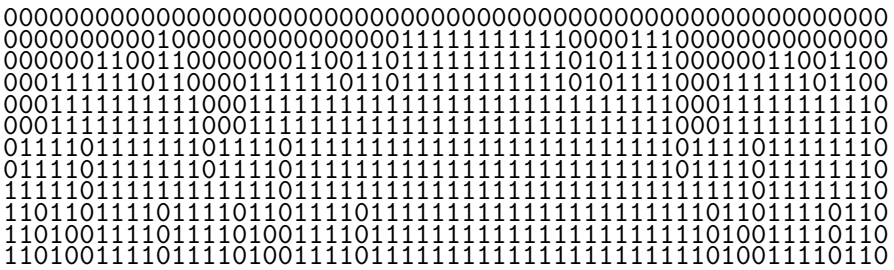

Figure A.3: Example of a sparsity pattern.

of unknowns we evaluate the derivative in forward or reverse mode.

This type of Jacobian is often sparse, i.e. there are entries of value 0: For example, the initial concentration component of the control vector has no impact on prognostics that are fluxes into the atmosphere. Furthermore, as a subset of the 57 parameters are PFT-specific their influence is limited to particular regions of the globe. For instance high latitude fluxes are insensitive to parameters specific to tropical forests. This sparseness of the Jacobian is determined by TAF's Automatic Sparsity Detection (ASD) mode. ASD is a source to source transformation similar to AD. Instead of propagating derivative values, however, ASD propagates only the sparsity information. In contrast to an entry of the Jacobian, which takes real values, an entry in the sparsity pattern only takes boolean values, i.e. true or false. TAF's ASD mode exploits this by storing sparsity information in the bits of integers, i.e. as integer bit-vectors. In our current setup based on 4 byte integers, each variable holds blocks of 32 (8×4) units of sparsity information. Operations on these integers efficiently propagate sparsity information block-wise, i.e. 32 units per operation. As a demonstration, Figure A.3 illustrates the sparsity pattern of the Jacobian for 12 prognostic quantities, namely the mean fluxes over the integration period and 12 latitude bands spanning the northern hemisphere. The pattern has been derived by ASD in reverse mode. The first row has only zero entries, because the model simulates no biospheric flux in that latitude. The last (58th) column is zero, because it corresponds to the initial atmospheric concentration, which has no impact on the surface fluxes. The remaining zeros correspond to parameters which have no influence on the fluxes of the respective latitude band, because they refer to PFTs which are not represented in this band. Curtis et al. [1974]; Newsam and Ramsdell [1983]; Geitner et al. [1996] exploit Jacobian sparsity by efficiently constructing the full Jacobian from Jacobian-vector products. In the current version of CCDAS we do not take advantage of sparsity yet, but might do so, as the dimensions of the Jacobian increase.

The performance of Jacobian and ASD evaluations has been tested on a Linux PC, with an Athlon 1.6 GHz processor and 1 GByte core memory. The integration period was limited to one year. All runs are for 58 unknowns (independents). Run times of forward mode AD and ASD are about 12 and 1.3 function evaluations, respectively. Figure A.4 shows performance numbers of reverse mode AD and ASD for a varying number of prognostics (dependents). Both, forward and reverse ASD, consume most of the CPU time to provide required variables, for which they use the same strategies as their AD counterparts. Reverse ASD for 1000 prognostics, i.e. about

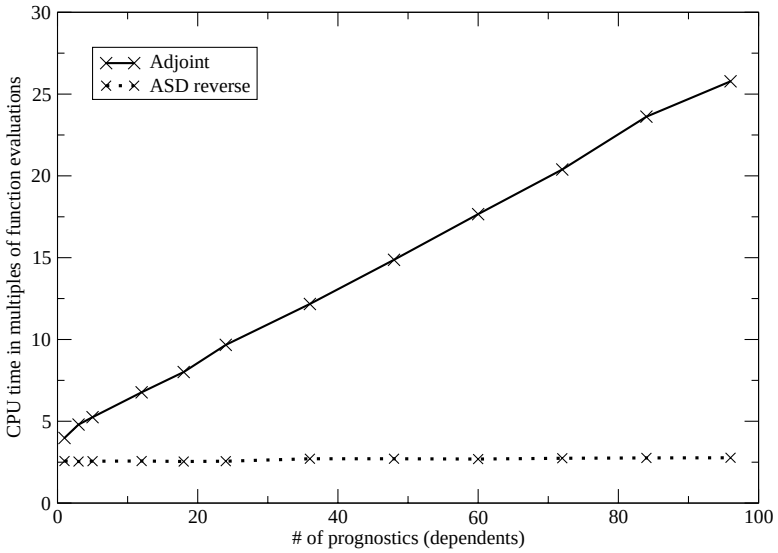

Figure A.4: Performance of Jacobian (solid line) and ASD (dashed line) evaluations in reverse mode for varying number of prognostics (dependents). Values are in multiples of the CPU time of one function evaluation.

30 bit-vectors, costs about 6 function evaluations (not shown in Figure A.4).

A.5 Conclusions

We have presented an example of a derivative based modelling system for data assimilation, which also serves as a frame for model development. We have given examples in which sensitivity information and algorithmic comparison with observations support model development. Rather than testing a given model formulation with a few selected sets of parameter values, CCDAS allows us to judge a model formulation with its *optimal* set of parameters. As we get more experience in operating the system, we expect it to make further important contributions to model development. The system's inverse modelling applications, in turn, benefit enormously from having the most recent model version available. In this system, AD is a key technology, since it provides a reliable and efficient way of keeping a suite of derivative codes up to date with the latest model version.

This example may well be generalised to other models and other fields. Especially when developing a new model from scratch, it appears beneficial to have the model code AD compliant in order to benefit from a derivative based system around the model.

References

Adcroft, A., Campin, J. M., Heimbach, P., Hill, C., Marshall, J., 2002. The MITgcm. Online documentation, MIT, Cambridge, USA.

Andres, R. J., Marland, G., Boden, T., Bischoff, S., 2000. Carbon dioxide emissions from fossil fuel consumption and cement manufacture 1751 to 1991 and an estimate for their isotopic composition and latitudinal distribution. In: Wigley, T. M. L., Schimel, D. (Eds.), The carbon cycle. Cambridge University Press, New York, USA.

Curtis, A. R., Powell, M. J. D., Reid, J. K., 1974. On the estimation of sparse Jacobian matrices. J. Inst. Math. Appl. 13, 117–119.

Enting, I. G., 2002. Inverse Problems in Atmospheric Constituent Transport. Cambridge University Press, Cambridge, U.K.

Galanti, E., Tziperman, E., Harrison, M., Rosati, A., Giering, R., Sirkes, Z., 2002. The equatorial thermocline outcroppin - a seasonal control on the tropical pacific ocean-atmosphere instability strength. J. Clim. 15 (19), 2721–2739.

Geitner, U., Utke, J., Griewank, A., 1996. Automatic computation of sparse Jacobians by applying the method of Newsam and Ramsdell. In: Berz, M., Bischof, C., Corliss, G., Griewank, A. (Eds.), Computational Differentiation: Techniques Applications, and Tools. SIAM, Philadelphia, USA, pp. 161–172.

Giering, R., Kaminski, T., 1998a. Recipes for adjoint code construction. ACM Trans. Math. Software 24, 437–474.

Giering, R., Kaminski, T., 1998b. Using TAMC to generate efficient adjoint code: Comparison of automatically generated code for evaluation of first and second order derivatives to hand written code from the minpack-2 collection. In: Faure, C. (Ed.), Automatic Differentiation for Adjoint Code Generation. INRIA, Sophia Antipolis, France.

Giering, R., Kaminski, T., Slawig, T., 2003. Applying TAF to a Navier-Stokes solver that simulates an Euler flow around an airfoil. to appear in Future Generation Computer Systems.

Gilbert, J. C., Lemaréchal, C., 1989. Some numerical experiments with variable-storage quasi-Newton algorithms. Mathematical Programming 45, 407–435.

GLOBALVIEW-CO_2, 2001. Cooperative Atmospheric Data Integration Project - Carbon Dioxide. CD-ROM, NOAA CMDL, Boulder, Colorado, [Also available on Internet via anonymous FTP to ftp.cmdl.noaa.gov, Path: ccg/co2/GLOBALVIEW].

Griewank, A., 1992. Achieving logarithmic growth of temporal and spatial complexity in reverse automatic differentiation. Optimization Methods and Software 1, 35–54.

Griewank, A., 2000. Evaluating Derivatives: Principles and Techniques of Algorithmic Differentiation. No. 19 in Frontiers in Appl. Math. SIAM, Philadelphia, Penn.

Griffies, S. M., Harrison, J. M., Pacanoski, R. C., Rosati, A., 2002. The FMS MOM4-beta user guide. Tech. rep., NOAA/Geophysical Fluid Dynamics Laboratory.

Heimann, M., 1995. The global atmospheric tracer model TM2. Tech. Rep. 10, Max-Planck-Institut für Meteorologie, Hamburg, Germany.

Houghton, R. A., Boone, R. D., Fruci, J. R., Hobbie, J., Mellilo, J. M., Palm, C. A., Peterson, B. J., Shaver, G. R., Woodwell, G. M., Moore, B., Skole, D. L., Myers, N., 1987. The flux of carbon from terrestrial ecosystems to the atmosphere in 1980 due to changes in land use: Geographic distribution of the global flux. Tellus 39B, 122–139.

Kaminski, T., Heimann, M., Giering, R., 1999. A coarse grid three-dimensional global inverse model of the atmospheric transport - 1. Adjoint model and jacobian matrix. J. Geophys. Res. 104 (D15), 18535–18553.

Kaminski, T., Knorr, W., Rayner, P. J., Heimann, M., 2002. Assimilating atmospheric data into a terrestrial biosphere model: A case study of the seasonal cycle. Glob. Biogeochem. Cycle 16 (4), doi:10.1029/2001GB001463.

Knorr, W., 1997. Satellitengestützte Fernerkundung und Modellierung des globalen CO_2-Austauschs der Landvegetation: Eine Synthese. Ph.D. thesis, Max-Planck-Institut für Meteorologie, Hamburg, Germany.

Knorr, W., 2000. Annual and interannual CO_2 exchanges of the terrestrial biosphere: Process-based simulations and uncertainties. Glob. Ecol. Biogeogr. 9 (3), 225–252.

Knorr, W., Heimann, M., 1995. Impact of drought stress and other factors on seasonal land biosphere CO_2 exchange studied through an atmospheric tracer transport model. Tellus 47B (4), 471–489.

Le Quéré, C., Orr, J. C., Monfray, P., Aumont, O., Madec, G., 2000. Interannual variability of the oceanic sink of CO_2 from 1979 through 1997. Global Biogeochem. Cycles 14, 1247–1265.

Marland, G., Boden, T. A., Andres, R. J., 2001. Global, regional, and national CO_2 emissions. In: Trends: A Compendium of Data on Global Change. Carbon Dioxide Information Analysis Center, Oak Ridge National Laboratory, U.S. Department of Energy, Oak Ridge, Tenn.

Marshall, J., Adcroft, A., Hill, C., Perelman, L., Heisey, C., 1995. A finite-volume incompressible Navier Stokes model for studies of the ocean on parallel computers. Tech. Rep. 36, MIT, Center for Global Change Science, Cambridge, USA.

Newsam, G. N., Ramsdell, J. D., 1983. Estimation of sparse Jacobian matrices. SIAM J. Alg. Disc. Meth. 4 (3), 404–417.

Nijssen, B., Schnur, R., Lettenmaier, D., 2001. Retrospective estimation of soil moisture using the vic land surface model, 1980-1993. J. Climate 14 (8), 1790–1808.

Rayner, P. J., Knorr, W., Scholze, M., Giering, R., Kaminski, T., Heimann, M., Le Quéré, C., 2001. Inferring terrestrial biosphere carbon fluxes from combined inversions of atmospheric transport and process-based terrestrial ecosystem models. In: Proceedings of 6th carbon dioxide conference. Sendai, pp. 1015–1017.

Rayner, P. J., Scholze, M., Knorr, W., Kaminski, T., Giering, R., 2003. The history of terrestrial carbon fluxes from 1980–2000: Results from a Data Assimilation System. In preparation for Global Biogeochem. Cycles.

Schnur, R., 2002. personal communication.

Scholze, M., Rayner, P. J., Knorr, W., Kaminski, T., Giering, R., 2002. A prototype Carbon Cycle Data Assimilation System (CCDAS): Inferring interannual variations of vegetation-atmosphere CO_2 fluxes. Abstract CG62A-05. Eos Trans. AGU Fall Meeting Suppl. 83 (47).

Stammer, D., Wunsch, C., Giering, R., Eckert, C., Heimbach, P., Marotzke, J., Adcroft, A., Hill, C., Marshall, J., 2002a. Global ocean circulation during 1992-1997, estimated from ocean observations and a general circulation model. J. Geophys. Res. 107, doi:10.1029/2001JC000888.

Stammer, D., Wunsch, C., Giering, R., Eckert, C., Heimbach, P., Marotzke, J., Adcroft, A., Hill, C. N., Marshall, J., 2002b. Volume, heat and freshwater transpoerts of the ocean circulation 1992-1997, estimated from a general circulation model constrained by WOCE data. J. Geophys. Res. , doi:10.1029/2001JC001115.

Takahashi, T., Wanninkhof, R. H., Feely, R. A., Weiss, R. F., Chipman, D. W., Bates, N., Olafsson, J., Sabine, C., Sutherland, S. C., 1999. Net sea-air CO_2 flux over the global oceans: An improved estimate based on the sea-air pCO_2 difference. In: Nojiri, Y. (Ed.), Extended abstracts of the 2nd International CO_2 in the Oceans Symposium, Tsukuba, Japan, January 18-22, 1999. pp. 9–15.

Tarantola, A., 1987. Inverse problem theroy - Methods for data fitting and model parameter estimation. Elsevier Science, New York, USA.

Wilson, M. F., Henderson-Sellers, A., 1985. A global archive of land cover and soils data for use in general-circulation climate models. Journal of Climatology 5 (2), 119–143.

Danksagung

Zum Gelingen dieser Arbeit haben viele Kollegen und Freunde beigetragen - ihnen allen sei herzlich gedankt. Insbesondere möchte ich mich bedanken bei:

Lennart Bengtsson für die Möglichkeit und Unterstützung, die Arbeit am Max-Planck-Institut für Meteorologie zu erstellen. Seine aufgeschlossene Art Wissenschaft zu betreiben war besonders motivierend. Die Freiheit, die er mir ließ, und das damit verbundene Vertrauen waren sehr hilfreich.

Hartmut Graßl für sein Interesse an der Arbeit und seine Bereitschaft, die Begutachtung der Dissertation zu übernehmen.

Martin Heimann für die wissenschaftliche "Fernbetreuung". Sein Enthusiasmus und vor allem seine weitreichenden Kenntnisse des Kohlenstoffkreislaufes, gemeinsam mit detaillierten und kritischen Diskussionen waren eine wichtige Basis für den Verlauf der Arbeit.

Wolfgang Knorr für die wissenschaftliche "Nahbetreuung". Ihm verdanke ich durch viele anregende Diskussionen und Gespräche unter anderem einen tieferen Einblick in die Prozesse der terrestrischen Biosphäre.

Eva-Maria Pfeiffer und Walter Michaelis als weitere Mitglieder des Promotionsausschusses.

Philippe Ciais, Fortunat Joos, Thomas Kaminski und vor allem Peter Rayner für die vielen hilfreichen Ratschläge und Kommentare zu der Arbeit und auch für die Elimination zahlreicher Rechtschreib- und sonstiger Fehler in der Arbeit.

Ute Merkel und Georg Bäuml, die als meine beiden Büro-Kollegen wesentlich zu der ausgesprochen netten und produktiven Atmosphäre beigetragen haben und mit bewundernswerter Ausdauer so manche "Du, sag mal, wie macht man eigentlich ...?"-Frage beantwortet haben.

Der größte Dank geht an meine Eltern für deren Unterstützung und Zuspruch, sowie an Carmen, die alle Höhen und Tiefen der Arbeit mitleben musste.

MPI-Examensarbeit-Referenz:

Examensarbeit Nr. 1-67 bei Bedarf bitte Anfragen:
MPI für Meteorologie, Abtlg.: PR, Bundesstr. 55, 20146 Hamburg

Examensarbeit Nr. 68 Februar 2000	**Die direkte Strahlungswirkung von Aerosolteilchen auf ein Klimamodell** Anke Maria Allner
Examensarbeit Nr. 69 Februar 2000	**Räumliche und zeitliche Variabilität von Wasserisotopen im polaren Niederschlag** (Spatial and Temporal Variability of Water Isotopes in Polar Precipitation) Martin Werner
Examensarbeit Nr. 70 März 2000	**Bestimmung des turbulenten Impulsflusses mit Hilfe von Doppler- und Interferometriemessungen eines Radar-RASS-Systems** Lutz Hirsch
Examensarbeit Nr. 71 Mai 2000	**Entwicklung und Test eines massenerhaltenden semi-Lagrangschen Transportverfahrens auf einer Kugel** Markus Peter Olk
Examensarbeit Nr. 72 Mai 2000	**Quantification of Natural Climate Variability in Paleoclimatic Proxy Data Using General Circulation Models: Application to Glacier Systems** Bernhard K. Reichert
Examensarbeit Nr. 73 Mai 2000	**Validation of Clouds in the ECHAM4 Model Using a Dynamical Adjustment Technique** Hans-Stefan Bauer
Examensarbeit Nr. 74 Juni 2000	**The Dynamical Link Between the Troposphere and Stratosphere and its Potential to Affect Climate** Judith Perlwitz
Examensarbeit Nr. 75 Juli 2000	**Fernerkundung von Eis- und Mehrschichtbewölkung über Meeresuntergrund aus Messungen rückgestreuter Solarstrahlung** Claudio Costanzo
Examensarbeit Nr. 76 Juli 2000	**Large-scale SST variability in the midlatitudes and in the tropical Atlantic** Dietmar Dommenget
Examensarbeit Nr. 77 Juli 2000	**HOAPS: Eine neue Klimatologie des Süßwasserflusses an der Meeresoberfläche abgeleitet aus Satellitendaten** Volker Jost
Examensarbeit Nr. 78 September 2000	**The potential influence of natural climate variability and uncertainty in the design of optimal greenhouse gas emission policies** Victor Ocaña

MPI-Examensarbeit-Referenz:

Examensarbeit Nr. 1-67 bei Bedarf bitte Anfragen:
MPI für Meteorologie, Abtlg.: PR, Bundesstr. 55, 20146 Hamburg

Examensarbeit Nr. 79 Oktober 2000	**Messungen des Reflexionsvermögen der Meeresober-fläche im infraroten Spektralbereich mit dem "Ocean Atmosphere Sounding Interferometer System" (OASIS)** Lars Fiedler
Examensarbeit Nr. 80 November 2000	**Vertikalmessungen der Aerosolextinktion und des Ozons mit einem UV-Raman-Lidar** Volker Matthias
Examensarbeit Nr. 81 Dezember 2000	**Photochemical Smog in Berlin-Brandenburg: An Investigation with the Atmosphere-Chemistry Model GESIMA** Susanne E. Bauer
Examensarbeit Nr. 82 Juli 2001	**Komponenten des Wasserkreislaufs in Zyklonen aus Satellitendaten – Niederschlagsfallstudien-** Klepp Christian-Philipp
Examensarbeit Nr. 83 Juli 2001	**Aggregate models of climate change: development and applications** Kurt Georg Hooss
Examensarbeit Nr. 84 Februar 2002	**Ein Heterodyn-DIAL System für die simultane Messung von Wasserdampf und Vertikalwind: Aufbau und Erprobung** Stefan Lehmann
Examensarbeit Nr. 85 April 2002	**Der Wasser- und Energiehaushalt der arktischen Atmosphäre** Tido Semmler
Examensarbeit Nr. 86 April 2002	**Auswirkungen der Assimilation von Meereshöhen-Daten auf Analysen und Vorhersagen von El Niño** Sigrid Schöttle
Examensarbeit Nr. 87 Juni 2002	**Atmospheric Processes in a young Biomass Burning Plume - Radiation and Chemistry** Jörg Trentmann
Examensarbeit Nr. 88 August 2002	**Model Studies of the Tropical 30 to 60 Days Oscillation** **S**tefan Liess
Examensarbeit Nr. 89 Dezember 2002	**Influence of Sub-Grid Scale Variability of Clouds on the Solar Radiative Transfer Computations in the ECHAM5 Climate Model** Georg Bäuml

ISSN 0938 - 5177